# Effect of Leaching Scale on Prediction of Total Dissolved Solids Release from Coal Mine Spoils and Refuse

Lucas Clay Ross

Thesis submitted to the faculty of Virginia Polytechnic Institute and State University in partial fulfillment of the requirements for the degree of

Master of Science

In

Crop and Soil Environmental Sciences

Walter L. Daniels, Chair

Matthew J. Eick

Stephen H. Schoenholtz

Carl E. Zipper

2/26/2015

Blacksburg, VA

Keywords: Mesocosms, overburden, electrical conductivity, leachate

# Effect of Leaching Scale on Prediction of Total Dissolved Solids Release from Coal Mine Spoils and Refuse

Lucas Clay Ross

## ABSTRACT

Coal surface mining in the Appalachian USA coalfields can lead to significant environmental impacts including elevated total dissolved solids (TDS) levels in receiving streams. Column leaching procedures are recommended by many studies for TDS prediction, but many question their applicability to field conditions. The objective of this study was to assess results from a simple column leaching method relative to larger scale leaching vessels (scales) using one coal mine spoil and two coarse coal refuse materials. A non-acidic mine spoil sample from SW Virginia (crushed to $\leq$ 1.25 cm) was placed into PVC columns (~10 cm x 40 cm) in the laboratory and leached unsaturated with simulated acidic rainfall. The same spoil was also placed into larger "mesocosms" (~1.5 $m^3$) with run-of-mine material and into barrels (~0.1 $m^3$; screened to $\leq$ 15 cm) under natural field environmental and leaching conditions. Similarly, two coarse coal refuse samples were placed into lab columns and field barrels. Comparative results suggest the column method was a reasonable predictor of TDS release from the coal mine spoil relative to the two larger scales studied. However, there were significant differences at times during the study, including during initial peak TDS elution (1,750 µS $cm^{-1}$ in columns vs. 2,250 µS $cm^{-1}$ in mesocosms). Field leaching also produced a distinct seasonal time-lagged EC pattern that was not observed in the columns. On the other hand, significantly different and dissimilar leaching results were noted for the refuse column vs. barrel leachates, calling into question their prediction ability for refuse.

# DEDICATION

To my parents.  Thank you for your continuous support, and everything that you do.

ACKNOWLEDGEMENTS

I would like to Dr. Lee Daniels, Dr. Matt Eick, Dr. Stephen Schoenholtz, and Dr. Carl Zipper for their guidance throughout my time as a graduate student. In particular, I would like to thank Dr. Daniels for encouraging and allowing me to continue my education for the past several years. I would also like to thanks Sara Koropchak, Zenah Orndorff, Julie Burger, Dan Johnson, John Parker, Steve Nagle, Katie Haering, Mike Beck, Whitney Nash, Luiz Spinelli Pinto, and Jon Dickerson for their help with various parts of my research. Without their help with column construction, column leaching, mesocosm and barrel construction and filling, leachate analysis, and much more, none of this would have been possible. Lastly, I would like to thank ARIES, the Powell River Project, and the OSM Applied Science Program for their support to make this research possible.

TABLE OF CONTENTS

LIST OF FIGURES

LIST OF TABLES

## INTRODUCTION AND LITERATURE REVIEW

### INTRODUCTION

In recent years, total dissolved solids (TDS) resulting from Appalachian coal mining operations have been identified as a significant problem for the aquatic biota in receiving headwater streams (Bernhardt et al., 2012; Green et al., 2000; Pond et al. 2008; Pond, 2010). TDS are the inorganic salts and other non-volatile dissolved materials in water. Leachates from coal mining operations often contain elevated levels of ions such as $HCO_3^-$, $SO_4^{2-}$, $Cl^-$, $Ca^{2+}$, $K^+$, $Mg^{2+}$, and $Na^+$ (Pond et al., 2008). TDS results from the rapid weathering of overburden material (mine spoil) that is displaced to mine the coal present under the land surface, and from coal preparation by-products (coal refuse). These materials often become the new surface of the landscape, with the excess material placed into highwall backfills, valley fills, and other disposal sites. Here, the materials are exposed to oxidized surface or near-surface conditions, leading to rapid weathering reactions, which create an ideal environment for TDS generation.

Levels of TDS in the field in streams are typically measured by electrical conductivity (EC), and often expressed in $\mu S\ cm^{-1}$. Field and laboratory EC data vary somewhat with temperature and are frequently corrected to standard temperature and then expressed as specific conductance (SC). Aquatic scientists often use a "rule of thumb" whereby TDS (in $mg\ L^{-1}$) is presumed to be approximately 0.70 x EC (Daniels et al., 2009; Hood and Oertel, 1984), but this relationship will vary based on the complement of ions measured.

TDS levels in streams receiving drainage from Appalachian coal mines have been found to be significantly higher compared to streams not affected by coal mining operations. By looking in detail at both affected and unaffected streams, researchers have concluded that TDS is

a major stressor in the mine influenced streams (Chapman et al., 2000; Pond et al. 2008; Timpano et al. 2010, 2015). Many of these studies investigated populations of benthic macroinvertebrates in streams to determine their overall health. These small aquatic organisms live on the bottom of streams, and are a very important part of the food web in these environments. Altered community structures and lowered biodiversity of these organisms in receiving streams has been confirmed, which is an indicator of declining overall stream health.

TDS elution from coal mine spoils and refuse has been examined by a number of researchers in the laboratory and in the field as discussed below. With the development of column leaching techniques (Orndorff et al., 2010; Parker, 2013), it is relatively straightforward to test these materials in the laboratory and learn about their TDS elution levels and patterns, but these techniques may not fully replicate field conditions. Therefore, their ability to accurately predict field TDS leaching behaviors needs to be evaluated and further confirmed.

Accordingly, this overall objective of this project was to characterize the release of TDS and component ions over time from a selected mine spoil and two coarse coal refuse materials using both laboratory columns and two larger leaching vessels (barrels and mesocosms) in the field. Specifically, we compared data collected from these combined leaching trials to determine how leaching scale (vessel size) affected the prediction of TDS elution from mine spoil and coal refuse.

## LITERATURE REVIEW

### Effect of TDS on Receiving Headwater Streams

In the Appalachians, coal mining leads to increased TDS in nearby waters due to the large areas of land and fresh geologic materials disturbed. Once a set of minable coal seams is permitted for surface mining, all of the earthen materials above it (overburden) must be removed, and eventually replaced. This is the most economical way to reach and mine shallow coal seams. In order to remove the overburden above the coal seam, explosives are used to break it up so that it can be hauled away to a backfill or adjacent valley fill by large machinery. Once the overburden is placed into its new landforms, unweathered materials from deeper in the mine pit cuts often comprise much of the final land surface and deeper volumes of fills. Unfortunately, due to what is known as the "swell factor," not all of the material can be replaced in the same location where it was removed from, which leads to the necessity for valley fills. Once the material is replaced, at least initially, there is less vegetation to intercept rainfall, leading to increased infiltration and runoff (Evans et al., 2014). The chemical composition and physical characteristics of the overburden material, along with rainfall, present optimal conditions for TDS generation (Bernhardt et al., 2012).

An important early study by Pond et al. (2008) showed a correlation between high levels of specific conductance in streams and decreased benthic macroinvertebrate biodiversity, which indicated a decrease in stream biotic integrity and associated mining impacted water quality. Their study found specific conductance levels in water affected by mine spoils reached as high as 2,540 $\mu S\ cm^{-1}$ with an average of 1,023 $\mu S\ cm^{-1}$, as opposed to an average of 62 $\mu S\ cm^{-1}$ in nearby un-mined headwater streams. In addition, they found significantly fewer taxa in mined

streams, along with other shifts in communities and lower overall biodiversity, causing concerns about the overall health of these streams.

More recent research by Pond et al. (2014) indicated negative impacts on receiving streams from mountaintop coal mining can last at least 30 years past reclamation. Researchers saw sustained strong chemical differences and loss of sensitive taxa in previously affected streams. These findings suggest that despite efforts to protect and restore the function of these streams with past regulations, aquatic life was not able to fully recover over the timeframe studied.

Another study by Bernhardt et al. (2012) found similar negative effects on streams receiving runoff from coal mining operations. This study investigated macroinvertebrate populations vs. several stressors related to mining. When looking at intolerant species, stream macroinvertebrates decreased significantly with percent of drainage area mined. These sensitive species decreased even more significantly with an increase in stream conductivity. Results from these collected studies (as summarized by Daniels et al., 2014a), clearly indicate a correlation between elevated TDS levels in receiving streams near coal mining operations and negative impacts on aquatic organisms. Collectively, these findings have created increased awareness of coal surface mining effects on headwater streams and fostered increased regulatory and research monitoring of TDS levels in receiving streams near coal mined lands.

## TDS Regulation

The first nationwide USA legislation created to monitor and regulate the reclamation of surface coal mines was the Surface Mining Control and Reclamation Act (SMCRA) of 1977, which is enforced by the Office of Surface Mining (OSM). While SMCRA based regulations

did not directly attempt to reduce TDS runoff from coal mine operations per se, they did include the use of pre-selected overburden materials as topsoil substitutes when necessary and beneficial, and the isolation of acid-forming material away from contact with surface runoff. Coal mining operations are also under regulation by the Clean Water Act, enforced by the Environmental Protection Agency (EPA), but that permit authority is delegated to OSM with EPA serving in an oversight role. Recently (2010), based on the research reviewed earlier (and other related studies) regarding the negative impacts of TDS release on benthic fauna in receiving streams with EC levels exceeding 300 – 500 µS $cm^{-1}$, the EPA issued new policy guidance using 300 µS $cm^{-1}$ as the maximum level allowed before action must be taken to reduce EC levels in streams, and 500 µS $cm^{-1}$ was considered an acute level (Cormier et al., 2013) and grounds for shutting down mining operations. The U.S. Federal Court then ruled that the EPA did not have the ability to implement this guidance (Walton 2012). It is currently up to individual states, the EPA, and OSM to establish formal regulatory criteria for TDS via the Clean Water Act.

TDS from Coal Mining Operations

During coal mining activities, forests are cleared, topsoil is removed, and rocks overlying coal seams are removed using explosives and large machinery. These rocks, known as overburden, become known as mine spoils once displaced, and often dominate the new land surface when used to reconstruct "approximate original contours" or placed into valley fills (Palmer et al., 2010). These unweathered materials are subject to rapid weathering processes as described below once they are subject to near-surface atmospheric conditions, which leads to increased TDS levels in receiving headwater streams.

The main short- and long-term mechanism for TDS generation in most fresh non-weathered mine spoils is acid-base reactions that occur as traces of sulfides react with rainfall and carbonate grain cements in the rocks (Orndorff et al., 2010). Also, simple dissolution reactions of carbonates, traces of entrained Cl, and direct dissolution of feldspars via hydrolysis and other primary mineral grains contribute to TDS release (Daniels et al., 2014a). The initial peak is a result of rapid pyrite oxidation and flushing of other fresh mineral surface salts produced via hydrolysis. A certain component of this "initial flush" also appears to be very fine colloidal particulate matter (Parker, 2013) from simple blasting and abrasion of the spoils as they are handled and placed in the mining operations. The primary mechanism of pyrite oxidation produces metals and acidity as shown below (Evangelou, 1995).

$$FeS_2 + 7/2O_2 + H_2O \rightarrow Fe^{2+} + 2SO_4^{2-} + 2H^+$$

$$Fe^{2+} + 1/4O_2 + H^+ \rightarrow Fe^{3+} + 1/2H_2O$$

$$Fe^{3+} + 3H_2O \rightarrow Fe(OH)_3 + 3H^+$$

$$FeS_2 + 14Fe^{3+} + 8H_2O \rightarrow 15Fe^{2+} + 2SO_4^{2-} + 16H^+$$

The resulting acidity will then react with the carbonate minerals, feldspars and other potential neutralizers (proton sinks) present in the mine spoils of the Appalachian region. The mechanism of this carbonate mineral dissolution and related neutralization reactions is presented below for calcium-dominated carbonate minerals (Berner and Morse, 1974).

$$CaCO_3 \rightarrow Ca^{2+} + CO3^{2-}$$

$$H^+ + CaCO_3 \rightarrow Ca^{2+} + HCO_3^-$$

$$2H^+ + CaCO_3 \rightarrow Ca^{2+} + H_2CO_3^-$$

$$H_2CO_3 + CaCO_3 \rightarrow Ca^{2+} + 2HCO_3^-$$

This series of weathering reactions generates large amounts of TDS. Specifically, ions such as sulfate, bicarbonate, $Ca^{2+}$, and $Fe^{3+}$ are the end products of these acid-base neutralization reactions that take place in fresh weathering coal mine spoils.

Total Dissolved Solids Column Leaching Studies

Total dissolved solids release from mine spoils has been studied heavily using column techniques in the laboratory. A study by Caruccio et al. (1993) determined this to be the best method for imitating field leaching conditions after comparing acid-base accounting, humidity weathering cells, columns tests and Soxhlet reactors. A wide array of column leaching techniques are available and are reviewed by Parker (2013).

TDS are the inorganic salts and other non-volatile dissolved materials in water. Leachates from coal mining operations often contain elevated levels of ions such as $HCO_3^-$, $SO_4^{2-}$, $Cl^-$, $Ca^{2+}$, $K^+$, $Mg^{2+}$, and $Na^+$ (Agouridis et al., 2012). TDS is extremely laborious to analyze for directly, and is usually estimated by electrical conductivity or specific conductance (EC corrected to 25˚C). This method is acceptable thanks to several studies confirming close correlation between TDS and EC (> 0.95; Daniels et al., 2009; Hood and Oertel, 1984) for given ionic complements in mine leachates.

A column study by Orndorff et al. (2010) found that non acid-forming mine spoils generate high EC levels at first that decrease over time, and often fall to presumed acceptable regulatory levels (e.g. 300 to 500 µS $cm^{-1}$). Additionally, column studies have found several other significant trends with TDS release from coal mine spoils. Orndorff et al. (2010) determined that spoils containing significant levels of sulfides release higher initial levels of

TDS and much more total dissolved elements over extended periods of time, and that partially oxidized and pre-weathered spoil materials from the upper-section of the geologic column were less likely to produce high TDS than deeper non-weathered fully reduced strata. Later, Daniels et al. (2013) also concluded that finer textured shales and mudrocks and high-sulfur sandstones yielded leachate with higher TDS levels than most coarse quartzitic sandstones.

Leachate pH

Many studies investigating TDS are also interested in leachate pH. In the Appalachians, these overburden pH values will depend on the amount of carbonates and reactive pyrite in the rock. The column leaching study by Orndorff et al. (2010) found the leachate pH for unweathered overburden to be between 7.0 and 8.0, while the leachate pH for weathered overburden was between 4.0 and 7.0. This value is similar to those found in a study by Roberts et al. (1988), which found the pH of weathered mine spoils to be 4.5 to 6.0 and the pH of unweathered spoils to be 6.5 to 8.0. Additionally, Agouridis et al. (2012) monitored leachate from weathered and unweathered sandstones using 0.4 ha cells in nearby eastern Kentucky and saw moderately alkaline pH values.

Trace Metals and Elements of Interest

Elements of interest in mine spoil leachates include Al, As, Ca, Cr, Cu, Fe, K, Mg, Mn, Na, Ni, S (as $SO_4^{2-}$), Se, Zn, and C (as $HCO_3^-$) (Orndorff et al., 2010). In terms of total mass, bulk TDS is usually dominated by Ca, $HCO_3^-$, K, Mg, and $SO_4^{2-}$. Daniels et al. (2009) found that As, Cr, Cu, Ni, Zn, and Se were present in the recalcitrant fraction of the overburden, and that very low levels of all except Se were released under due to low solubility under normal environmental conditions (moderate leachate pH). However, despite very low concentrations of

Se in the overburden, Se levels in initial leachates exceeded the MCL for drinking water (0.05 mg $L^{-1}$; Daniels et al., 2009).

Concentrations of $SO_4^{2-}$, Ca, Fe, $HCO_3^-$, and Mn in the same study leachates "were controlled primarily by acid-base reactions, pH solubility controls, and relative saturation (Daniels et al. 2009)." Sulfate release is controlled by the acid-base reactions displayed above along with the initial amounts of sulfide-S in the spoil. Sulfur elution typically peaks during initial leaches and then rapidly drops over time. Mine spoils that were weathered contained lower concentrations of Ca compared to unweathered spoils. Thus the release patterns for Ca were similar to $SO_4^{2-}$ (Daniels et al., 2009).

Iron elution in column leaching studies does not follow the same pattern seen with sulfate, another pyrite oxidation product. Relatively high pH values (e.g. 6.0 to 8.0) can cause much of the Fe to precipitate in the columns as various oxy-hydroxide forms. In the previous study cited above, Mn was present in much higher concentrations due to its increased solubility within this moderate pH range. Bicarbonate release depends heavily on saturation level of the spoil. Bicarbonate release often increases over the course of a column leaching study, because it is a result of carbonate dissolution in the spoil (Daniels et al., 2009).

Long-term Field Scale Studies

In particular, vast differences have been noticed between TDS production with weathered and unweathered material. Agouridis et al. (2012) studied TDS potentials from a range of spoils in large field lysimeters and concluded that EC levels from unweathered mine spoil is usually higher compared to weathered mine spoils. In the same study, EC levels from an unweathered gray sandstone showed initial peak EC levels of over 1500 µS $cm^{-1}$, and fell to below 500 µS $cm^{-1}$ within two years. Another recent study by Evans et al. (2014) which examined over 100

valley fill discharge points in southwest Virginia indicated that it required, on average, 10-15 years beyond mine closure and revegetation for SC to fall below 500 µS $cm^{-1}$. On the other hand, a study by Sena et al. (2014) examined water chemistry coming off field plots and found that EC levels returned to target levels (300 – 500 µS $cm^{-1}$) within 9 growing seasons when mine spoils were placed according to the Forestry Reclamation Approach (Burger et al., 2005). They also found that weathered material was preferred for vegetation growth, but long-term water quality did not differ significantly based on extent of weathering. Lindberg et al. (2011) investigated SC levels from two streams that had been affected by mining nearly 20 years after reclamation. They found SC levels between approximately 1000 µS $cm^{-1}$ and 2000 µS $cm^{-1}$. They also compared SC levels throughout the year and found that among the months of July, September, October, and December, October produced the highest SC levels while July produced the lowest SC levels. Also, Hartman et al. (2005) studied four streams that were affected by valley fills between 5 and 20 years old. They found SC levels to range between 502 µS $cm^{-1}$ and 1479 µS $cm^{-1}$.

TDS from Coal Refuse

Coal refuse is waste rock material mined with coal that is removed during the coal preparation process (Stewart et al., 1997). There are two main types of coal refuse. Fine refuse is mainly very small (< 2 mm) pieces of coal from the coal preparation process, while coarse refuse is primarily rock that was mined along with the coal (Buttermore et al., 1978) along with low grade (high ash) coal fragments. A study by Stewart and Daniels (1992) showed widely varying characteristics among different sources of refuse. In terms of saturated paste EC produced by the refuse itself, significant differences were seen based on age of the refuse piles. In a large column study, Stewart et al. (2001) documented very high EC (> 10,000 µS $cm^{-1}$)

leaching from non-neutralized high sulfur SW Virginia coal refuse materials which was driven by pyrite oxidation processes. Results from refuse column leaching studies differ from similar studies using coal mine spoils. Coal refuse materials produce much higher levels of initial and long-term TDS compared to mine spoils (Daniels et al., 2014b). This difference is due to the finer texture of the refuse materials and much higher content of reactive sulfides compared to mine spoils (Daniels et al., 2009).

## MATERIALS AND METHODS

### Geology and Sample Collection

The mine spoil used during this study was collected at an active surface mining site (Elevation ~900 m) adjacent to the Powell River Project Research and Education Center (http://www.prp.cses.vt.edu) from the Pennsylvanian age Harlan Formation in Wise County, Virginia. This material was selected by our research group for being "typical" of unweathered sandstone spoils that were analyzed as a part of a larger regional (50+) sample set under study for TDS prediction (Daniels et al. 2013). It has also been studied extensively by Parker (2013). Compared to other materials tested, the Harlan spoil exhibited a relatively typical TDS elution curve with a high initial peak, followed by a rapid decrease and subsequent leveling off over time. According to the USGS (1993), the Harlan Formation is primarily composed of sandstone with siltstone, shale, and coal seams. The spoil collected for this study was an unweathered medium grained sandstone material. This assessment (unweathered) was based upon the material's uniform light gray color with no evidence of oxidized reddish brown Fe-oxide staining on fracture faces or in the rock matrix.

Coarse coal refuse materials from two coal processing plants in Tennessee were also chosen for this study. Originally, a total of nine coarse coal refuse samples were collected from Tennessee, Virginia, and West Virginia for use in a larger study (Daniels et al., 2014b). Of these, four samples were chosen by our research group and OSM based on their initial characterization to be studied further using the column leaching technique. Furthermore, two of these materials were selected to use for scaling effects study due to their significantly different total-S and calcium carbonate equivalent (CCE) values (Daniels et al., 2014b). One sample (TNR-1) was taken from the retaining dam construction area (compacted coarse refuse) of the

Gum Branch slurry impoundment in Campbell, Tennessee and was approximately one week old at the time of collection. The second sample (TNR-3) was taken from the Kopper Glo coal processing plant in Claiborne, Tennessee. This sample was taken from the dewatered coarse refuse beltline feed from the preparation plant.

Spoil and Refuse Characterization Methods

Electrical conductivity (EC) and pH of the Harlan spoil and two coarse refuse samples were determined using saturated paste extracts (Rhoades, 1996). The samples were crushed to pass through a 2 mm sieve, mixed with deionized water to form a paste-like consistency, equilibrated for approximately 1.5 hours, then filtered and analyzed. Calcium carbonate equivalent (CCE) was determined using AOAC method 955.01 (AOAC International, 2002). A Leco S632 sulfur analyzer was used to determine total S for each sample. A 0.5 g sample of each sample was acid digested using EPA Method 3051A, Revision 1 (USEPA, 2007a) to determine the concentrations of Al, As, Cd, Ca, Cu, Fe, K, Mg, Mn, Na, Ni, Pb, Se, and Zn. These acid digest were analyzed with Thermo Electron Corporation ICP-MS, X-Series USEPA method SW 846 6020A, revision 1 (USEPA, 2007b). For all standard characterization analyses listed above, blanks, internal standards, or other appropriate QA/QC measures such as use of replicates were employed to ensure accuracy of all standard lab measurements. In general, when the relative values of duplicate samples vary by more than 5% (of absolute value), the samples are re-run by lab staff. Values presented in characterization tables are averages of two duplicate samples.

Overall Leaching Array Design

The Harlan spoil was placed into three different sized leaching vessels to monitor resulting leachates over time. First, the spoil was placed into leaching columns, the smallest sized vessel, in a lab at Virginia Tech and watered with simulated acid rain as specified by Halverson and Gentry (1990), as described later in this section. In parallel, the spoil was placed into two larger sized vessels at the Virginia Tech Turfgrass Research Center (TRC). These vessels, referred to as barrels (medium sized) and mesocosms (largest leaching vessels), were subject to natural weather conditions, and leachates were produced by rainfall or snowfall events. All three sizes of leaching vessels were run in triplicate.

Additionally, the coarse coal refuse materials were placed in two different sized leaching vessels. These materials were placed in columns and barrels. Similar to the Harlan spoil, the columns and barrels were located in a lab at Virginia Tech and at the TRC, respectively. Again, each size x refuse material combination was run in triplicate.

In this study, the difference in leaching vessel size was considered as a scaling effect although the comparisons are limited to three scales and associated vessel sizes and material size consist described here. Also, as described in the following sections, each vessel size was filled with different material sizes. For the Harlan spoil, the column material was crushed and screened to < 1.25 cm, while the material placed in the barrels was screened to < 15 cm, and the mesocosms were composed of < 15 cm material with larger rocks up to 45 cm mixed in. Similarly, for both coarse coal refuse samples, the material placed in the columns was crushed and screened to < 1.25 cm, while the material placed in the barrels was unaltered.

Mesocosm Design – Large Leaching Tanks

The mesocosms were constructed from plastic tanks and placed within a wooden frame (Fig. 1). They had capacities of approximately 1.5 cubic meters each, with a length and width of 135 cm and a depth of 80 cm. Three replications were placed side by side. Once the vessels were in place, they were plumbed to a thick-walled PVC pipe which drained down to three 200 L (55 gal.) drums where the leachates were collected (Fig. 2). The three leachate collecting barrels were placed mostly underground, and downhill from the mesocosms containing the mine spoil, so the leachate drained by gravity to the barrels allowing for sufficient collection volume.

Figure 1. View of three plastic tanks used as mesocosms before final wooden external frame was added. Photo by W. Lee Daniels. Used with permission.

Figure 2. Leachate collecting barrels (right) down-gradient from large tanks (left). Photo by Kathryn Haering. Used with permission.

The opening of the PVC collection pipes was covered by a coarse mesh (filter fabric) material to minimize sediments in the leachate. Next, a ~20 cm layer of washed quartz gravel was placed on the bottom of each mesocosm (Fig. 3). The quartz gravel was rinsed thoroughly in five-gallon buckets before placement. The quartz gravel had an average diameter of 3 to 4 cm. The gravel was added to limit spoil contact with the leachate draining pipes and minimize possible clogging problems.

Figure 3. Quartz gravel being added. Photo by Kathryn Haering. Used with permission.

Approximately 20 cm of washed quartz was also placed in the bottom of each leachate collecting barrel (Fig. 4) to ensure that they stayed in place (e.g. would not be buoyant if the surrounding soil became saturated). A small PVC pipe was anchored in the gravel, so that water collection tubing could reach the bottom of the barrel for leachate collection.

Figure 4. Leachate collecting barrel with PVC pipe anchored in quartz gravel. Photo by Kathryn Haering. Used with permission.

Next, a layer of filter fabric was placed on top of the quartz gravel in the mesocosms before the placement of the spoil. The filter fabric was used to further limit possible clogging of the pipes by any fine spoil particles that could have been washed down with leachates.

Figure 5. Dried Harlan spoil being placed on top of filter fabric layer. Photo by Kathryn Haering. Used with permission.

Following the filter fabric, approximately 50 cm of the Harlan spoil/rocks was placed into the mesocosms on November 5, 2012 (Fig. 5). Prior to placement in the mesocosms, the spoil was air dried and mixed on a large tarp (Fig. 6). While adding the spoil with ~20L (5-gal.) buckets (Fig. 7), care was taken to evenly distribute the material among the three tanks to create uniform environments. As the spoil was added, it was lightly tamped down to prevent voids possibly allowing preferential flow (Fig. 8). Rocks as large as 25 to 45 cm were placed randomly into the mesocosms throughout the filling process (Fig. 9) in an effort to better reflect the coarse rocky nature of field run of mine spoils. Lastly, the mesocosms were covered with bird netting (Fig. 9) and surrounded by a fence to discourage tampering by humans or wildlife (Fig. 10).

Figure 6. Spoil being emptied onto tarp for air drying. Photo by Kathryn Haering. Used with permission.

Figure 7. Spoil being added to tanks with a five gallon (~23 L) bucket. Photo by Kathryn Haering. Used with permission.

Figure 8. Spoil being lightly tamped down to limit voids. Photo by Kathryn Haering. Used with permission.

Figure 9. Mesocosms nearly completed. Photo by Kathryn Haering. Used with permission.

Figure 10. Mesocosms filled with spoil, and bird netting added. Photo by Kathryn Haering. Used with permission.

Figure 11. Completed installation of mesocosms. Photo by Kathryn Haering. Used with permission.

Leaching Barrels - Mine Spoil and Coal Refuse in Barrels

The Harlan mine spoil and two coal refuse materials were placed into the medium sized vessels. Fifty-five gallon drums (~200 L) were used as leaching barrels for the medium sized vessels in the experiment. They had an inside diameter of 55 cm and depth of 85 cm. The same Harlan formation mine spoil used for the mesocosms was placed into these three leaching barrels on November 5, 2012. Additionally, the two coal refuse materials from Tennessee were placed into six more leaching barrels at a later date (April 25, 2013), using the same design. Like the mesocosms, these leaching barrels were placed and monitored at the TRC.

Leaching Barrel Design

First, circular holes were excavated in the site soil to allow about 1/4 of the leaching barrels to be placed below grade and for excess soil to be mounded around their base. This provided both stability and insulation to prevent freezing of leachates. Once in place, the barrels were constructed following the same procedure as the larger tanks.

First, a layer of the same quartz gravel described above for the larger tanks was placed approximately 20 cm deep. This layer of washed quartz gravel on the bottom of the barrels

allowed room for leachate to collect below the spoil or refuse, so that under normal circumstances the spoil or refuse material above did not become saturated. Next, two PVC pipes were anchored in the gravel, extending from the bottom to the top of the barrel. The pipes allowed for leachate collection and for air flow return as leachates were evacuated under suction. Next, a piece of landscape fabric was placed on top of the gravel to limit fine mine spoil or refuse particles from collecting in the bottom of the barrel and clogging the collection pipes.

Finally, after the materials had been dried and mixed on a tarp, approximately 45 cm of material was placed in each barrel (Fig. 12). As with the large tanks, care was taken to evenly distribute the material among the three barrels for each material. The largest rock fragments placed into the leaching barrels, however, were limited to < 15 cm, so the spoils in these leaching units were not as coarse as in the larger tank mesocosms. Lastly, bird netting was placed over the barrels to decrease the chance of contamination. We also installed a "blank" barrel to receive local rainfall that was constructed using the same methods, and included everything except the mine spoil or coal refuse (Fig. 13).

Figure 12. Refuse barrels complete with two PVC pipes and bird netting. Photo by John Parker. Used with permission.

Figure 13. Three Harlan spoil barrels completed (foreground) and blank barrel (background). Photo by Kathryn Haering. Used with permission.

Mesocosm and Leaching Barrel Water Collection and Analysis

The tank mesocosms and leaching barrels were monitored and sampled over time, especially after each rainfall or snowmelt event. The first leachate collection from tanks and barrels containing Harlan spoil occurred on December 27, 2012, while the first leachate was collected from the barrels containing coarse refuse on April 29, 2013. Samples were drawn from all tanks and barrels through October 9, 2014, totaling 67 leaching events for the Harlan spoil and 47 for the coarse refuse. Whenever water was present and weather conditions allowed, all leachate collection vessels were pumped dry as soon as possible (usually within 48 hours). The leachate was pumped into a 20 L carboy, which was rinsed with deionized water after each sample was collected. Total volume was noted for each collection, and a 500 mL subsample was split for further lab analyses. Precautions were taken to ensure that subsamples taken were representative of the full sample. It less than 20 L was collected, the carboy was inverted several times to ensure mixing of the sample before taking a subsample. If more than 20 L of leachate was collected, the subsample was created using equal proportions of each 20 L carboy.

Upon return to the lab, untreated samples were measured immediately for EC and pH. These measurements were performed in glass test tubes using standard EC and pH meters, for each sample collected throughout the study period. The EC values were recorded after allowing samples to equilibrate to approximately room temperature in the laboratory. Next, three subsamples of each individual leachate sample were separated for further analysis. For sample one, 15 mL was decanted into a test tube, and three drops of 8 N nitric acid added to preserve for metal analysis. A Thermo Electron Corporation ICP-MS, X-series USEPA method SW 846 6020A, revision 1 (USEPA 2007b), located in Durham Hall at Virginia Tech, was subsequently used to analyze for total Al, As, Ca, Cd, Cl, Cu, Fe, K, Mg, Mn, Na, Ni, Pb, Se, and Zn. Secondly, a 60 mL sample was decanted into 60 mL amber vials (with no head space) and analyzed by a Shimadzu Carbon Analyzer located in Latham Hall at VT for inorganic C within three days of collection. Values given as total inorganic C were converted to bicarbonate by multiplying by 5.0, due to the fact that one-fifth of the molecular weight of bicarbonate is inorganic carbon. Lastly, a third sample was decanted into 25 mL bottles for total S analysis by a Spectro ARCOS ICPES Model FHS16 with CETAC Autosampler Type: ASX-520 using USEPA method SW 846 6010B, revision 2 (USEPA, 2001) in the Virginia Tech Extension Soil Testing Lab. Total sulfur values were converted to sulfate by multiplying by 3.0, based on the molar mass ratio of S to $SO_4$. Individual leachate EC and pH measurements were recorded for each sample during the study period, metal and sulfur analyses were performed for each sample from the first leaching event through January 16, 2014, while bicarbonate analysis was performed for each sample from the first leaching event through March 10, 2014.

Mine Spoil and Coal Refuse in Leaching Columns

The Harlan mine spoil and two coal refuse samples were also run in unsaturated leaching columns (replicated three times) in the laboratory (Fig. 14). These columns represented the smallest scale leaching environment. The basic column leaching procedures are described below and follow those of Orndorff et al. (2010) and more recently, Parker (2013).

Figure 14. Image of a column set-up in the laboratory. Photo by W. Lee Daniels. Used with permission.

The first step in setting up the columns was spoil preparation. The spoil was air dried and crushed to pass through a 1.25 cm diameter sieve and then back-blended in order to maintain the entire mass of spoils. The cone and quarter method was used to divide the spoil into 1200 $cm^3$ samples and to uniformly redistribute the coarse and fine materials.

Next, the columns were constructed and packed with spoil material. Columns were constructed out of PVC pipe with an inner diameter of 7.4 cm, length of 40 cm, and a concave PVC end cap with attached plastic nipple and tygon tubing. Further information on this column design can be found in Orndorff et al. (2010). The mass of spoil added to each column was recorded in addition to the volume. A perforated circular plastic disk was placed in the bottom

of the columns to support the filter paper, mesh, and spoil. Nylon mesh with a nominal 0.1 mm opening size and Whatman #1 filter paper (11µm pore size) was placed on top of the plastic disk to limit both fine and coarse particulates from leaching out of the columns or blocking the drainage tube. A 2.5 cm layer of acid-washed sand was placed on top of the filter paper, which helped promote uniform leachate drainage and acted as a leachate reservoir to insure the bottom of the spoil samples remained unsaturated (as confirmed by Parker, 2013). Then, a 1200 $cm^3$ sample of spoil was added to each column in small lifts to avoid coarse and fine particle stratification. Finally, 2.5 cm of coarse acid-washed sand was placed on top of the spoil to promote uniform infiltration of the leaching solution.

Lastly, the columns were leached with 2.54 cm of simulated acid rain (pH 4.6), as specified by Halverson and Gentry (1990), that was gently added to each column for each leaching event (twice per week). After the water had leached through the column (typically, $\leq$ 24 hours), a clamp was placed on the tubing to prevent oxygen movement into the bottom of the column, and samples were collected and analyzed using the same methods described above for the mesocosms and leaching barrels. Additionally, weights were taken for all collected leachate samples to allow for mass leaching calculations.

Statistical Analysis

Leachate data (e.g. pH, EC, Se) for the three sandstone spoil leaching techniques (columns, barrels, and tanks) were first compared qualitatively (graphically) to describe variance over time among treatments. This was accomplished by simple plots of each leachate component concentration vs. time (or water volume) using SigmaPlot,$^{tm}$ Version 11, with one standard error of the mean (SE) plotted above and below each mean leachate value. Where

comparative treatment lines for a given graph were separated by > 2 SE, we considered them to differ statistically at p = ~ 0.05.

The rate/volume of water additions to the field barrels and tanks vs. the lab columns was obviously different and these data were first normalized by water volume (e.g. net cm of leachates) for statistical comparisons with the same assumptions regarding $\geq$2 SE indicating significant differences. Simple time series plots (date vs. component concentration) were used to compare the tanks vs. the barrels for both the Harlan spoil and coarse refuse.

## RESULTS AND DISCUSSION

### EFFECT OF LEACHING TEST SCALE ON TDS RELEASE FROM COAL MINE SPOIL

#### Spoil Characterization

Selected chemical and physical properties of the Harlan spoil are presented in Table 1. Particle size analysis indicated that the bulk crushed spoil consisted of approximately 41% rock fragments (> 2 mm) and 59% fines (< 2 mm). The saturated paste pH was slightly alkaline (pH 7.68). According to Orndorff et al. (2010) this is "typical of fresh, relatively unweathered materials of this region due to hydrolysis reaction involving broken primary mineral grains and carbonate dissolution." The saturated paste EC of the original spoil was 882 µS $cm^{-1}$. The total S content of the spoil (0.04%) was very low. Also, the spoil had a relatively high apparent neutralization capacity (4.84% CCE). This aligns with the alkaline leachate pH observed over time and the initial saturated paste pH. The total elemental analysis of the bulk spoil is presented in Table 2 for alkali cations and Table 3 for metals. Levels of Al, Ca, Fe, K, Mg, and Na are characteristic of similar overburden material from the central Appalachian region (Schatzel and Stewart, 2012). The trace metal content of the spoil ranged from below detection to 46.0 mg $kg^{-1}$ for Zn. The Cd and Se levels in the spoil were below detection , so the detection limit was used to report the potential maximum amount that could be in the spoil samples.

Table 1. Selected chemical and physical properties of the Harlan spoil used in the columns, barrels, and mesocoms. EC = Elecrical Conductivity; CCE = Calcium Carbonate Equivalent.

| Material | Saturated Paste | | CCE | Total S | Particle Size Analysis | | | | | |
|---|---|---|---|---|---|---|---|---|---|---|
| | pH | EC µS $cm^{-1}$ | % | % | % Coarse >2 mm | % Fines <2 mm | % Sand | % Silt | % Clay | Textural Class |
| **Harlan Spoil** | 7.68 | 882 | 4.84 | 0.04 | 41 | 59 | 75 | 16 | 9 | Sandy Loam |

Table 2. Total mass (mg $kg^{-1}$) of Ca, K, Mg, and Na per kg of mine spoil used in the columns, barrels, and mesocosms.

| Material | Ca mg $kg^{-1}$ | K mg $kg^{-1}$ | Mg mg $kg^{-1}$ | Na mg $kg^{-1}$ |
|---|---|---|---|---|
| **Harlan Spoil** | 20,100 | 6,700 | 3,700 | 850 |

Table 3. Total mass (mg $kg^{-1}$) of As, Cd, Cu, Mn, Na, Ni, Pb, Se, Zn per kg of mine spoil used in the columns, barrels, and mesocosms. Cadmium and Se levels were below the detection limit, so Cd and Se content are expressed at their respective detection limits.

| Sample ID | Al mg $kg^{-1}$ | As mg $kg^{-1}$ | Cd mg $kg^{-1}$ | Cu mg $kg^{-1}$ | Fe mg $kg^{-1}$ | Mn mg $kg^{-1}$ | Ni mg $kg^{-1}$ | Pb mg $kg^{-1}$ | Se mg $kg^{-1}$ | Zn mg $kg^{-1}$ |
|---|---|---|---|---|---|---|---|---|---|---|
| **Harlan Spoil** | 25,300 | 4.2 | < 0.13 | 12.9 | 20,200 | 496 | 16.9 | 8.54 | < 0.25 | 46.0 |

Effect of Various Sizes (Scales) of Leaching Container

*Leachate Electrical Conductance (EC)*

The overall trends in leachate EC were similar among all three scales (Fig. 15), but there were a few key differences among the columns, barrels and mesocosms. First, the initial peak EC value for the mesocosms (~2250 µS $cm^{-1}$) was approximately 500 µS $cm^{-1}$ higher than the barrels and columns. According to Orndorff et al. (2010), this initial peak is a result of rapid pyrite oxidation and flushing of other fresh mineral surface salts produced via hydrolysis. The higher peak in the mesocosms was likely due to the accumulation of sulfate weathering salts during the nearly two month period between the initial filling the mesocosms and collection of the first leachates. During this time there were several smaller rainfall events that were able to interact with and wet spoil, but were not significant enough to yield collectable leachate. The rainfall event that eventually yielded the first leachates was very heavy, allowing the accumulated weathering salts to be flushed through at more concentrated levels than observed in the columns or barrels. It is also interesting to note that the initial EC values produced by the

barrels were intermediate between the columns and mesocosms, again reflecting an effect of leaching scale.

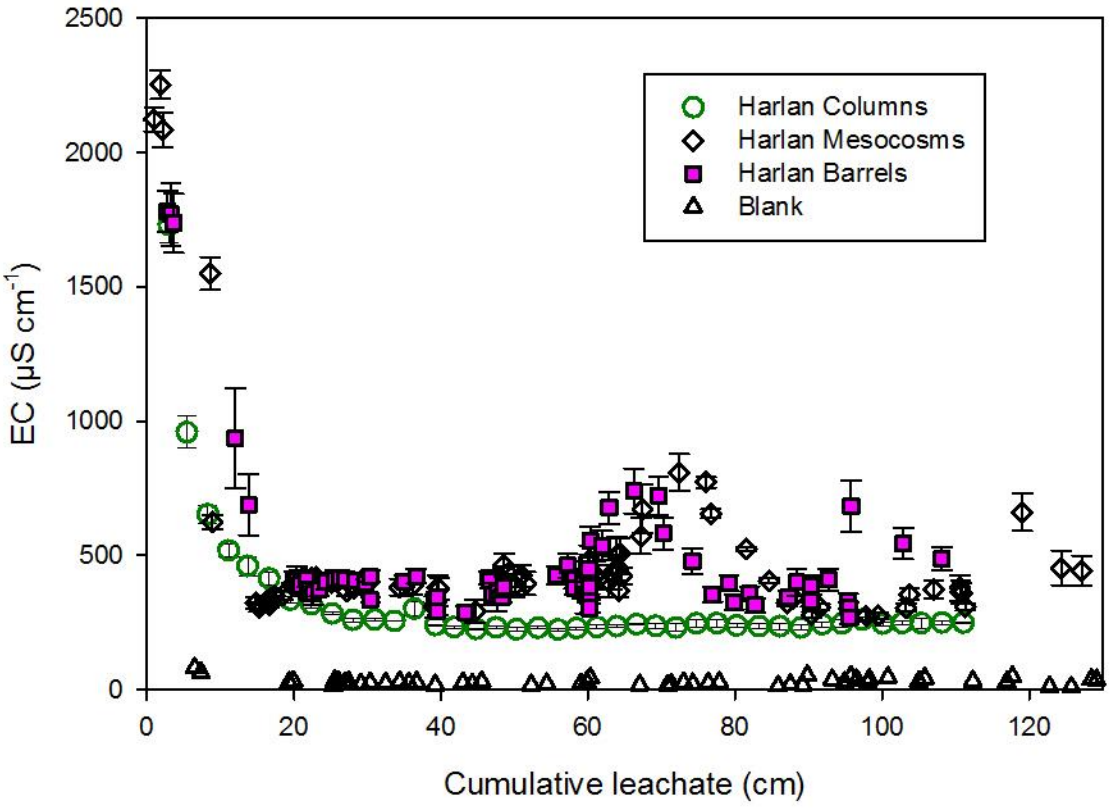


Figure 15. Leachate EC versus cumulative volume eluted for columns, mesocosms, and barrels. Values plotted are means (n=3 except for blank n=1) per sample event with one standard error above and below. Leach number 1 for Harlan the columns is obscured by first data point for Harlan barrels.

After their initial peaks, all three leaching scales exhibited the expected rapid decline in EC, which lasted until about 20 cm of cumulative leachate. From about 20 cm to 50 cm of cumulative leachate, the three scales leveled off to a very gently sloping decline, but the barrel and mesocosm leachate EC values were significantly higher than the columns. During this

period of gradual EC decline, the columns fell from approximately 330 µS $cm^{-1}$ to 225 µS $cm^{-1}$, whereas the mesocosms and barrels fluctuated between 320 µS $cm^{-1}$ and 400 µS $cm^{-1}$.

After this interval of slow decline (20 to ~50 cm), both the mesocosms and the barrels exhibited a second peak, while the column leachate EC stayed relatively consistent. The secondary peaks for the mesocosms and barrels were not significantly different in absolute value, and reached between 730 µS $cm^{-1}$ and 810 µS $cm^{-1}$. The barrels peaked at approximately 66 cm of cumulative leachate, while the mesocosms peaked at approximately 72 cm of cumulative leachate. These peaks corresponded to rainfall events that followed a dry period in the late summer and fall of 2013, which likely allowed more weathering salts to accumulate and become concentrated as discussed above.

Following these secondary peaks, the barrels and mesocosms declined again to < 500 µS $cm^{-1}$, but then showed another peak near the conclusion of the study period, while the columns continued to stay relatively constant. These subsequent peak EC values were slightly lower than the secondary peak, reaching approximately 680 µS $cm^{-1}$ for the barrels and 660 µS $cm^{-1}$ for the mesocosms. The interval in which this third peak occurred differed greatly for the barrels and mesocosms. The peak for the barrels occurred at approximately 96 cm of cumulative leachate vs. approximately 119 cm of cumulative leachate for the mesocosms. However, both of these later peaks corresponded to a very dry period with little rainfall during the early fall of 2014. Both the barrels and mesocosms declined to below 500 µS $cm^{-1}$ by the end of the study.

Leachate EC during the first few leaching events (1750 – 2250 µS $cm^{-1}$) was much higher than the saturated paste EC (882µS $cm^{-}1$) for all treatments. Also, the long-term EC from all treatments remained below (often significantly) the saturated paste EC.

*Leachate pH*

Leachate from all three scales exhibited similar pH values (Fig. 16) and patterns over time. With the exception of a few short leaching intervals, pH values for the three scales were not significantly different. Leachate pH increased over the first few leaching events, and stabilized at 7.5 – 8.0 after approximately 10 cm of cumulative leaching.

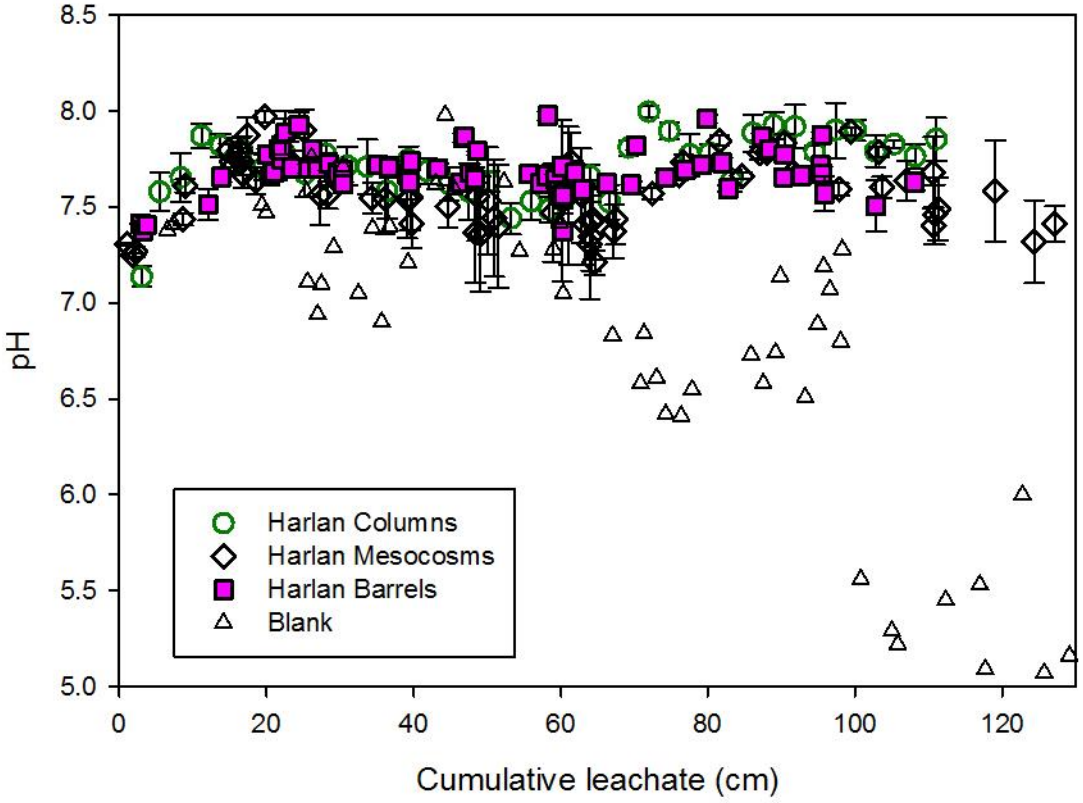


Figure 16. Leachate pH versus cumulative volume eluted for columns, mesocosms, and barrels. Values plotted are means (n=3 except for blank n=1) per sample event with one standard error above and below.

This pattern was expected due to (a) the initial weakly buffered acidic nature of the column leaching solution and local rainfall coupled with (b) neutralization reactions that quickly

established, equilibrating the pH into the 7.5 to 8.0 range. A column leaching study by Orndorff et al. (2010) also saw pH values between 7.0 and 8.0 for unweathered mine spoils. The reason for the much lower pH of the blank barrel, particularly in the latter half of the study, has not been established, but obviously reflects inputs of some acidic component in either local rainfall or perhaps other dusts or aerosols from activities at the TRC.

*Leachate Sulfate*

The pattern of sulfate release (Fig. 17) from the Harlan spoil very closely mirrored that of the EC release. As with EC, the main differences among the three scales were the initial peak values, the secondary peaks found only in the barrels and mesocosms, and that the barrels and mesocosms maintained slight but significantly higher values over the course of the study period. Initially, the peak sulfate value for the mesocosms (~1000 mg $L^{-1}$) was significantly higher (by approximately 350 mg $L^{-1}$) than both the barrels and the columns. This initial sulfate peak was likely caused by rapid pyrite oxidation (Orndorff et al., 2010). This was followed by a rapid decline by 15 cm of cumulative leachate and then relatively low levels were maintained until ~50 to 60 cm of cumulative leaching.

Both the barrels and mesocosms exhibited a secondary peak of 418 mg $L^{-1}$ and 465 mg $L^{-1}$, respectively. The barrel peak occurred slightly before the mesocosms, at approximately 66 cm of cumulative leachate, while the mesocosm peak occurred at 73 cm of cumulative leachate. Similar to the initial peak seen in all three scales, these two secondary peaks were most likely produced by trace sulfide weathering, aided by the warm and humid alternating wet/dry conditions in the late summer and early fall that only the barrels and mesocosms were exposed to. Lastly, following their second peak, the barrels and mesocosms appeared to level off at significantly higher sulfate levels (by approximately 75 mg $L^{-1}$) than the columns

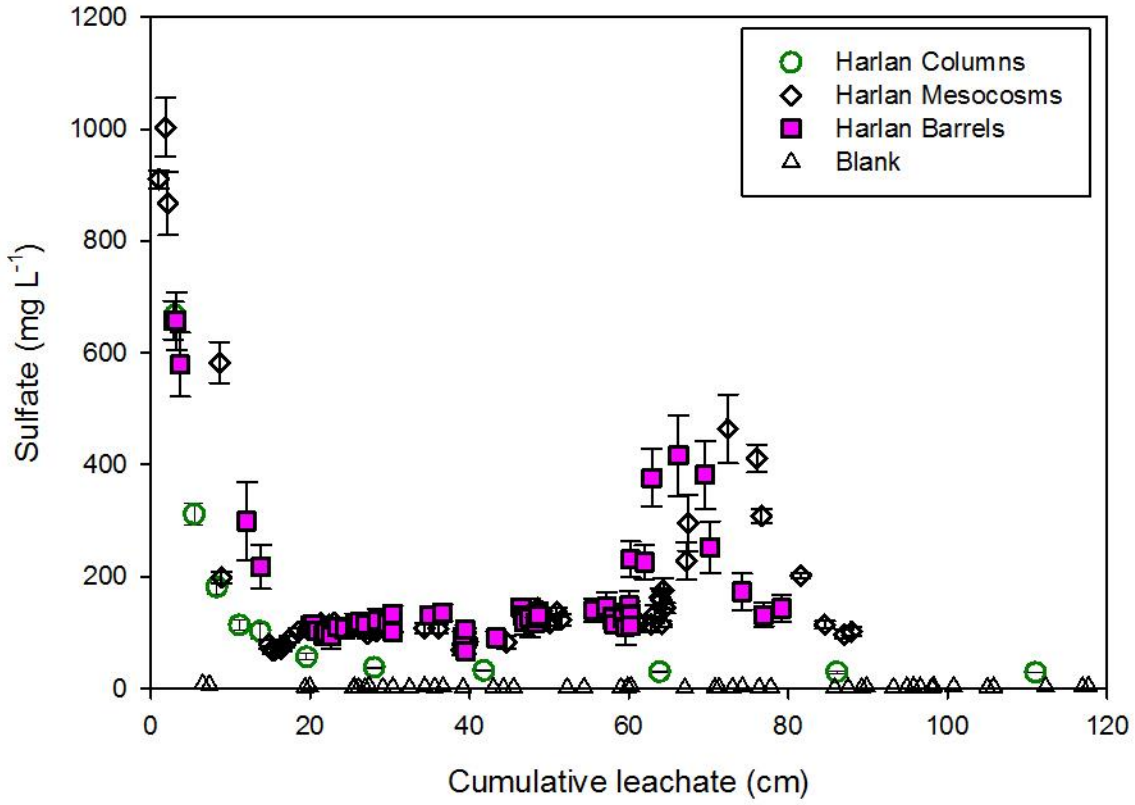


Figure 17. Leachate sulfate versus cumulative volume eluted for columns, mesocosms, and barrels. Values plotted are means (n=3 except for blank n=1) per sample event with one standard error above and below. Leach number 1 for the Harlan columns is obscured by first data point for Harlan barrels.

*Leachate Bicarbonate*

For bicarbonate release (Fig. 18), the three scales showed an overall similar pattern for the Harlan spoil. The key differences were starting value, peak timing, and variance. First, the barrels and mesocosms started out at around 45 mg $L^{-1}$ compared to 85 mg $L^{-1}$ for the columns. This could be due to the spoil preparation methods requiring that the spoil be crushed, and therefore much more reactive, before placement in the columns, while the spoil was not altered before placement into the mesocosms and barrels. Secondly, the columns quickly reached their

peak bicarbonate values after about 10 cm of cumulative leachate, while the barrels and mesocosms leveled off at this point (10 cm), but then slowly continued to increase and reached their peak values at around 60 cm. The peak values were not significantly different between the columns, barrels, and mesocosms, and were approximately 115 mg $L^{-1}$, 110 mg $L^{-1}$, and 138 mg $L^{-1}$, respectively.

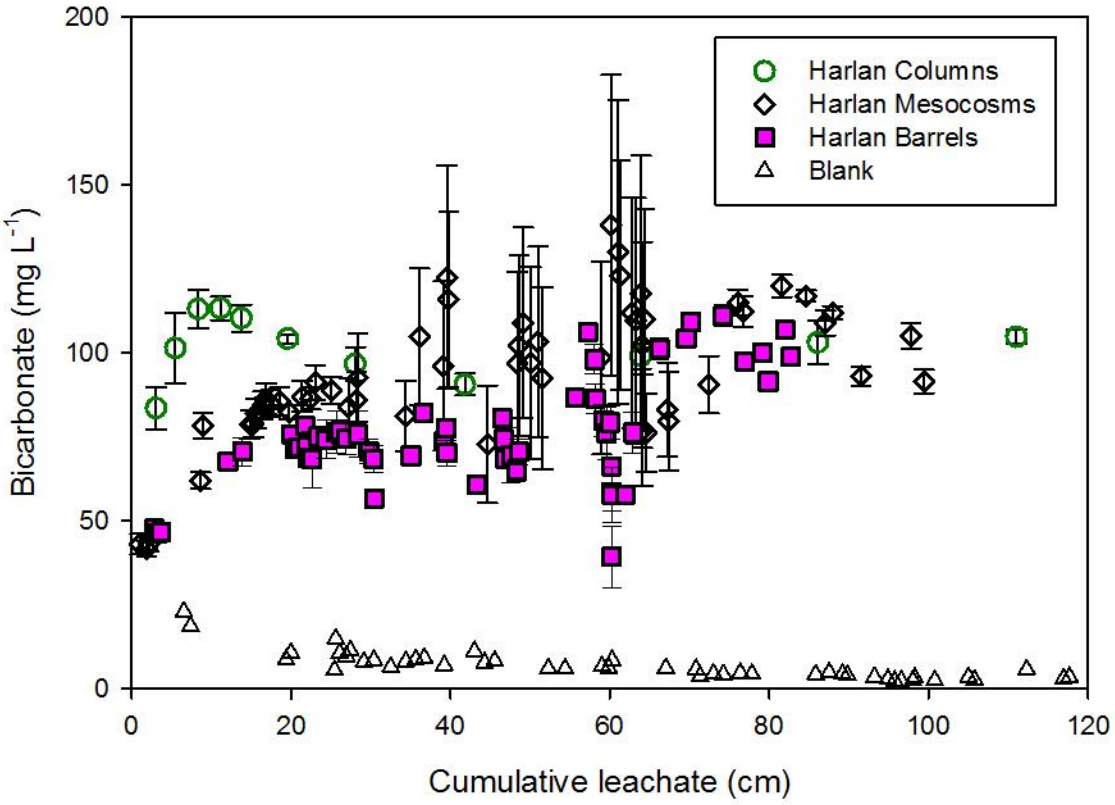


Figure 18. Leachate bicarbonate versus cumulative volume eluted for columns, mesocosms, and barrels. Values plotted are means (n=3 except for blank n=1) per sample event with one standard error above and below.

Lastly, between about 40 cm and 70 cm of cumulative leaching, the bicarbonate values of the barrels and the mesocosms had large standard errors, indicating large variation among

replicates. This variation occurred when the barrels and mesocosms were subject to a dry period during the late summer and early fall of 2013, and was likely exaggerated by the natural variation of packing and associated aeration, hydration, and gas exchange in the larger scale vessels. After about 70 cm of leachate, all three scales leveled off and continued to fluctuate around 100 mg $L^{-1}$.

*Leachate Arsenic (As)*

The overall pattern of As release was very similar for the three scales of Harlan spoil (Fig. 19). The barrels and mesocosms peaked at approximately 2.5-3 µg $L^{-1}$. Although the columns peaked at approximately 16 µg $L^{-1}$, this value appeared to be skewed by a single replicate value (actual values were 36.4 µg $L^{-1}$, 10.1 µg $L^{-1}$, and 2.4 µg $L^{-1}$ for the three replicates).

All three scales decreased to the detection limit of 0.3 µg $L^{-1}$ within 20 cm of cumulative leachate and only a very small second peak was seen in the barrels and mesocosms just after 60 µg $L^{-1}$ of cumulative leachate, which never exceeded 1.0 µg $L^{-1}$.

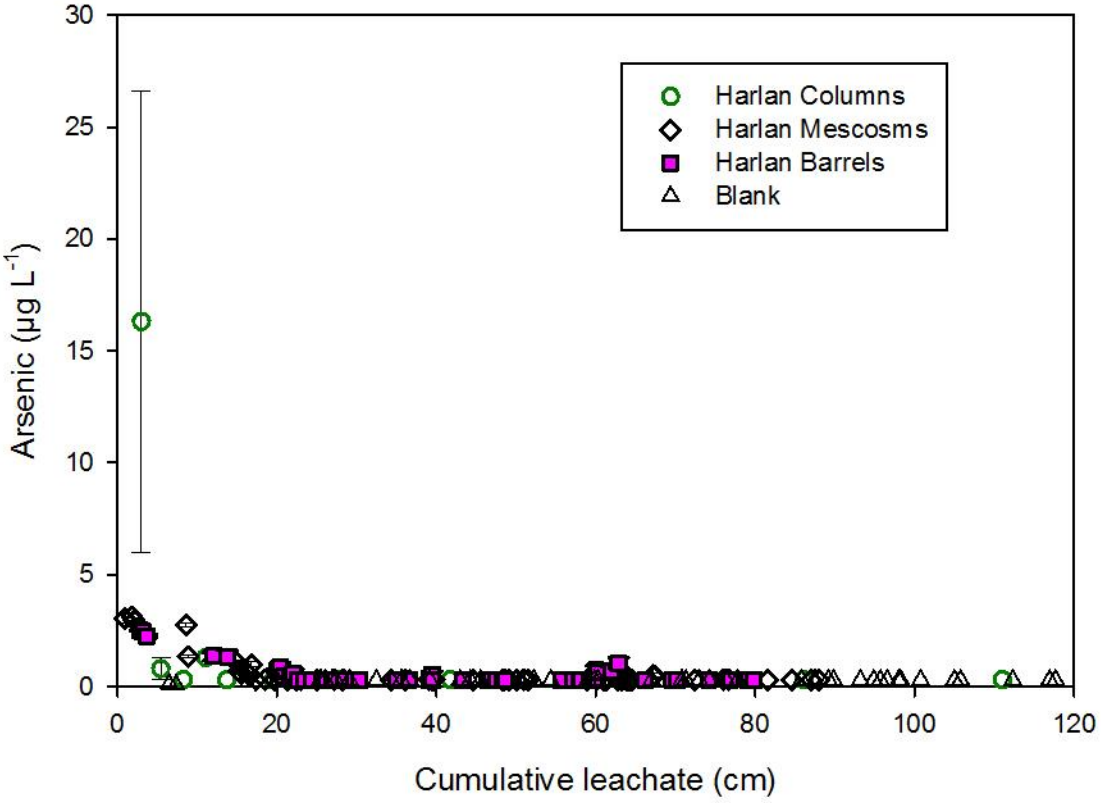


Figure 19. Leachate As versus cumulative volume eluted for columns, mesocosms, and barrels. Values plotted are means (n=3 except for blank n=1) per sample event with one standard error above and below. Detection limit = 0.3 µg $L^{-1}$.

*Leachate Selenium (Se)*

The pattern of Se release (Fig. 20) was similar to As, but the initial peak was much more pronounced. However, the mesocosms had a much higher initial peak value of approximately 90 µg $L^{-1}$, while the columns and barrels had a peak of 54 µg $L^{-1}$ and 60 µg $L^{-1}$, respectively. These peaks were followed by a rapid decline during the first 20 cm of cumulative leachate followed by a leveling off around the detection limit of 0.8 µg $L^{-1}$ for the majority of the rest of the study period. However, there was a small, but noticeable, peak in the barrels and mesocosms at around 70 cm of cumulative leachate that reached no higher than 4 µg $L^{-1}$.

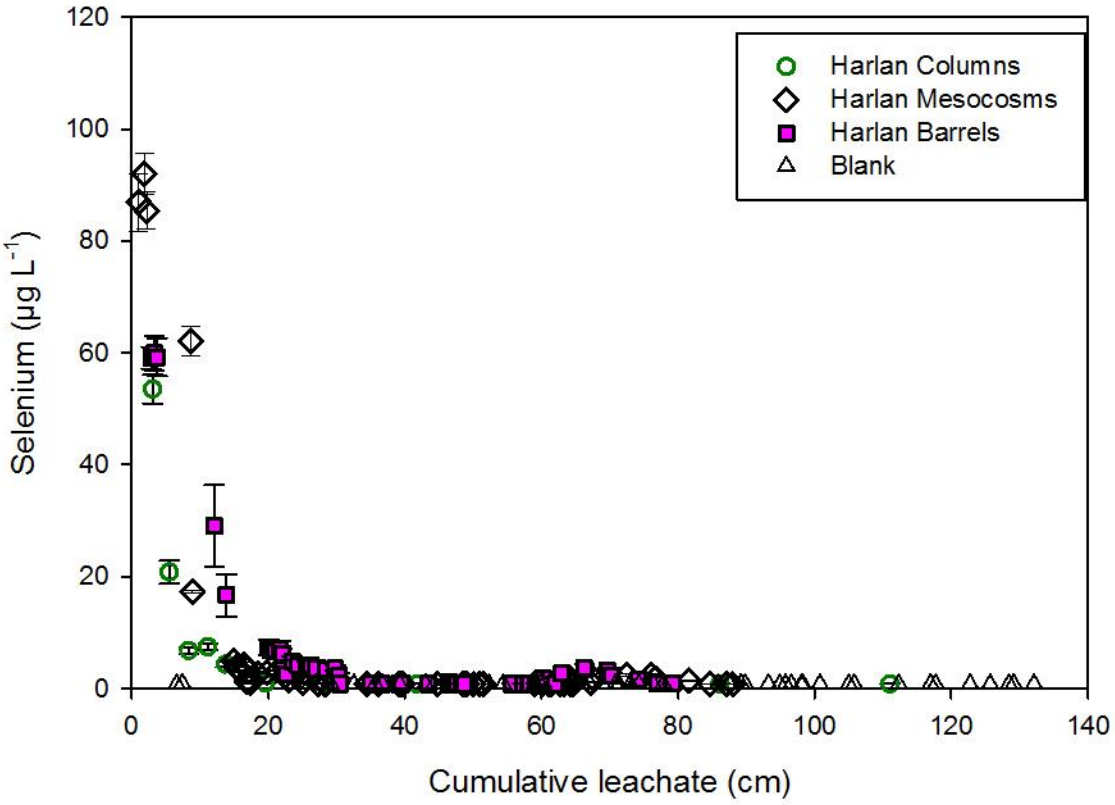


Figure 20. Leachate Se versus cumulative volume eluted for columns, mesocosms, and barrels. Values plotted are means (n=3 except for blank n=1) per sample event with one standard error above and below. Detection limit = 0.8 µg $L^{-1}$.

*Leachate Calcium (Ca)*

Calcium release (Fig. 21) mirrored the patterns observed for EC and sulfate. The peak Ca value was approximately 100 mg $L^{-1}$ higher in the mesocosms compared to the barrels and columns. Between their initial peak and then 20 cm of cumulative leachate, the barrels and mesocosms exhibited a significantly slower, but still very rapid, decrease to approximately 60 mg $L^{-1}$. From this point on, the three scales had very similar levels of Ca release with the exception of the characteristic secondary summer seasonal spike seen in the barrels and mesocosms. In this case, the spike reached approximately 125 mg $L^{-1}$ in the barrels and 135

mg $L^{-1}$ in the mesocosms. Again, the location of the peak was slightly separated, and occurred approximately 4 cm of cumulative leaching apart.

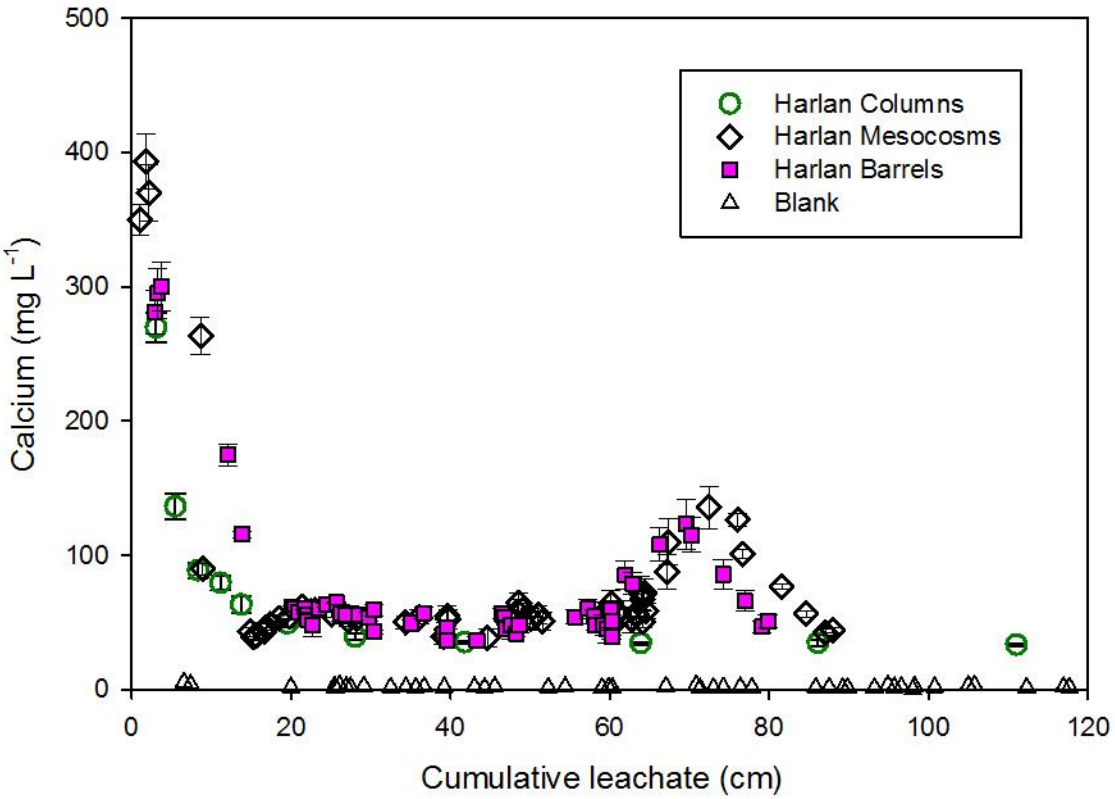


Figure 21. Leachate Ca versus cumulative volume eluted for columns, mesocosms, and barrels. Values plotted are means (n=3 except for blank n=1) per sample event with one standard error above and below. Detection limit = 0.01 mg $L^{-1}$.

*Leachate Magnesium (Mg)*

As with sulfate and Ca, Mg release mirrored EC release for the Harlan spoil (Fig. 22). The initial peak values for all three scales were significantly different. As expected, the mesocosms peaked the highest at approximately 55 mg $L^{-1}$, while the barrels and columns peaked at approximately 36 mg $L^{-1}$ and 30 mg $L^{-1}$, respectively. For the majority of the study period, the Mg levels in the barrel and mesocosm leachates remained slightly, but significantly,

higher than the columns. After their initial drop, all three leaching scales leveled off with the exception of the second peak in the barrels and mesocosms which reached approximately 22 mg $L^{-1}$ to 24 mg $L^{-1}$, respectively. This peak was separated by approximately 6 cm of cumulative leaching, with the barrel peak occurring first.

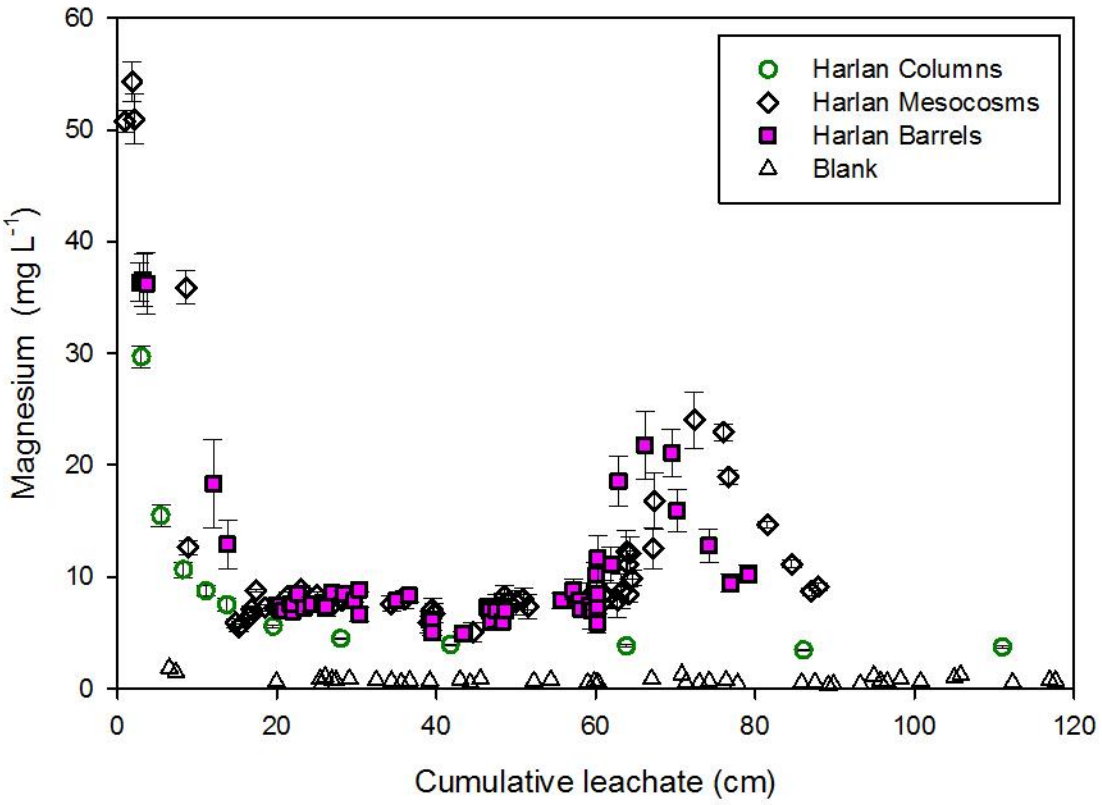


Figure 22. Leachate Mg versus cumulative volume eluted for columns, mesocosms, and barrels. Values plotted are means (n=3 except for blank n=1) per sample event with one standard error above and below. Detection limit = 0.005 mg $L^{-1}$.

*Leachate Potassium (K)*

All three scales exhibited very similar release patterns for K with the Harlan spoil (Fig. 23). They peaked at the beginning, decreased rapidly, and leveled off to a slow decline. The columns had a significantly higher initial peak at approximately 46 mg $L^{-1}$, while the barrels and

mesocosms peaked at approximately 23 mg $L^{-1}$ and 20.5 mg $L^{-1}$, respectively. This was presumably due to spoil preparation techniques and the finer textured grind of the column material. By 15 cm of cumulative leachate, all three scales leveled off at approximately 10 µg $L^{-1}$ and slowly declined through the rest of the study period. While K release for the columns was significantly higher early on, after 20 cm of leachate the barrels and mesocosms remained higher than the columns for the majority of the remainder of the study.

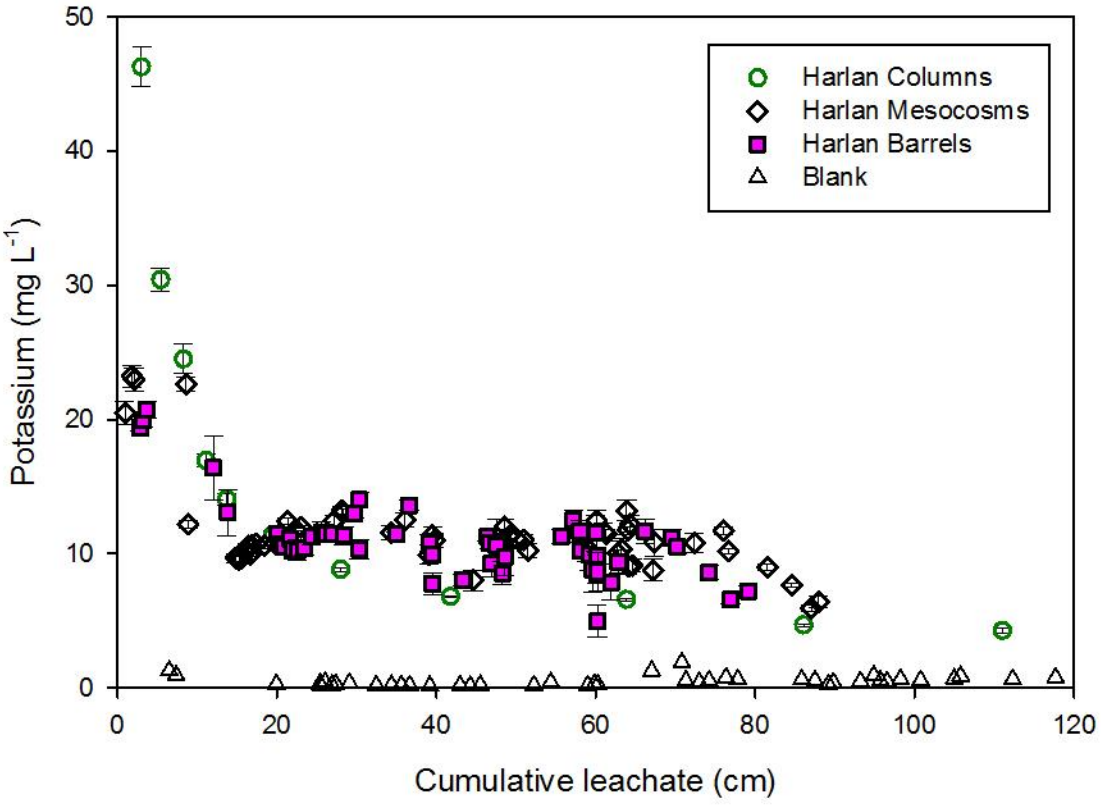


Figure 23. Leachate K versus cumulative volume eluted for columns, mesocosms, and barrels. Values plotted are means (n=3 except for blank n=1) per sample event with one standard error above and below. Detection limit = 0.005 mg $L^{-1}$.

*Leachate Sodium (Na)*

Sodium release for the Harlan spoil (Fig. 24) followed similar patterns for all three scales. However, the columns had a significantly higher initial peak at approximately 7 mg $L^{-1}$ compared to the barrels and mesocosms which peaked at 4.9 mg $L^{-1}$ and 5.3 mg $L^{-1}$, respectively. The higher peak in the columns was likely caused by the material preparation process and finer textured, ground material in the columns. Immediately after this initial peak, the three scales did not differ significantly in overall Na release. By 20 cm of cumulative leachate, all three scales had rapidly decreased to between approximately 0.70 mg $L^{-1}$ and 0.95 mg $L^{-1}$ and continued to slowly drop afterwards.

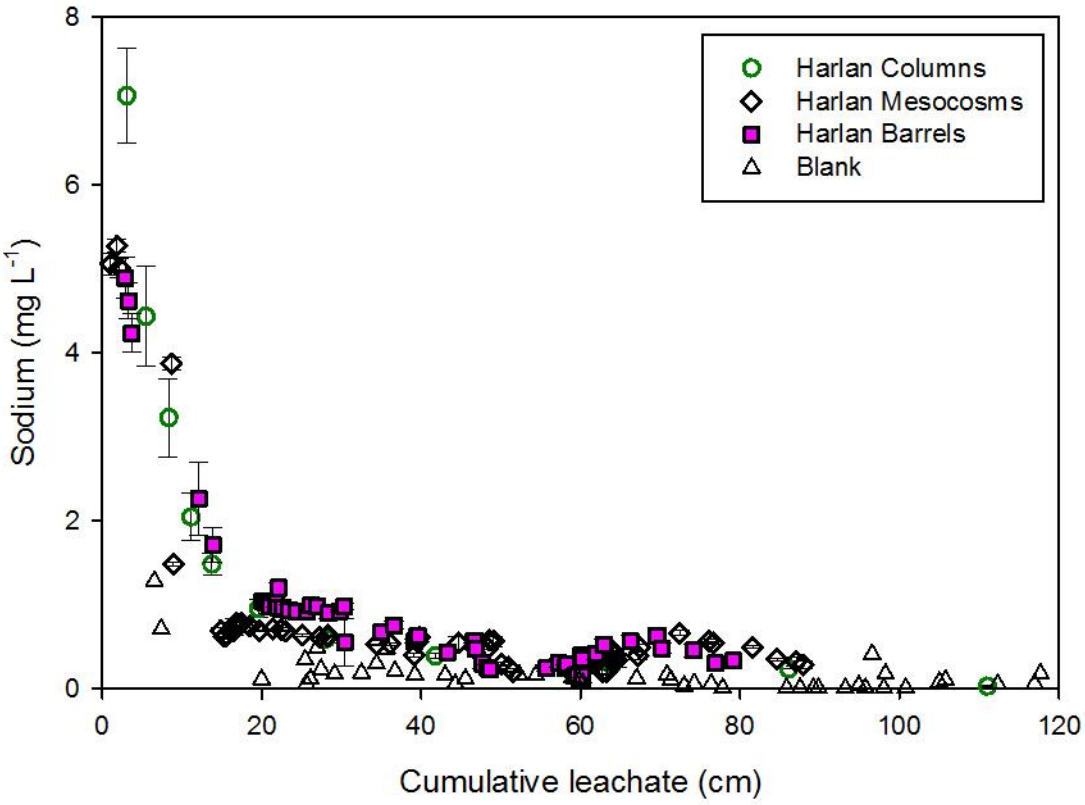


Figure 24. Leachate Na versus cumulative volume eluted for columns, mesocosms, and barrels. Values plotted are means (n=3 except for blank n=1) per sample event with one standard error above and below. Detection limit = 0.005 mg $L^{-1}$.

*Leachate Iron (Fe)*

The patterns of Fe release (Fig. 25) for the three scales of Harlan spoil were quite different from one another and fundamentally different from the bulk EC components discussed above. Iron in the Harlan spoil leachates likely came from the oxidation of pyrite, or the dissolution and oxidation of siderite. The columns began with their peak elution and then decreased rapidly, while the barrels and mesocosms initially began low and reached their peak between approximately 30 cm and 40 cm of cumulative leachate.

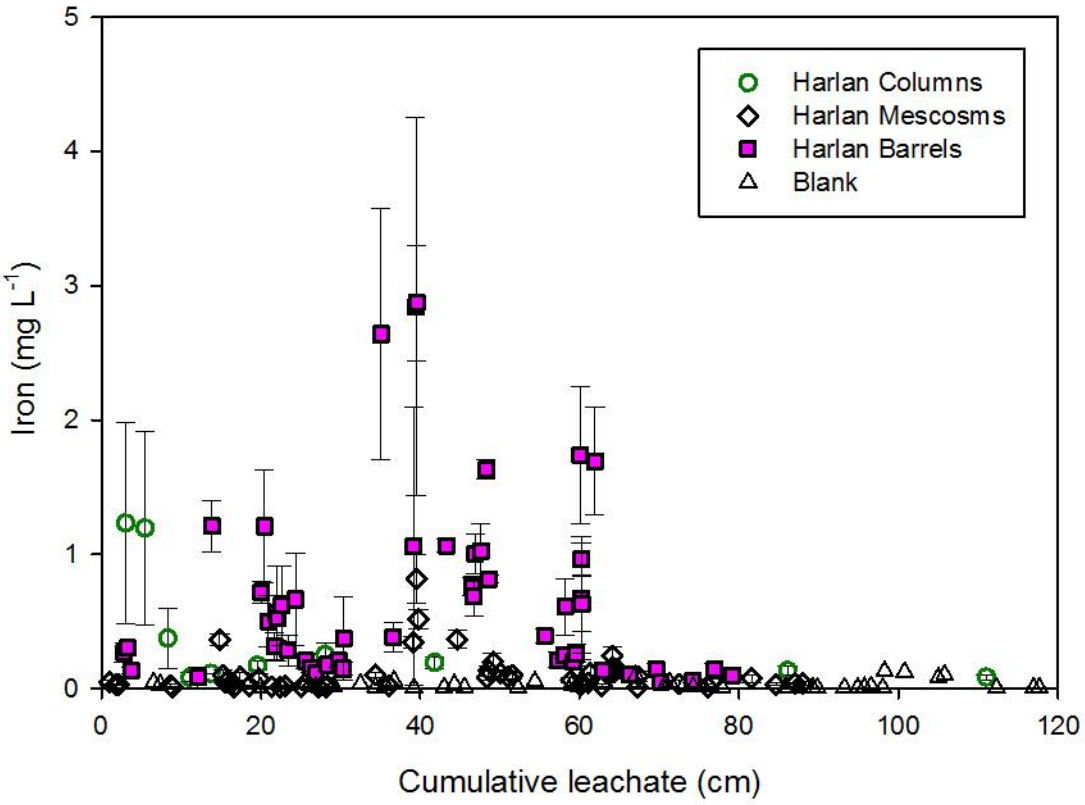


Figure 25. Leachate Fe versus cumulative volume eluted for columns, mesocosms, and barrels. Values plotted are means (n=3 except for blank n=1) per sample event with one standard error above and below. Detection limit = 5.0 µg $L^{-1}$.

In the barrels and mesocosms, Fe released initially by pyrite oxidation and/or siderite weathering likely precipitated as oxy-hydroxides which would have been very insoluble for some time before being released, causing the later peak compared to the columns. According to Moricz et al. (2012), Fe hydrolyzes and precipitates above pH 4.0. The regular leaching of the columns likely kept the spoil closer to saturation, limiting oxygen diffusion, and thus preventing iron from precipitating. The peaks for the columns, barrels, and mesocosms were approximately 1.2 mg $L^{-1}$, 2.9 mg $L^{-1}$, and 0.82 mg $L^{-1}$, respectively. While these numbers were quite different numerically, they were not significantly different. However, for much of the interval between 10

and 60 cm of cumulative leachate, the barrels released significantly more total Fe than the columns and mesocosms. After 60 cm of cumulative leachate there was no significant difference among the three leaching scales and the overall Fe release rates were all relatively low.

*Leachate Manganese (Mn)*

In terms of Mn release, all three scales produced an early peak (Fig. 26), similar to most EC leachate components analyzed in this study, but at relatively low levels. The columns (~440 µg $L^{-1}$) and mesocosms (~385 µg $L^{-1}$) peaked highest, declined rapidly to under 100 µg $L^{-1}$, and then continued to decline over time. On the other hand, the barrels initially peaked just below 200 µg $L^{-1}$, immediately decreased to below 50 µg $L^{-1}$, but then showed an interval of elevated Mn levels between 35 cm and 65 cm of cumulative leachate. The maximum peak during this interval was approximately 118 µg $L^{-1}$and was unique to the barrels. After 65 cm of cumulative leachate, the barrels aligned with the columns and mesocosms at very low levels.

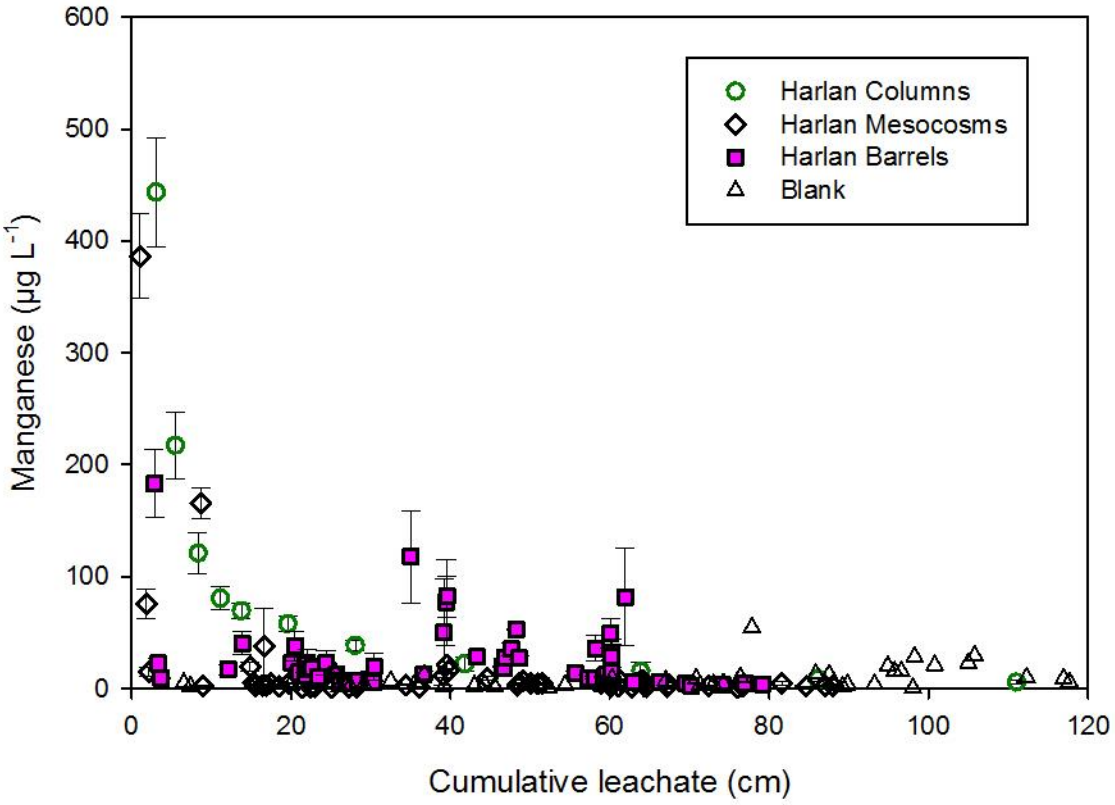


Figure 26. Leachate Mn versus cumulative volume eluted for columns, mesocosms, and barrels. Values plotted are means (n=3 except for blank n=1) per sample event with one standard error above and below. Detection limit = 5.0 µg $L^{-1}$.

*Leachate Aluminum (Al)*

The three scales showed similar patterns of Al release (Fig. 27), but the barrels and mesocosms released significantly higher levels during the 10 cm to 60 cm interval of cumulative leaching. The pattern for all three scales was to produce low levels at the beginning, followed by an increase which peaked around 40 cm of cumulative leachate; followed by a decrease to very low levels after 60 cm of cumulative leachate. The barrels peaked earlier and their overall level of Al release was significantly higher than the other scales. This could have been due to colloidal Al in very small mineral fragments, which were created during the blasting process,

washing out of the barrels. Also, there could have been more Al hydrolysis in the barrels, causing the higher peak. Throughout this time period, the barrels often reached >500 µg $L^{-1}$ and peaked at approximately 1400 µg $L^{-1}$. On the other hand, the mesocosms peaked just below 500 µg $L^{-1}$ and the columns peak just below 200 µg $L^{-1}$. After the conclusion of the peak elution period at around 60 cm of cumulative leachate, there was no significant difference in Al release among the three scales.

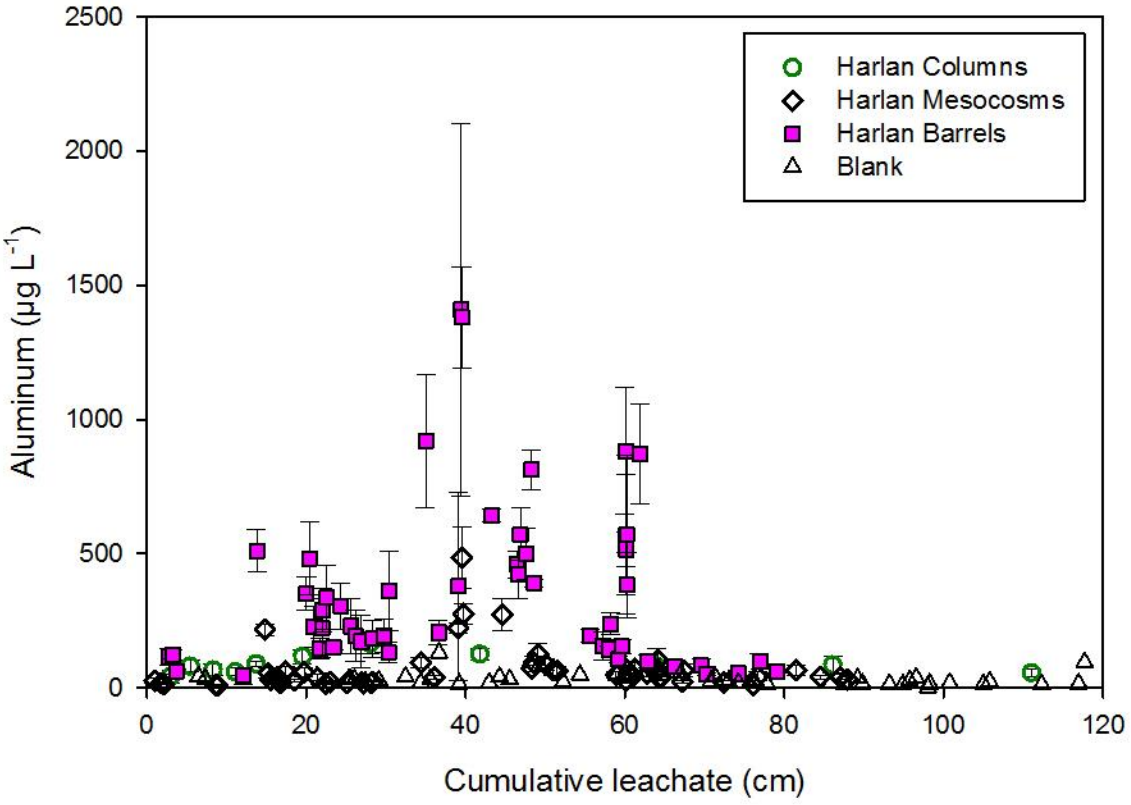


Figure 27. Leachate Al versus cumulative volume eluted for columns, mesocosms, and barrels. Values plotted are means (n=3 except for blank n=1) per sample event with one standard error above and below. Detection limit = 1.0 µg $L^{-1}$.

*Leachate Lead (Pb)*

The release pattern of Pb (Fig. 28) was similar to that of Fe, but at much lower levels. The column and mesocosm leachate stayed below the detection limit of Pb, 0.5 µg $L^{-1}$, for much of the study period. On the other hand, between about 10 cm and 60 cm of cumulative leachate, the barrels exhibited significantly higher, but very low, levels of Pb. Lead release peaked at approximately 4.5 µg $L^{-1}$ in the barrels at around 40 cm of cumulative leachate. While the mesocosms and columns varied from the detection limit a handful of times, they never exceeded 1.5 µg $L^{-1}$.

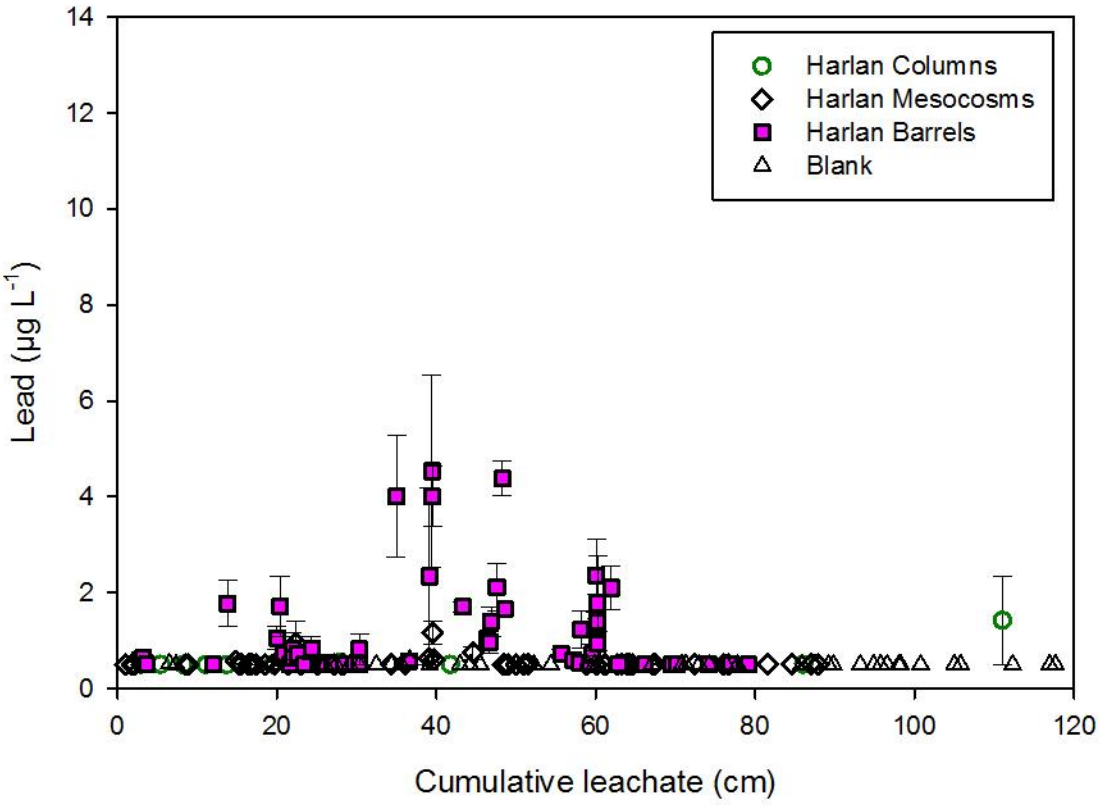


Figure 28. Leachate Pb versus cumulative volume eluted for columns, mesocosms, and barrels. Values plotted are means (n=3 except for blank n=1) per sample event with one standard error above and below. Detection limit = 0.5 µg $L^{-1}$.

*Leachate Copper (Cu)*

While the columns exhibited a rapid and steady decline in Cu levels (Fig. 29) to the detection limit of 0.6 µg $L^{-1}$ before 10 cm of cumulative leachate and stayed very low, the barrels and mesocosms continued to release low but detectable amounts of Cu throughout the study period. Between 10 cm and 40 cm of cumulative leachate, there was no significant difference between the three scales, because all were at or near the detection limit. Both the barrels and mesocosms exhibited a second interval of increased Cu elution after 40 cm of cumulative leachate. During this interval, the barrels reached 3 µg $L^{-1}$ just after 60 cm of cumulative leachate and the mesocosms reached 2 µg $L^{-1}$ at the same point. It is also interesting to note that significant (but low) levels of Cu were also collected in the blank barrel indicating some local source of acidic components.

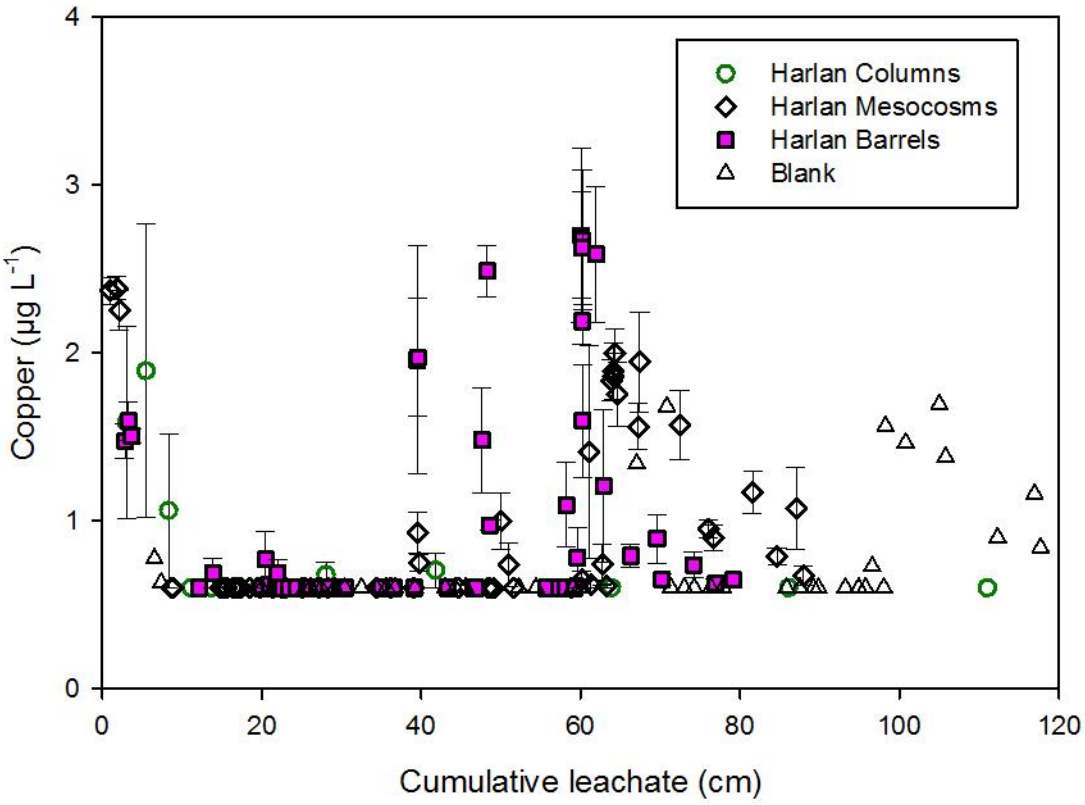


Figure 29. Leachate Cu versus cumulative volume eluted for columns, mesocosms, and barrels. Values plotted are means (n=3 except for blank n=1) per sample event with one standard error above and below. Detection limit = 0.6 µg $L^{-1}$.

*Leachate Nickel (Ni)*

During the first three leaching events, the Ni release (Fig. 30) from the Harlan spoil was significantly higher in the columns than the barrels and mesocosms. The columns peak value was approximately 41.5 µg $L^{-1}$, while only 5 µg $L^{-1}$ to 6 µg $L^{-1}$ leached from the barrels and mesocosms. This difference could have been caused by initial elution of colloidal particles and difference in material preparation in the columns and was also noted by Parker (2013). After 10 cm of cumulative leachate, all three scales stayed between 1.0 µg $L^{-1}$ and 6.0 µg $L^{-1}$, although the

barrels and mesocosms were much more variable between leaching events compared to the columns.

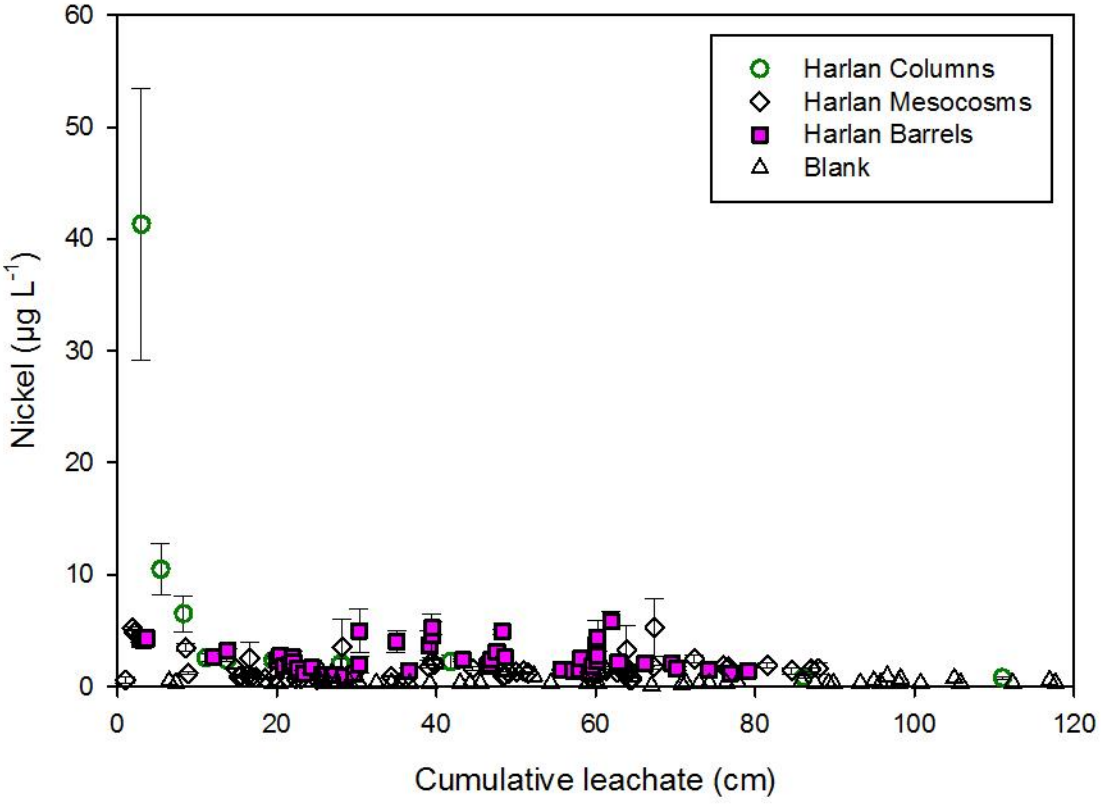


Figure 30. Leachate Ni versus cumulative volume eluted for columns, mesocosms, and barrels. Values plotted are means (n=3 except for blank n=1) per sample event with one standard error above and below. Detection limit = 0.3 µg $L^{-1}$.

*Leachate Zinc (Zn)*

Both the columns and the mesocosms had similar peak initial Zn levels (Fig. 31) of between 16.5 µg $L^{-1}$ and 17.5 µg $L^{-1}$. On the other hand, the barrels fluctuated greatly, periodically rose above 10 µg $L^{-1}$ between 20 and 60 cm of cumulative leachate, and peaked at approximately 13 µg $L^{-1}$. After their initial peak, the columns and mesocosms stayed well below

10 µg $L^{-1}$, but the mesocosms exhibited a second noticeable peak just after 60 cm of cumulative leachate. The cause of the much higher Zn levels in the blank towards the end of the study was unknown, but based on timing could have been caused by emissions from the Virginia Tech power plant or perhaps the local uses of Zn in foliar research applications at the TRC.

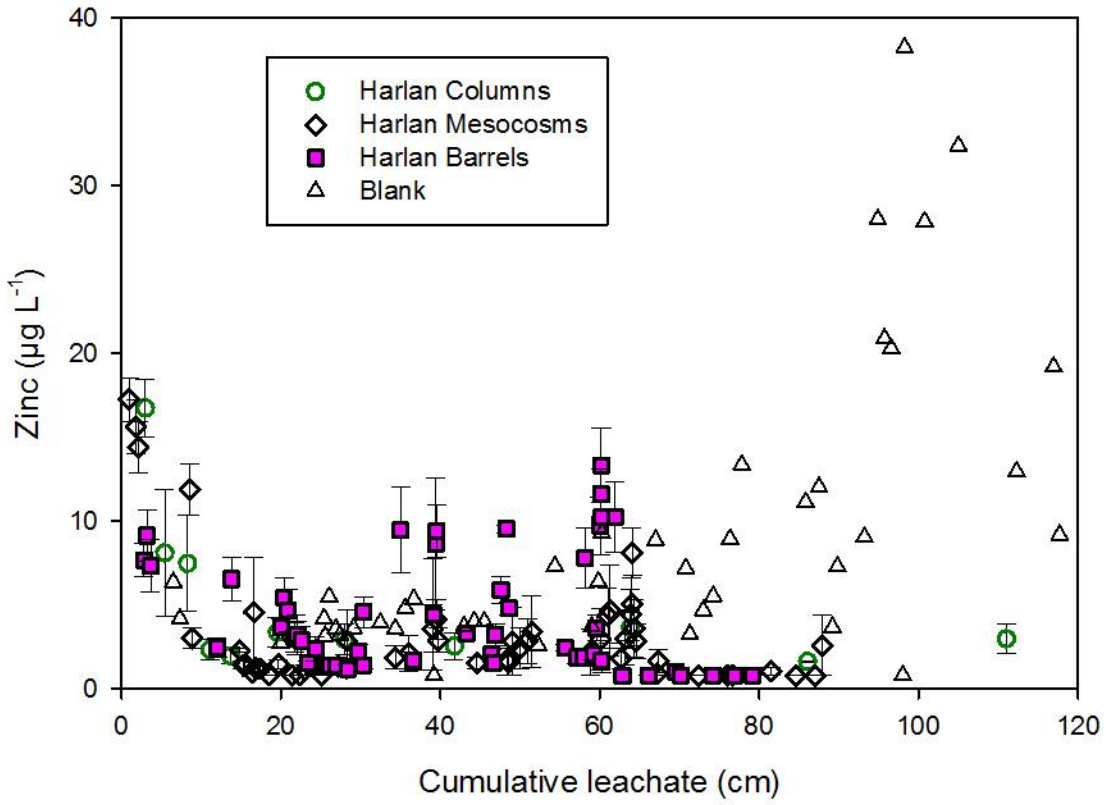


Figure 31. Leachate Zn versus cumulative volume eluted for columns, mesocosms, and barrels. Values plotted are means (n=3 except for blank n=1) per sample event with one standard error above and below. Detection limit = 0.8 µg $L^{-1}$.

*Leachate Cadmium (Cd)*

For the majority of the study period, leachate Cd levels in leachates from all three scales were at or below the detection limit (Fig. 32) of 0.1 µg $L^{-1}$ and thus there were not any treatment effects. Cadmium is very insoluble at pH > 7.0, particularly in the presence of carbonates. The

two individual higher values are outliers, most likely due to a flush of colloidal particles in one or more replications.

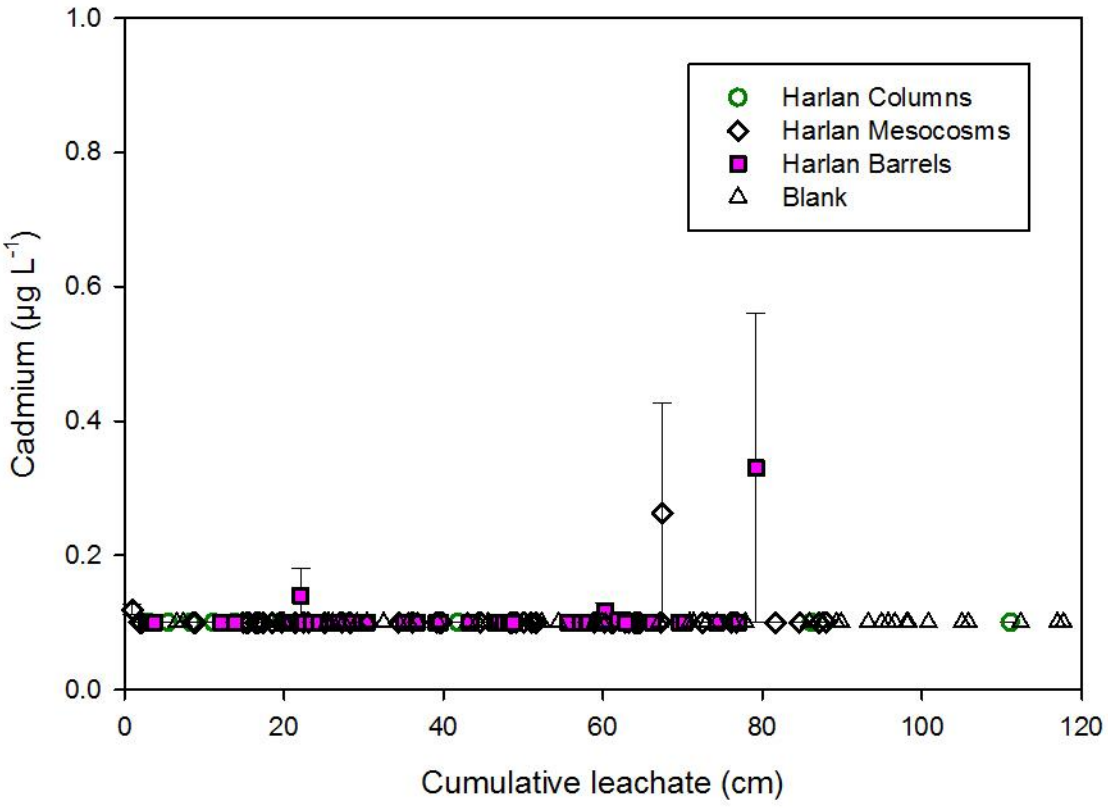


Figure 32. Leachate Cd versus cumulative volume eluted for columns, mesocosms, and barrels. Values plotted are means (n=3 except for blank n=1) per sample event with one standard error above and below. Detection limit = 0.1 µg $L^{-1}$.

*Leachate Chloride (Cl)*

Levels of Cl (Fig. 33) in the leachates were very low overall, peaked early, and then rapidly decreased to the detection limit of 5 µg $L^{-1}$. The peak from the columns (almost 11 µg $L^{-1}$) was significantly higher than the peak of the barrels and mesocosms. This could have been caused by the finer textured grind of the column material vs. the unaltered spoils placed in the barrels and mesocosms. The barrels and mesocosms peaked between 6.0 µg $L^{-1}$ and 6.6

µg $L^{-1}$ and were not significantly different. All three scales decreased to the detection limit by 6 cm of cumulative leachate.

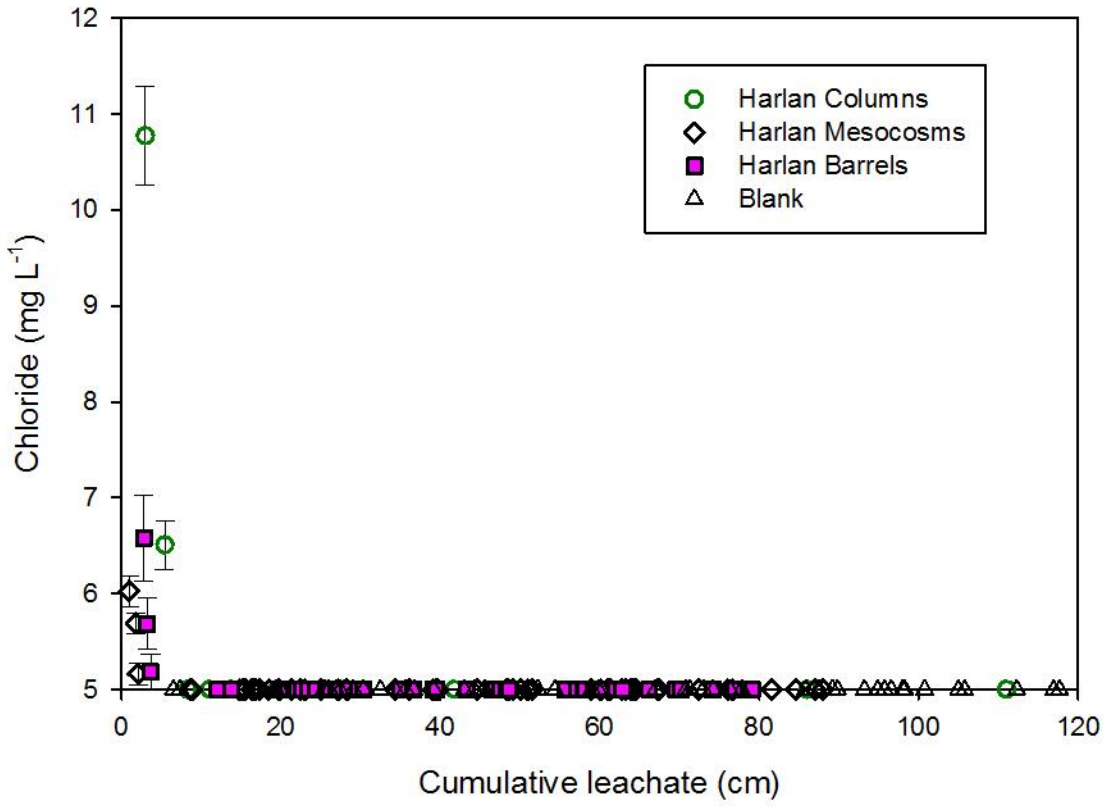


Figure 33. Leachate Cl versus cumulative volume eluted for columns, mesocosms, and barrels. Values plotted are means (n=3 except for blank n=1) per sample event with one standard error above and below. Detection limit = 5.0 mg $L^{-1}$.

Comparison of Field Leaching Behavior for Barrels and Mesocosms by Date

Figure 34 displays cumulative rainfall vs. date. This graph displays drier periods in the late summer and early fall of each year, when there was less cumulative rainfall added and visible gaps between rainfall events. This graph also displays the cumulative leachate that was collected from the mesocosms, barrels, and blank. It is interesting to note that the barrels produced less leachate compared to the mesocosms. Also, differences between rainfall and the

blank leachate were likely due to evaporation losses during the summer months or small differences in rainfall events between the location of the rain gauge and experiment site. For the balance of this results section, Figures 35 through 53 show the "sampling date" (rather than cumulative leachate volume) on the x-axis and "parameter of interest" on the y-axis. Leachate data is displayed for the Harlan spoil from the barrels and mesocosms that were placed in the field, and leached under natural environmental conditions. This allows for analysis of how leachate characteristics differed over time, between different seasons, and between the two sizes of leaching containers. All graphs begin in December 2012, and extend to January 2014, except for bicarbonate which extends to March of 2014, and pH and EC which extend through November 2014.

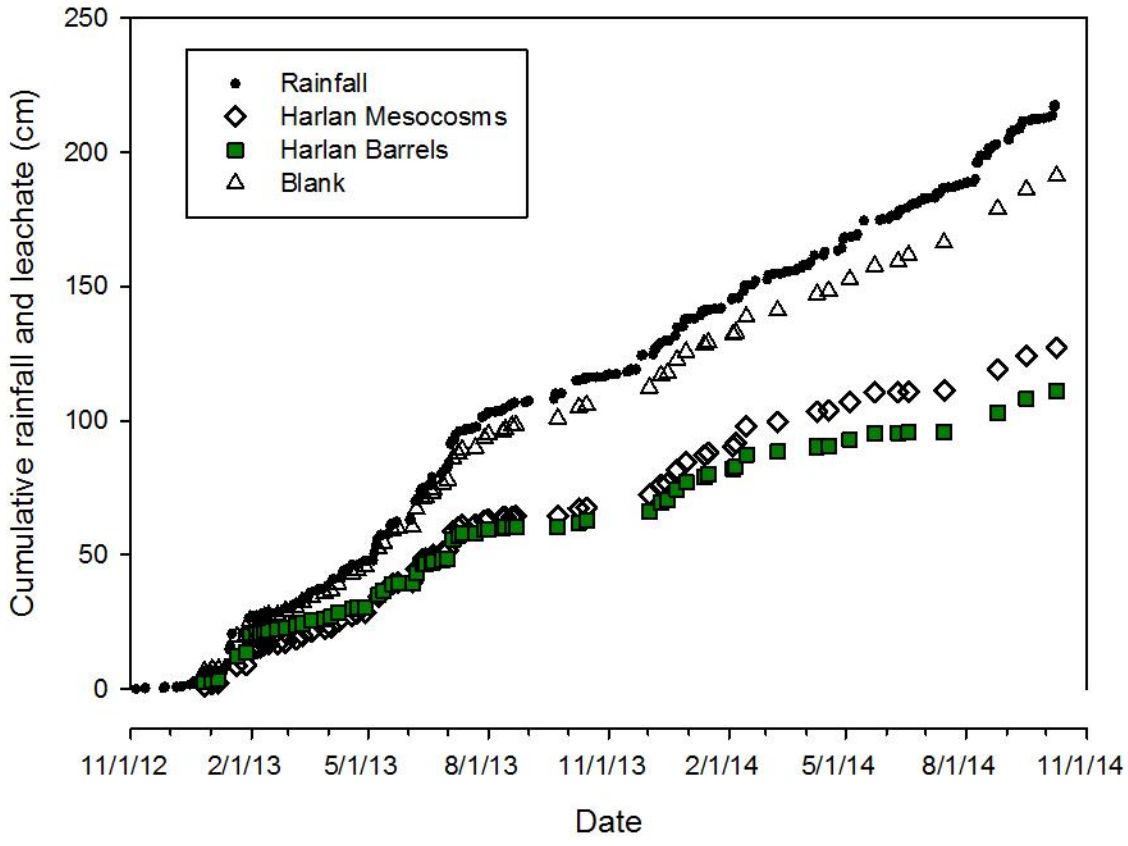


Figure 34. Cumulative rainfall and leachate versus date for mesocosms, barrels, and blank. Values plotted are cumulative rainfall for each measureable rainfall event, or cumulative leachate for each leachate collection.

*Leachate EC*

Leachate EC levels in the barrels and mesocosm s (Fig. 35) differed significantly only during the first month of leachate collection, when the mesocosms peaked significantly higher than the barrels. During this time, the mesocosms peaked around 2,250 µs $cm^{-1}$, while the barrels peaked at 1780 µs $cm^{-1}$. These peaks were followed by a rapid decline to below 500 µs $cm^{-1}$, before peaking two more times during the study period.

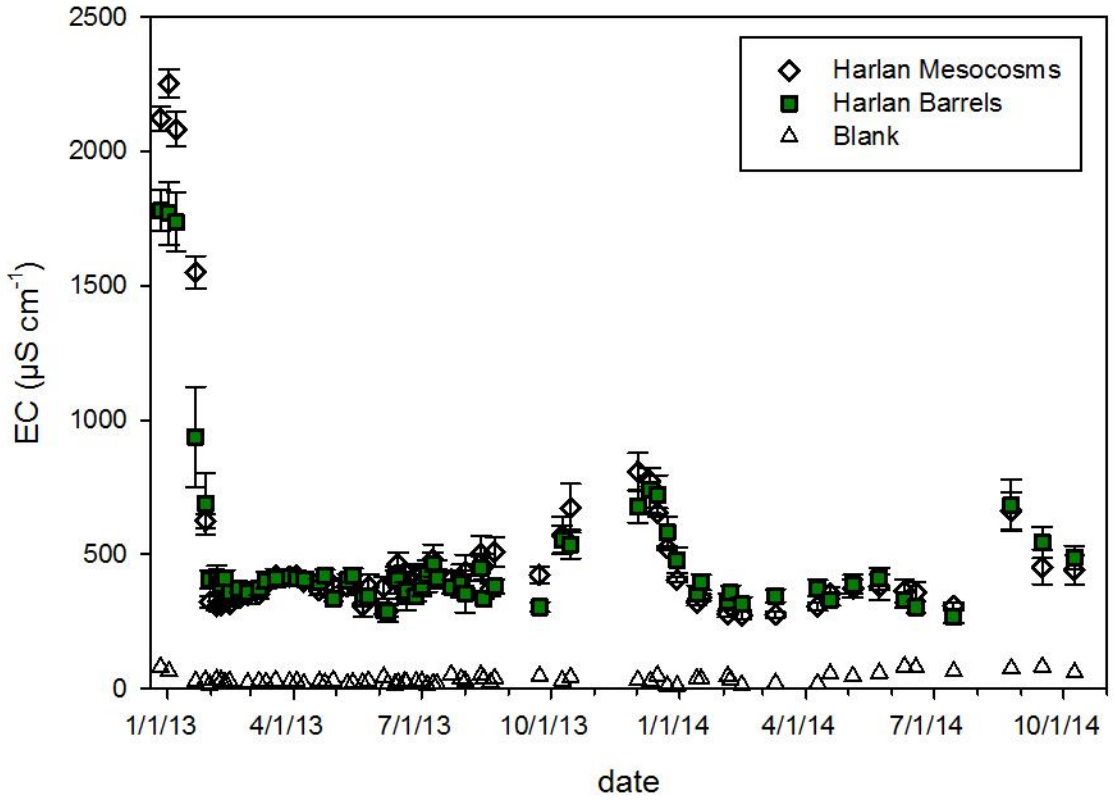


Figure 35. Leachate EC versus date for mesocosms and barrels. Values plotted are means (n=3 except for blank n=1) per sample event with one standard error above and below.

The two subsequent peaks each occurred after long dry periods with little rainfall. Both peaks reached above 500 µs $cm^{-1}$, and did not differ significantly in absolute value between the barrels and mesocosms. The second peak began in the early fall of 2013, and ended in early winter following almost 1.5 months of no collectable leachate, and then peaked at approximately 800 µs $cm^{-1}$. Lastly, the third peak occurred during the late summer of 2014 after more than one month without collectable leachate, and peaked around 675 µs $cm^{-1}$.

*Leachate pH*

Leachate pH levels in the barrels and mesocosm s (Fig. 36) did not show a significant treatment effect over time. As expected, both scales started out at lower levels, but quickly equilibrated between ~7.5 to 8 within the first two months. The pH level fluctuated only slightly after this time, and the two scales did not differ significantly. The reason for the much lower apparent rainfall pH values is unknown, but it is interesting that these later dates also exhibited higher Cu and Zn levels. Thus, some input of acidic deposition components is suspected, perhaps very fine particulates from the upwind Virginia Tech coal fired power plant or perhaps a regional deposition pattern.

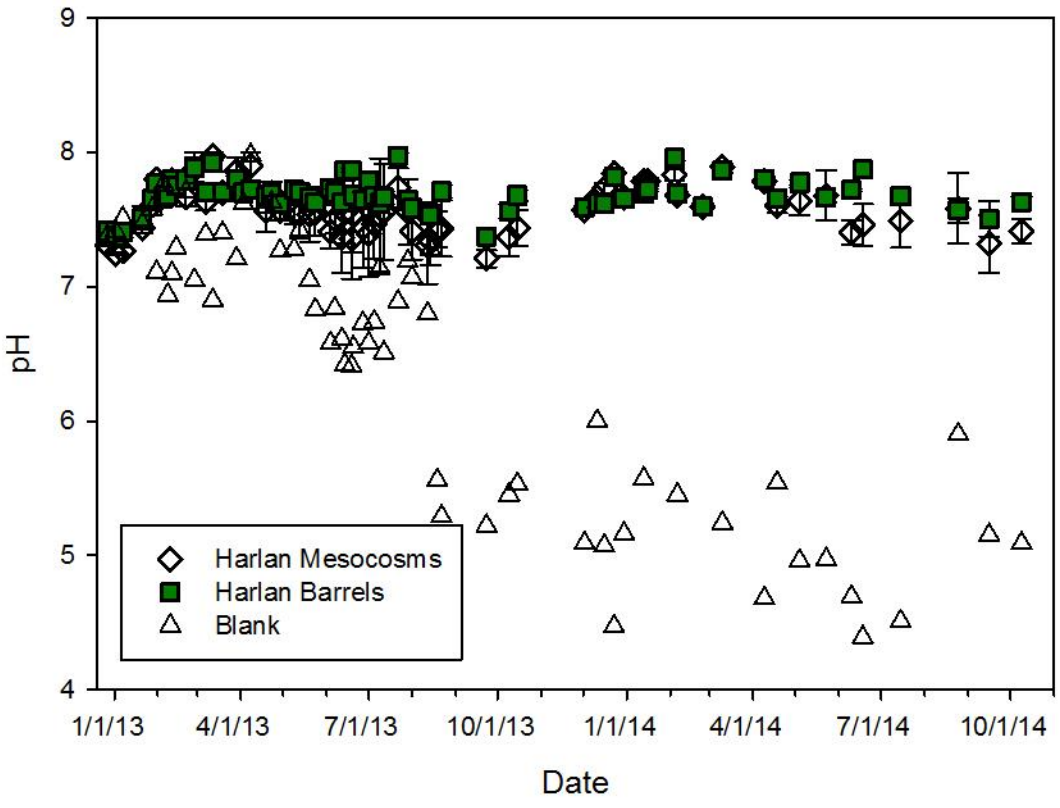


Figure 36. Leachate pH versus date for mesocosms and barrels. Values plotted are means (n=3 except for blank n=1) per sample event with one standard error above and below.

*Leachate Sulfate*

Sulfate levels in the leachate (Fig. 37) only differed significantly between the mesocosms and barrels during the first month of leachate collection. Within this time period, sulfate levels in the mesocosm leachate peaked at just over 1,000 mg $L^{-1}$, while the barrels peaked at 660 mg $L^{-1}$. Following this peak, EC also dropped rapidly and by early February 2013, and $SO_4^{2-}$ was below 150 mg $L^{-1}$ in both the mesocosms and barrels. Sulfate levels remained stable until the dry period of the fall to early winter of 2013, when a second peak of around 450 mg $L^{-1}$ occurred in both the mesocosms and barrels. This pattern corresponded directly to EC levels in the leachate.

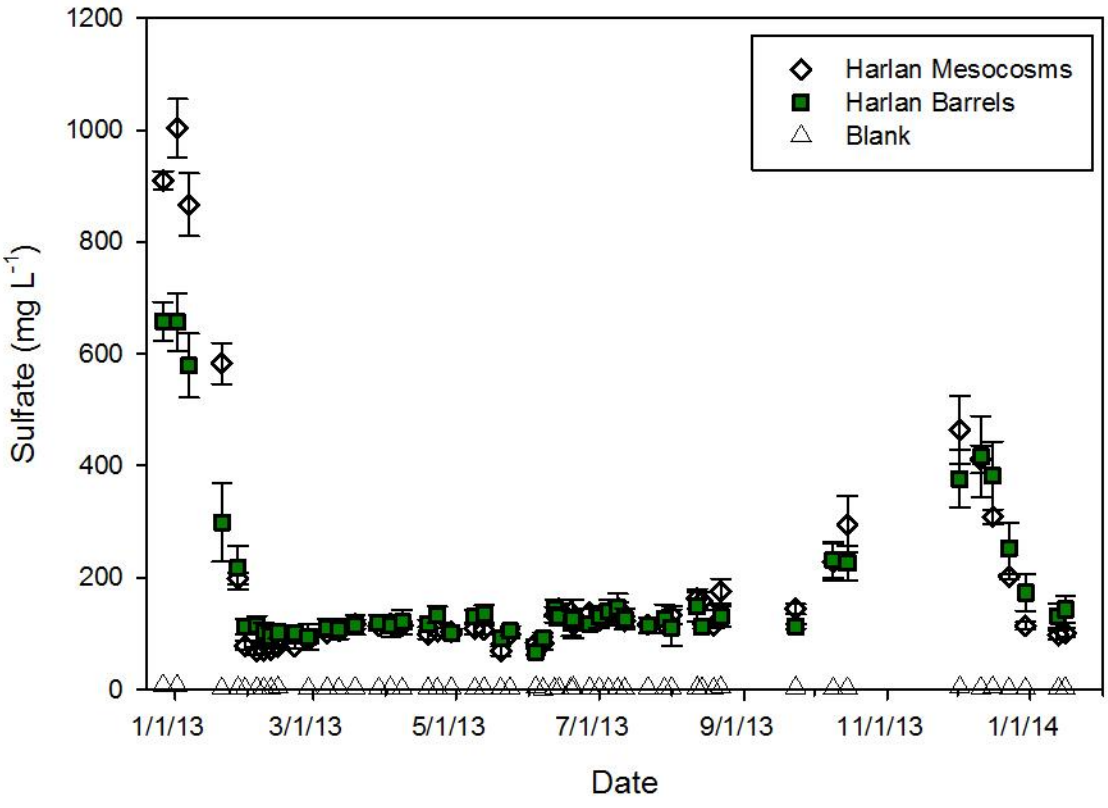


Figure 37. Leachate sulfate versus date for mesocosms and barrels. Values plotted are means (n=3 except for blank n=1) per sample event with one standard error above and below.

*Leachate Bicarbonate*

There were several key differences seen between the bicarbonate levels in the barrel and mesocosm leachate over time (Fig. 38). Bicarbonate levels during the first few leaching events were just below 50 mg $L^{-1}$ for both scales. Leachate bicarbonate levels rose after the first month, and for the majority of the leaching events until November 2013, the bicarbonate levels in the mesocosm leachates were significantly higher than in the barrels. However, bicarbonate levels in the mesocosms varied widely among replications, but were consistently higher than observed for the barrels. This large variance could have been caused by the more heterogeneous physical packing and associated differences in aeration among the replications in the mesocosms that contained much larger rock fragments.

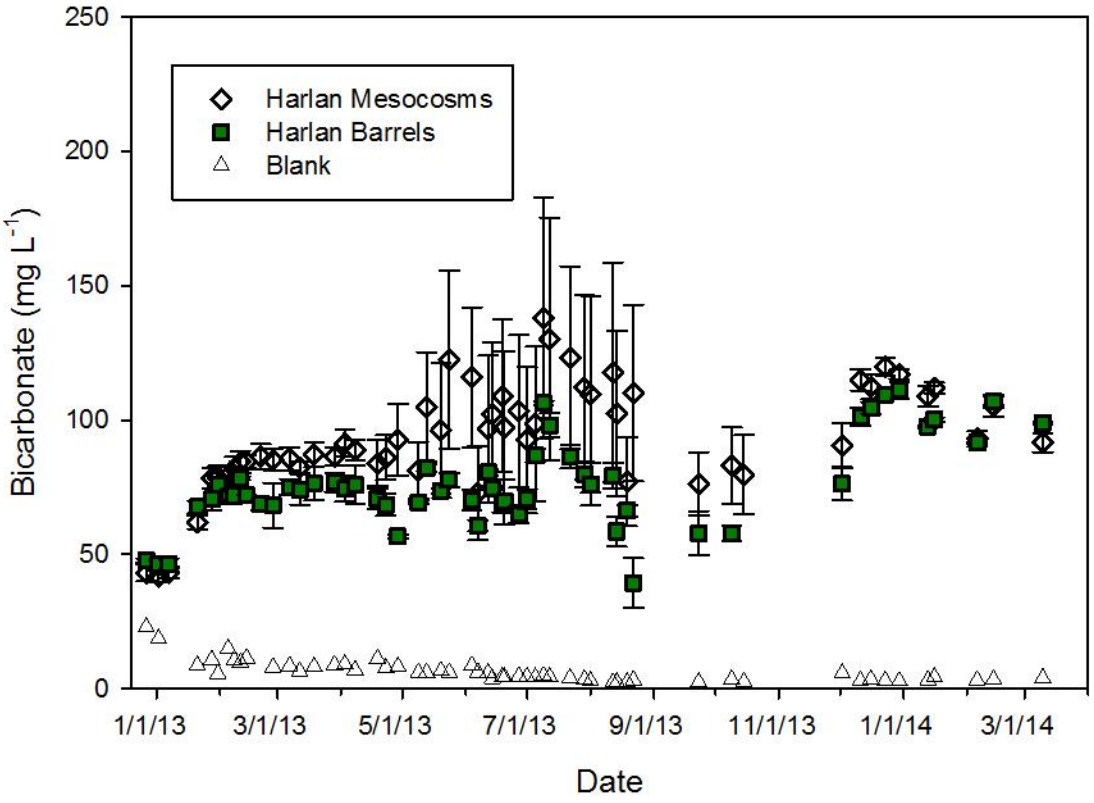


Figure 38. Leachate bicarbonate versus date for mesocosms and barrels. Values plotted are means (n=3 except for blank n=1) per sample event with one standard error above and below.

*Leachate Arsenic (As)*

There were two main differences in As elution between the barrels and mesocosms (Fig. 39). The initial peak was higher in the mesocosms during the first month, and the barrel leachate showed higher levels of As during the fall of 2013. Initially, the mesocosms peaked at just over 3.0 µg $L^{-1}$ in the mesocosms, compared to 2.5 µg $L^{-1}$ in the barrels. During the following months both dropped to the detection limit of 0.3 µg $L^{-1}$ until the barrels again reached 1.0 µg $L^{-1}$ in the late fall of 2013 after several dry periods of weather. After this time period, As levels in the leachates once again dropped below the detection limit.

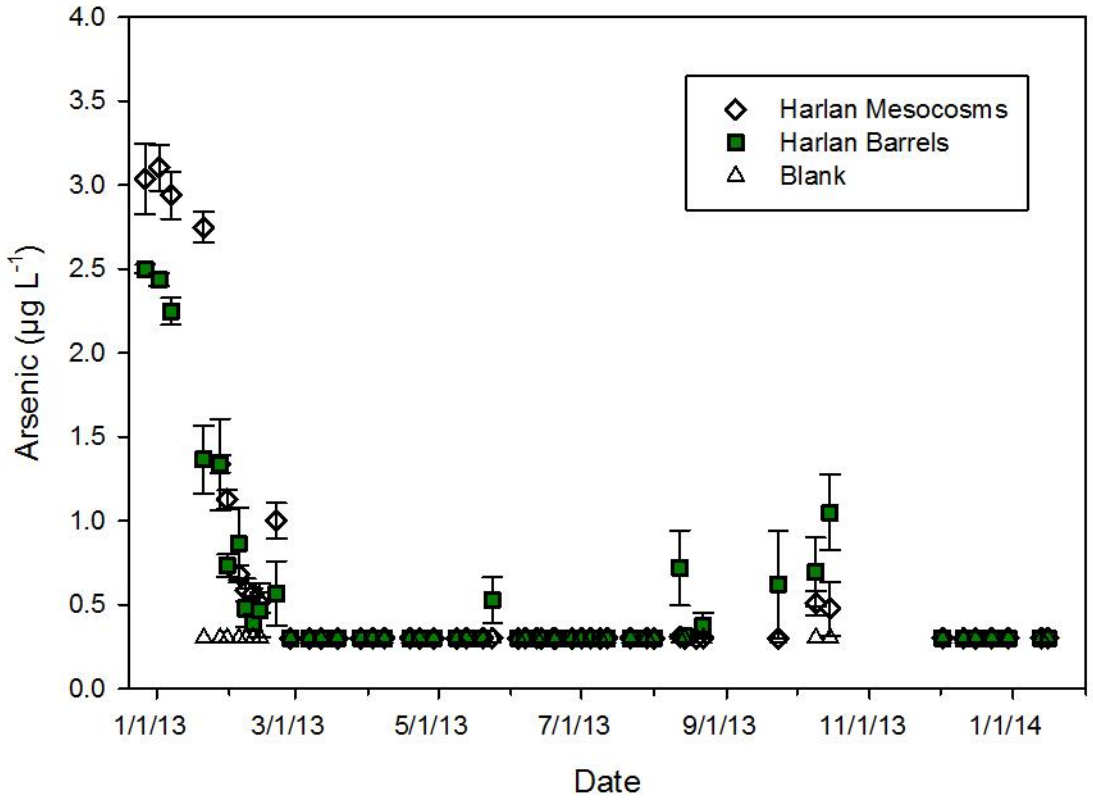


Figure 39. Leachate As versus date for mesocosms and barrels. Values plotted are means (n=3 except for blank n=1) per sample event with one standard error above and below. Detection limit = 0.3 µg $L^{-1}$.

*Leachate Selenium (Se)*

Selenium release during the first month was significantly higher from the mesocosms compared to the barrels (Fig. 40). During this time, selenium release from the mesocosms peaked at 92 µg $L^{-1}$, compared to 60 µg $L^{-1}$ in the barrels. After the first month, no treatment effects were seen. Se release dropped rapidly towards the detection limit of 0.8 µg $L^{-1}$, and then fluctuated very little over time.

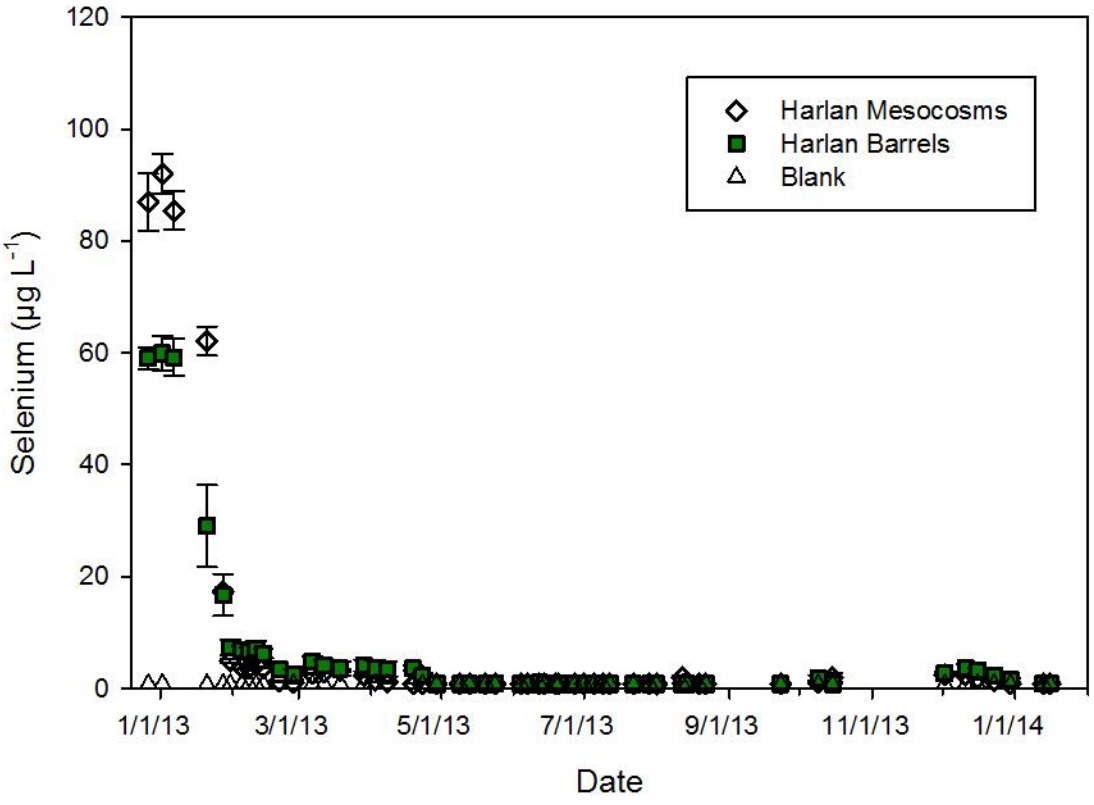


Figure 40. Leachate Se versus date for mesocosms and barrels. Values plotted are means (n=3 except for blank n=1) per sample event with one standard error above and below. Detection limit = 0.8 µg $L^{-1}$.

*Leachate Calcium (Ca)*

Similar to $SO_4^{2-}$, differences in Ca levels in the leachates (Fig. 41) corresponded to EC levels. The mesocosms peaked significantly higher (at almost 400 mg $L^{-1}$) than the barrels (300 mg $L^{-1}$) during the first month, then levels dropped to approximately 50 mg $L^{-1}$ until the fall of 2013 when the second peak began. The peak reached approximately 130 mg $L^{-1}$ in early winter- and again followed the dry period of weather.

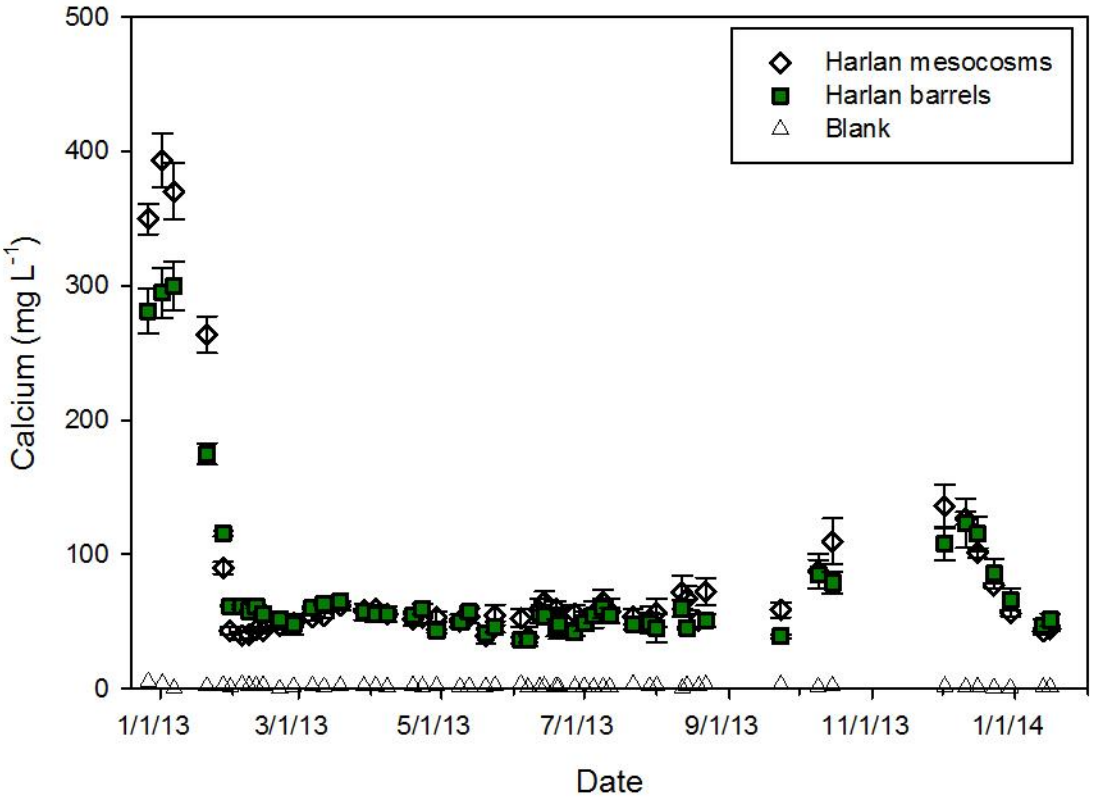


Figure 41. Leachate Ca versus date for mesocosms and barrels. Values plotted are means (n=3 except for blank n=1) per sample event with one standard error above and below. Detection limit = 0.01 mg $L^{-1}$.

*Leachate Magnesium (Mg)*

As expected, Mg levels in the leachates (Fig. 42) also mirrored EC release patterns. The mesocosms peaked significantly higher at 55 mg $L^{-1}$ compared to the barrels at 37 mg $L^{-1}$. Levels then dropped quickly to below 10 mg $L^{-1}$ after the first month until they peaked again in the fall of 2013. This peak reached approximately 23 mg $L^{-1}$ in both the barrels and mesocosms before dropping back to below 10 mg $L^{-1}$ during the winter months of 2014.

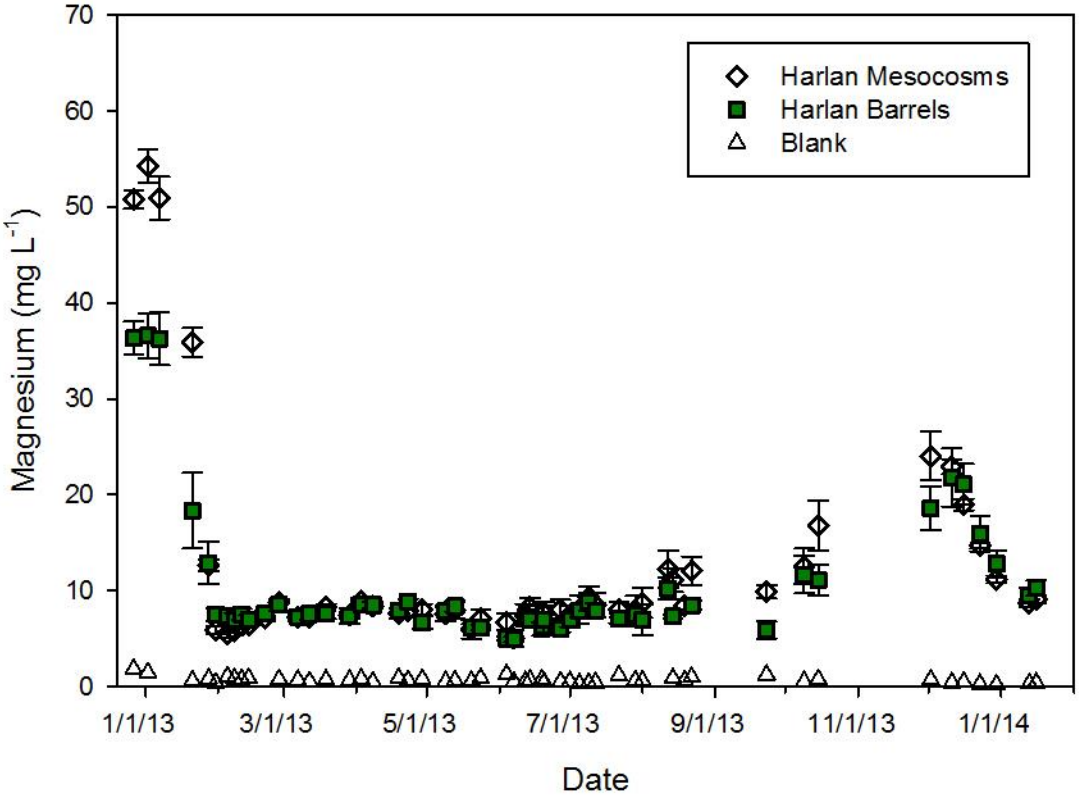


Figure 42. Leachate Mg versus date for mesocosms and barrels. Values plotted are means (n=3 except for blank n=1) per sample event with one standard error above and below. Detection limit = 0.005 mg $L^{-1}$.

*Leachate Potassium (K)*

Potassium elution peaked during the first month of leachate collection (Fig. 43), and this was the only time period where K levels were significantly different between the barrels (21 mg $L^{-1}$) and mesocosms (23 mg $L^{-1}$). Following this peak, K levels in the leachates dropped quickly by the second month to around 10 mg $L^{-1}$ and continued to slowly drop during the rest of the study period.

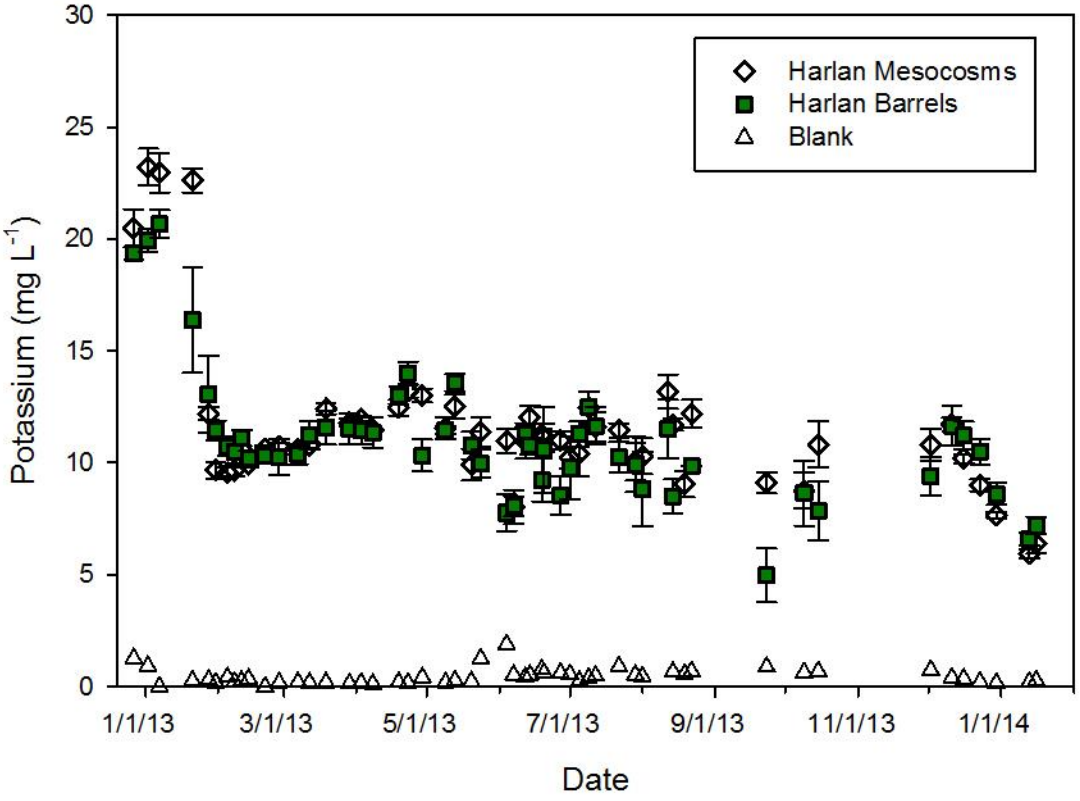


Figure 43. Leachate K versus date for mesocosms and barrels. Values plotted are means (n=3 except for blank n=1) per sample event with one standard error above and below. Detection limit = 0.005 mg $L^{-1}$.

*Leachate Sodium (Na)*

The comparative patterns of Na release (Fig. 44) showed treatment effects for the first five months of the study. During the first month of the study, the mesocosm leachate contained significantly higher concentrations of Na. The barrels initially peaked at 4.9 mg $L^{-1}$ while the mesocosms peaked at 5.3 mg $L^{-1}$. Next, the Na elution from the barrels was significantly higher than the mesocosms for months two through four. For the remainder of the study there was no significant difference in Na elution.

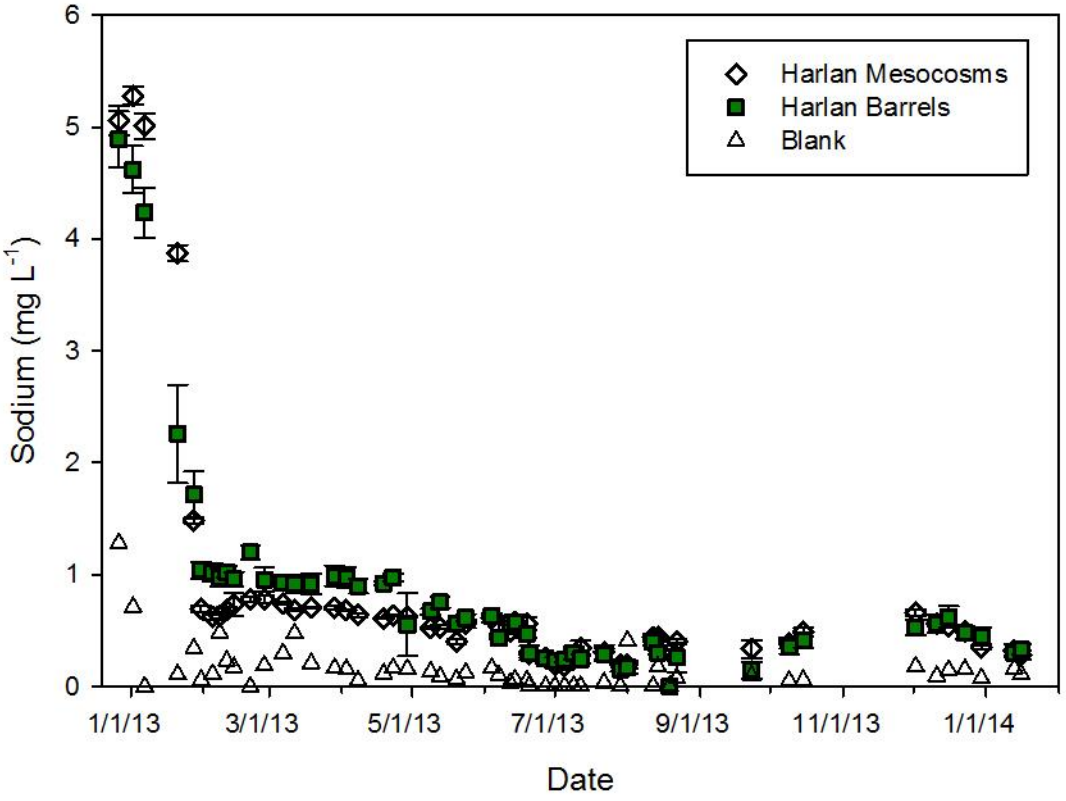


Figure 44. Leachate Na versus date for mesocosms and barrels. Values plotted are means (n=3 except for blank n=1) per sample event with one standard error above and below. Detection limit = 0.005 mg $L^{-1}$.

*Leachate Iron (Fe)*

Iron levels in the barrel leachate (Fig. 45) were commonly significantly higher compared to the mesocosm leachate throughout the study period. The Fe levels in the mesocosms often stayed below 0.20 mg $L^{-1}$, while Fe levels in the barrels remained above this level during the majority of the study. Iron levels in both scales reached their peak in late May of 2013, presumably due to the insolubility of Fe before this time while it was bound as an oxy-hydroxide precipitate. Another possible cause of this peak was time-lagged siderite dissolution. The barrels reached a peak of 2.9 mg $L^{-1}$, while the mesocosms reached a peak of only 0.82 mg $L^{-1}$.

Towards the end of the study, Fe levels in both scales converged below 0.20 mg $L^{-1}$ and remained there for the last two months.

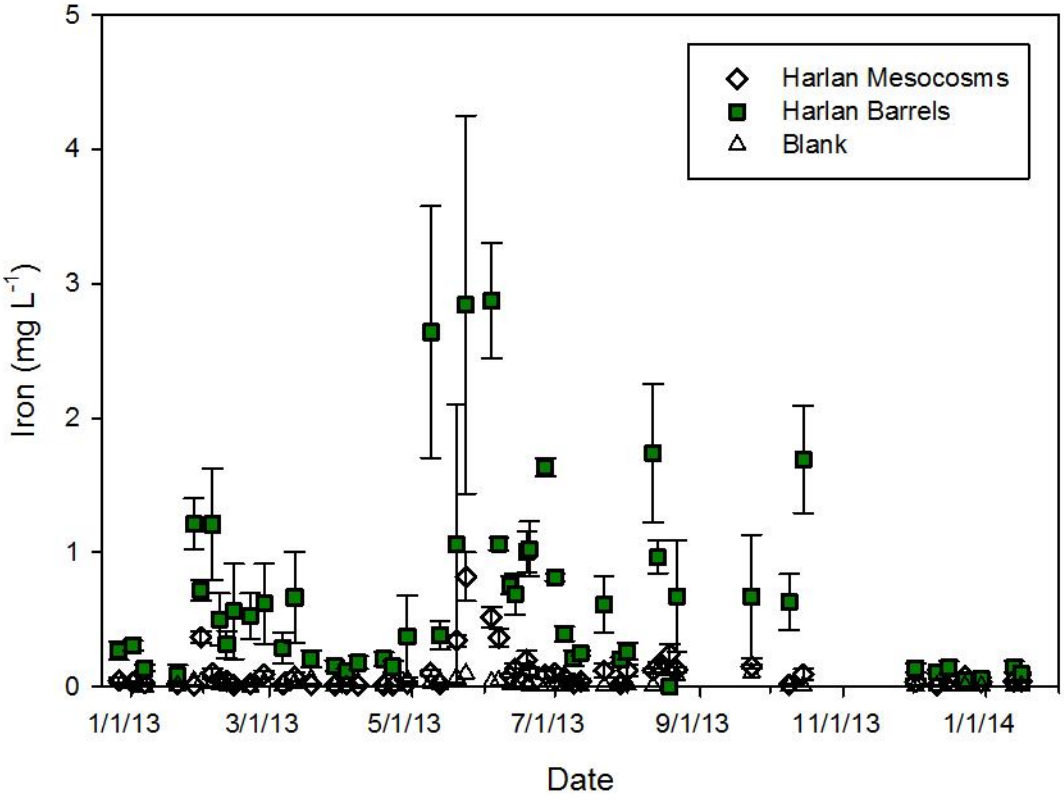


Figure 45. Leachate Fe versus date for mesocosms and barrels. Values plotted are means (n=3 except for blank n=1) per sample event with one standard error above and below. Detection limit = 5.0 µg $L^{-1}$.

*Leachate Manganese (Mn)*

Initially, Mn levels in the mesocosm leachate (Fig. 46) peaked significantly higher than the barrel leachate, but as time elapsed, Mn levels remained higher in the barrels. The initial peak reached 385 µg $L^{-1}$ in the mesocosms, and 185 µg $L^{-1}$ in the barrels. By the end of the first month, Mn levels in both scales dropped significantly. The Mn levels in the mesocosms stayed below 50 µg $L^{-1}$ for the remainder of the study, but the barrels showed a secondary peak of just

over 100 µg $L^{-1}$. By the end of the study, both scales converged at very low levels below 10 µg $L^{-1}$.

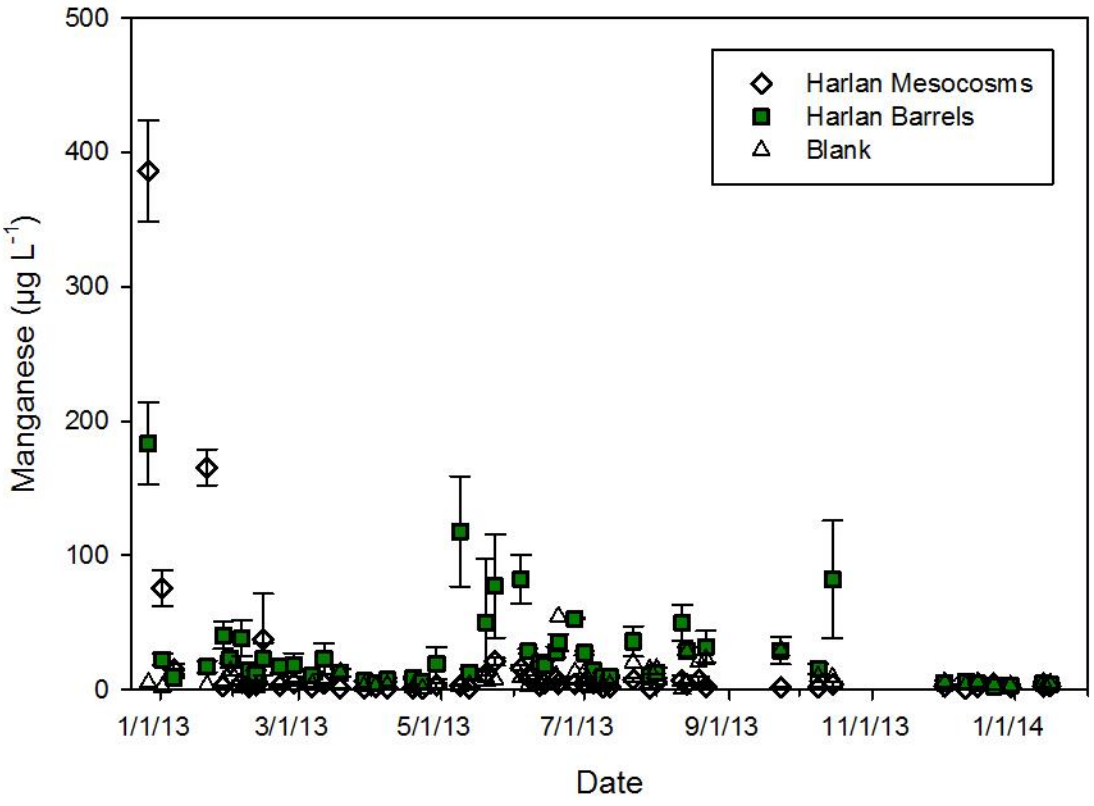


Figure 46. Leachate Mn versus date for mesocosms and barrels. Values plotted are means (n=3 except for blank n=1) per sample event with one standard error above and below. Detection limit = 5.0 µg $L^{-1}$.

*Leachate Aluminum (Al)*

Aluminum levels in the leachates (Fig. 47) differed significantly between the barrels and the mesocosms. Both started low, peaked during the summer of 2013, and decreased to very low levels by the end of the study period. During the period of increased elution (February 2013 through October 2013), the barrels consistently produced significantly higher Al levels compared to the mesocosms. For the duration of this period, the mesocosms were consistently below 200

µg $L^{-1}$, while the barrels usually remained above this level. The barrels peaked at 1,400 µg $L^{-1}$, while the mesocosms peaked at 490 µg $L^{-1}$.

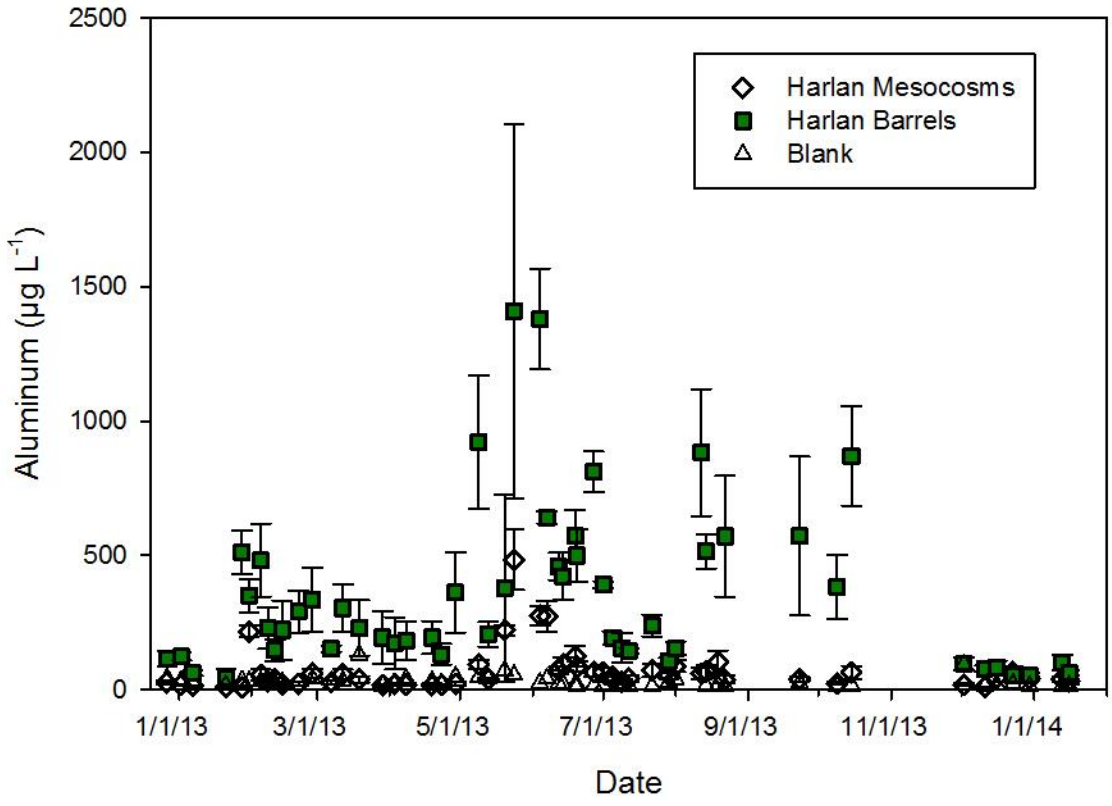


Figure 47. Leachate Al versus date for mesocosms and barrels. Values plotted are means (n=3 except for blank n=1) per sample event with one standard error above and below. Detection limit = 1.0 µg $L^{-1}$.

*Leachate Lead (Pb)*

Lead levels in the barrel leachates (Fig. 48) were often significantly higher in the barrels compared to the mesocosms. In all leachates, Pb levels were very low at the beginning and end of the study with a peak occurring in the late spring of 2013. Lead elution peaked in late May, with the barrels peaking at 4.5 µg $L^{-1}$ and the mesocosms peaking at 1.1 µg $L^{-1}$. There is some

possibility that the later Pb elution in the barrels was related to the delayed Fe elution as well, since Fe-oxides can effectively bind Pb.

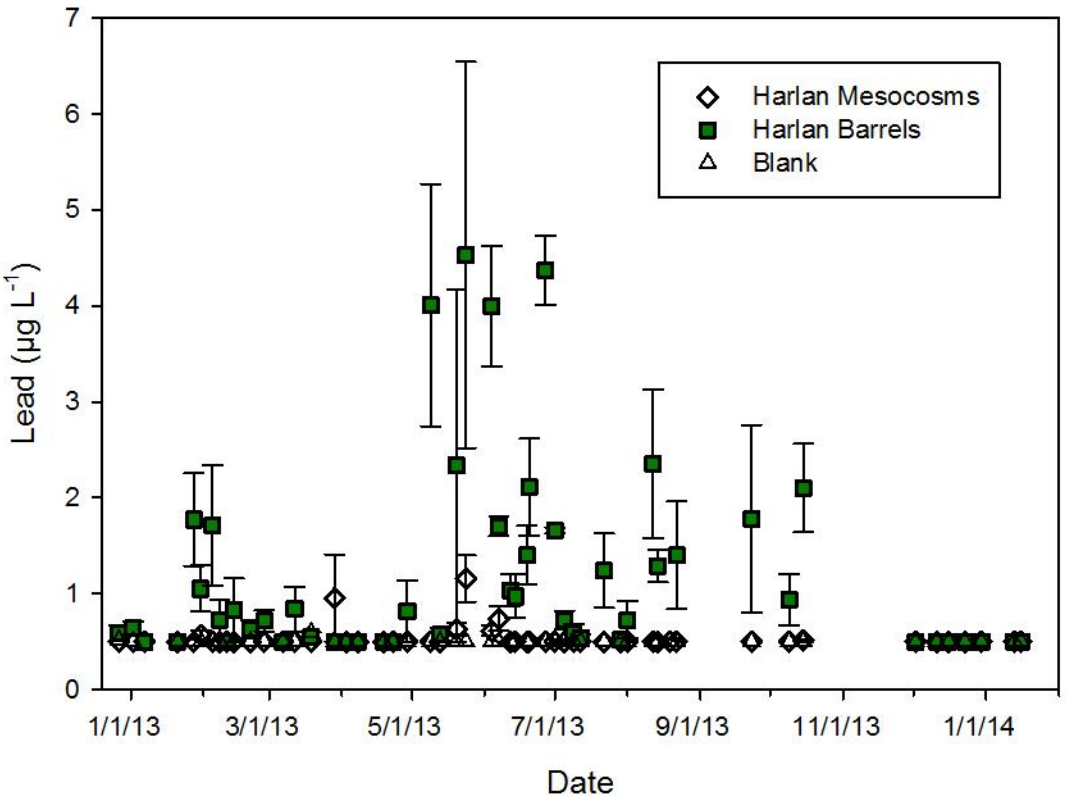


Figure 48. Leachate Pb versus date for mesocosms and barrels. Values plotted are means (n=3 except for blank n=1) per sample event with one standard error above and below. Detection limit = 0.5 µg $L^{-1}$.

*Leachate Copper (Cu)*

During the first month, Cu levels in the mesocosms (2.4 µg $L^{-1}$) peaked significantly higher than the barrels (1.6 µg $L^{-1}$; Fig. 49). However, by the end of the first month, Cu levels in the barrels and mesocosms dropped to the detection limit (0.6 µg $L^{-1}$) and, with few exceptions, remained there until late May of 2013. From this time through the end of the study (March 2013), Cu levels rose and fluctuated greatly in both the barrels and mesocosms. Both scales

produced a secondary peak in mid-August (2.7 µg $L^{-1}$ in the barrels and 2.1 µg $L^{-1}$ in the mesocosms). Throughout this time period, Cu levels in the barrels were often significantly higher than the mesocosms. Also during this time period, Cu levels in the blank were elevated as well, but did not reach the levels seen in the barrels and mesocosms. By January 2014, Cu levels were dropping towards the detection limit.

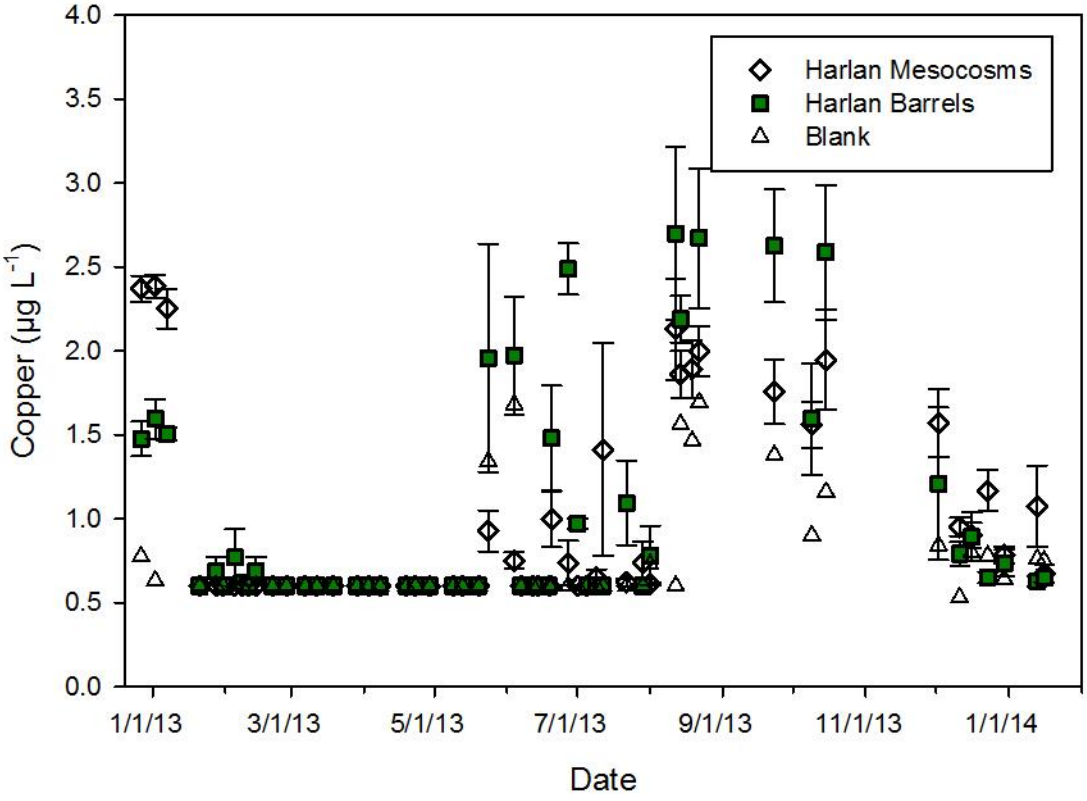


Figure 49. Leachate Cu versus date for mesocosms and barrels. Values plotted are means (n=3 except for blank n=1) per sample event with one standard error above and below. Detection limit = 0.6 µg $L^{-1}$.

*Leachate Nickel (Ni)*

Nickels levels in the leachates (Fig. 50) showed no consistent treatment effect although mean values for the barrels were generally higher than the mesocosms except for at the end of

the study. The barrels and mesocosms showed an initial peak of 4.3 µg $L^{-1}$ and 5.2 µg $L^{-1}$, respectively. Ni levels then dropped to low levels, but rose to higher levels once again by late spring of 2013, where they remained into the winter.

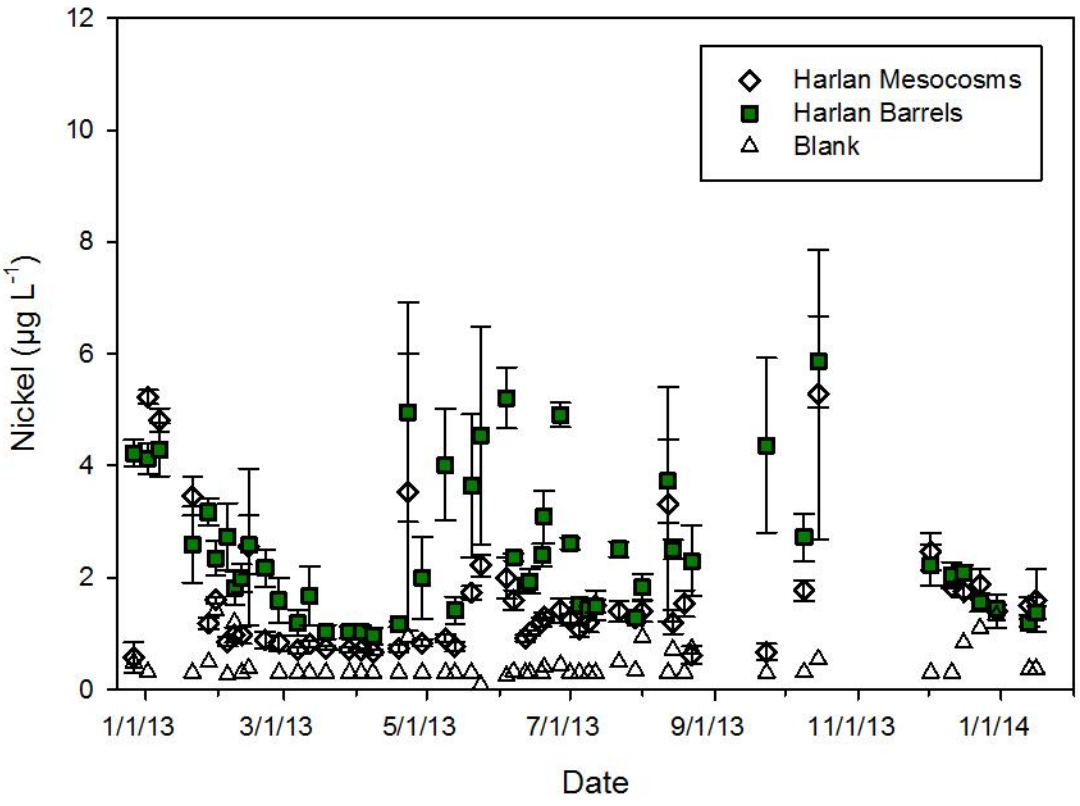


Figure 50. Leachate Ni versus date for mesocosms and barrels. Values plotted are means (n=3 except for blank n=1) per sample event with one standard error above and below. Detection limit = 0.3 µg $L^{-1}$.

*Leachate Zinc (Zn)*

Initially, Zn levels in the mesocosms were significantly higher (Fig. 51), but as time elapsed, levels were significantly higher in the barrels. The initial peak Zn levels were 17 µg $L^{-1}$ in the mesocosms, and 9 µg $L^{-1}$ in the barrels. Following these peaks, both leaching scales showed a steady decline to below 2 µg $L^{-1}$, but then Zn levels rose again beginning in May 2013.

During this period of increased Zn elution, the barrel leachates often showed higher concentrations compared to the mesocosms. A secondary peak occurred in both scales in August 2013 due to inputs from rainfall following a dry reaction period; 13 µg $L^{-1}$ in the barrels and 8 µg $L^{-1}$ in the mesocosms. By the end of the study period, Zn levels returned to very low levels. As noted earlier, this later pattern of Zn release also coincided with high Zn appearing in the blank barrel and thus may be indicative of a combination of release due to weathering reactions coupled with atmospheric additions.

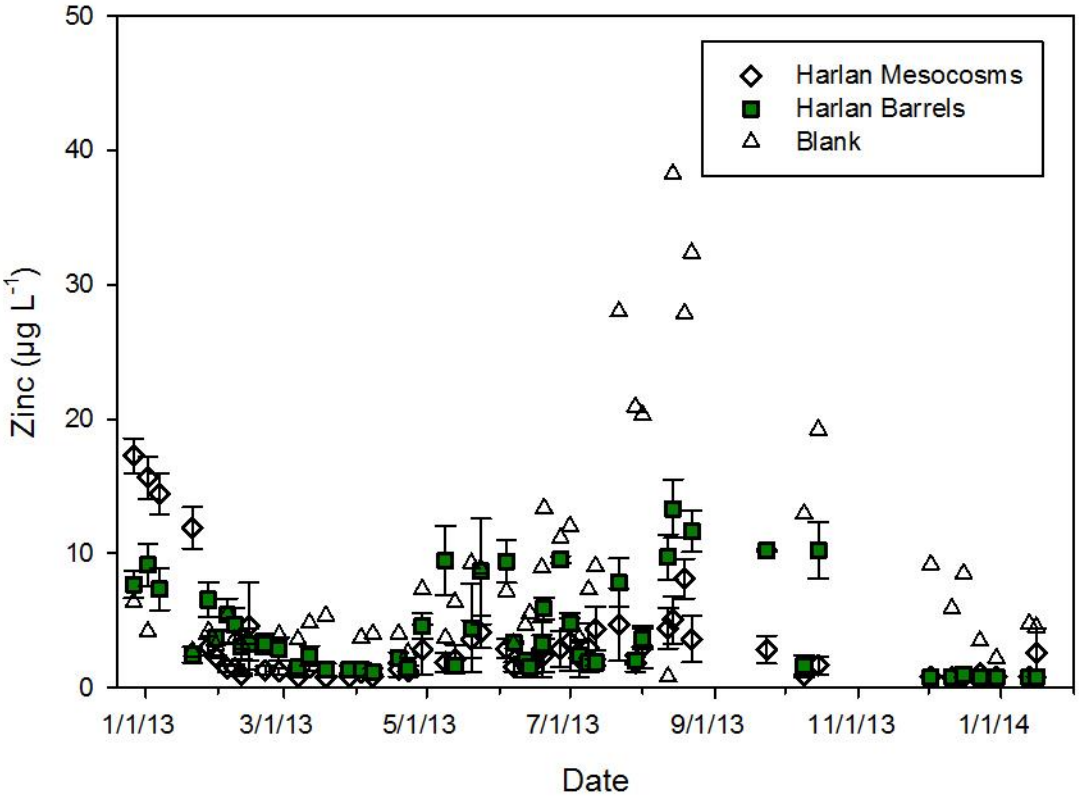


Figure 51. Leachate Zn versus date for mesocosms and barrels. Values plotted are means (n=3 except for blank n=1) per sample event with one standard error above and below. Detection limit = 0.8 µg $L^{-1}$.

*Leachate Cadmium (Cd)*

Cadmium release from the barrels and mesocosms showed no treatment effect (Fig. 52). With few exceptions, Cd levels in the leachate stayed at or below the detection limit of 0.1 µg $L^{-1}$. The two isolated high values at later time are outliers and most likely related to colloidal flux.

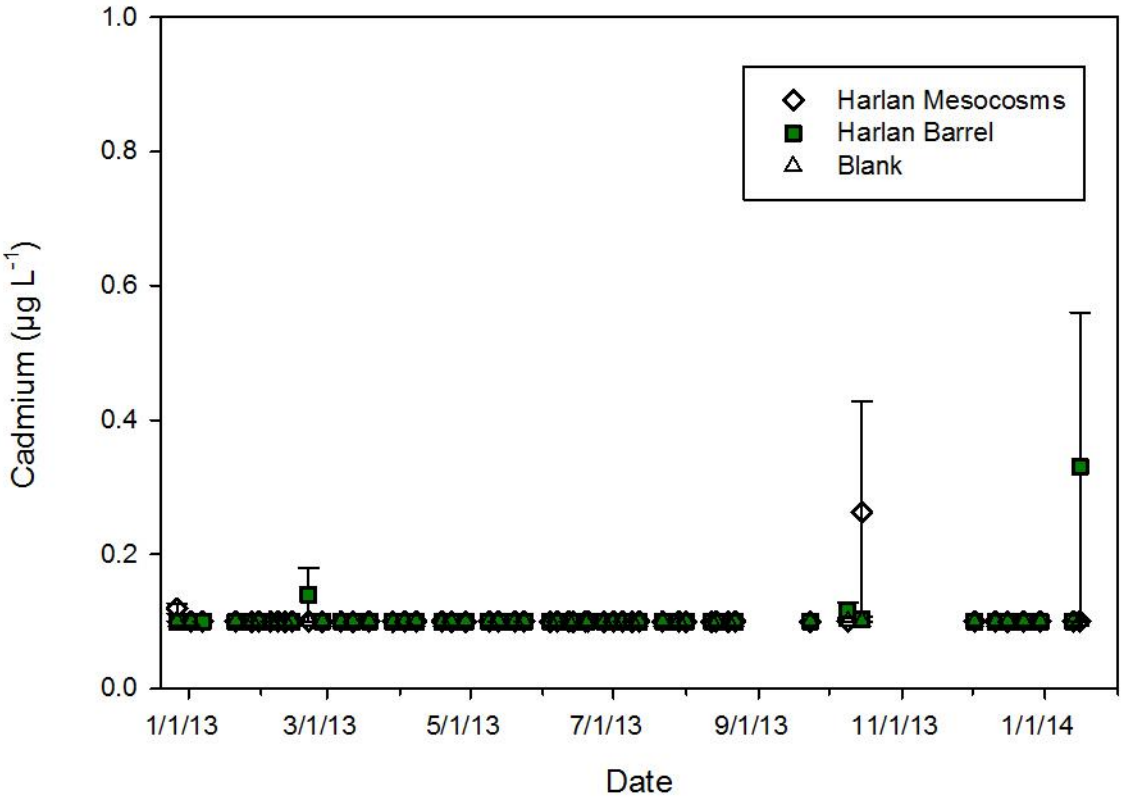


Figure 52. Leachate Cd versus date for mesocosms and barrels. Values plotted are means (n=3 except for blank n=1) per sample event with one standard error above and below. Detection limit = 0.1 µg $L^{-1}$.

*Leachate Chloride (Cl)*

There was no significant difference in Cl release between the barrels and mesocosms (Fig. 53), and no treatment effect was seen. Chloride release from the barrels and mesocosms

peaked during the first leaching cycle, and dropped rapidly during the first month to the detection limit (5 mg $L^{-1}$).

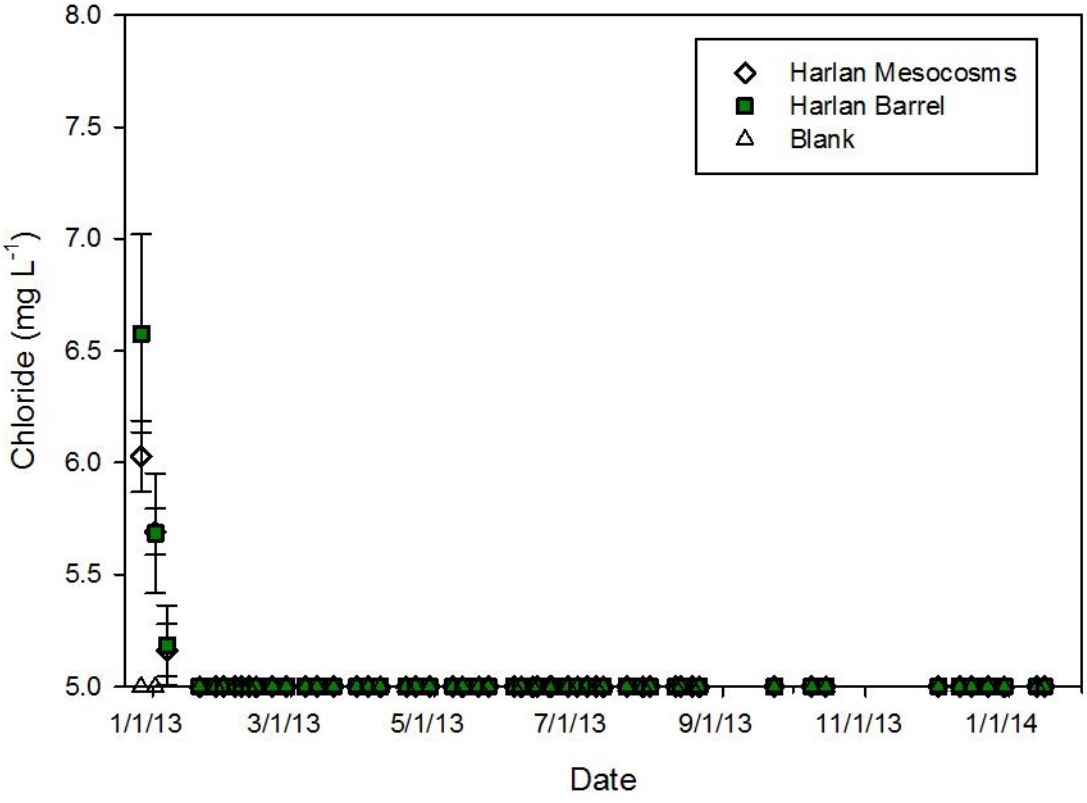


Figure 53. Leachate Cl versus date for mesocosms and barrels. Values plotted are means (n=3 except for blank n=1) per sample event with one standard error above and below. Detection limit = 5.0 mg $L^{-1}$.

## EFFECT OF LEACHING TEST SCALE ON TDS RELEASE FROM COAL REFUSE

### Refuse Characterization

Selected chemical and physical properties of the two coal refuse samples selected for the leaching study are presented in Table 4. Particle size analysis of the original bulk refuse samples showed approximately 69% rock fragments (> 2 mm) and 31% fines (< 2 mm) in the TNR-1 materials, and 62% rock fragments with 38% fines in the TNR-3 material. The pH of the

original coarse refuse samples using the saturated paste extract was 7.41 for TNR-1 and 8.36 for TNR-3. The saturated paste EC was 2,510 µS $cm^{-1}$ for the TNR-1 coarse refuse and 2,520 µS $cm^{-1}$ for TNR-3. The total S content of the TNR-1 coarse refuse was 0.76%, and S was higher in the TNR-3 material at 1.13%. Also, the CCE was 3.95% for the TNR-1 material, and higher in the TNR-3 material at 6.78%. Thus, under normal assumptions of acid-base accounting (ABA; Skousen et al., 2002) neither of these materials would be expected to be net acid-forming, but the TNR-3 material had a higher ratio of potential neutralizers (NP) to maximum potential acidity (MPA) derived from S. The total elemental analysis of the bulk spoil is presented in Tables 5 and 6.

Table 4. Selected chemical and physical properties of the coarse refuse samples used in the columns and barrels. CCE = Calcium Carbonate Equivalent; ABA = Acid–Base Accounting; EC = Electrical Conductivity; MPA = Maximum Potential Acidity; NP = Neutralization Potential.

| Sample ID | Saturated Paste | | CCE | Total S | ABA | | Particle Size Analysis | | | | | |
|---|---|---|---|---|---|---|---|---|---|---|---|---|
| | pH | EC µS $cm^{-1}$ | % | % | MPA Mg per 1000 Mg | NP Mg per 1000 Mg | % Coarse >2 mm | % Fines <2 mm | % Sand | % Silt | % Clay | Textural Class for <2 mm |
| **TNR-1** | 7.41 | 2,510 | 3.95 | 0.76 | 23.75 | 39.5 | 69 | 31 | 32 | 35 | 33 | Clay Loam |
| **TNR-3** | 8.36 | 2,520 | 6.78 | 1.13 | 35.31 | 67.8 | 62 | 38 | 42 | 39 | 19 | Loam |

Table 5. Total mass concentration (mg $kg^{-1}$) of Ca, K, Mg, and Na of coarse refuse samples used in the columns and barrels.

| Sample ID | Ca | K | Mg | Na |
|---|---|---|---|---|
| **TNR-1** | 2,200 | 11,400 | 4,800 | 550 |
| **TNR-3** | 2,100 | 10,600 | 5,000 | 945 |

Table 6. Total mass concentration (mg $kg^{-1}$) of Al, As, Cd, Cu, Fe, Mn, Ni, Pb, Se, and Zn of coarse refuse samples used in the columns and barrels.

| Sample ID | Al | As | Cd | Cu | Fe | Mn | Ni | Pb | Se | Zn |
|---|---|---|---|---|---|---|---|---|---|---|
| **TNR-1** | 48,900 | 14.0 | 0.26 | 28.7 | 21,500 | 149 | 32.8 | 17.3 | 3.09 | 85.4 |
| **TNR-3** | 43,500 | 34.1 | 0.17 | 34.5 | 25,400 | 199 | 28.6 | 15.6 | 3.05 | 71.0 |

Effect of Various Sizes of Leaching Container

*Leachate pH*

Leachate pH differed greatly between scales and different refuse materials (Fig. 54). First, the TNR-1 leachate was typically 2.0 to 3.0 pH units lower in the columns compared to the barrels. This may have been due to the differences in material preparation techniques for the two scales which could have caused differences in the reaction kinetics of the different neutralizers and pyritic-S forms present. The material was ground, and therefore much finer, before being placed in the columns, while the material was placed into the barrels without alteration. In this instance, the grinding process may have exposed internal reactive sulfides while exposing more surface area to weathering processes.

In particular, the TNR-3 refuse material exhibited a very different pattern of reactivity and TDS release in the columns and barrels. For the first 30 cm of cumulative leaching, pH values were similar and stable for both the columns and the barrels (approximately 7.5 to 8.0). However, after 30 cm of cumulative leaching, the pH in the barrel leachates quickly plummeted to 3.5 and continued to slowly drop. In contrast, the leachate pH in the columns stayed relatively stable at just below 8.0.

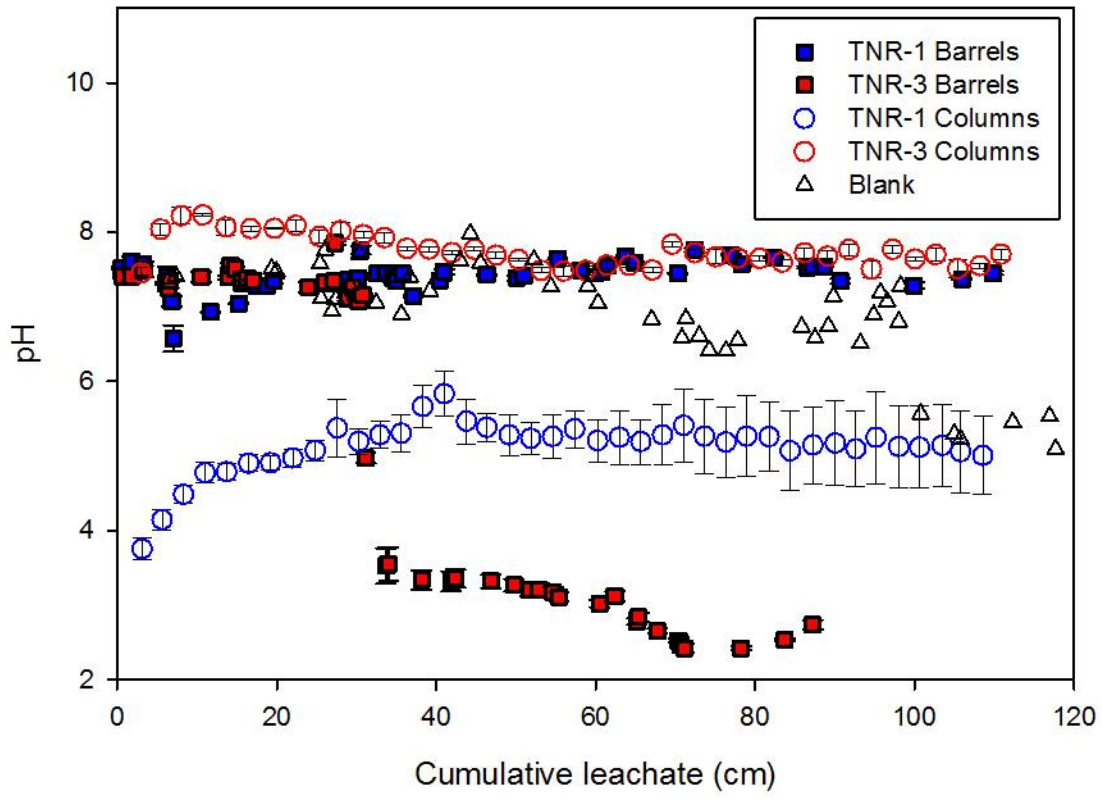


Figure 54. Leachate pH versus cumulative volume eluted for columns and barrels of TNR-1 and TNR-3 refuse material. Values plotted are means (n=3 except for blank n=1) per sample event with one standard error above and below.

It is possible that pyrite oxidation was inhibited in the columns by maintaining a more saturated environment directly adjacent to particle surfaces, while the barrels were able to wet and dry more under natural weather conditions, thus allowing pyrite oxidation to occur and reduce the leachate pH. Another possibility is that the finer particle sizing in the columns allowed more reactive surface area of the neutralizers (carbonates and feldspars) present in the refuse while in the barrels, they were much less reactive for some reason. Regardless, since the columns were also run under overall unsaturated conditions, this large difference was quite unexpected.

*Leachate EC*

Leachate for the TNR-1 columns initially produced very high electrical conductivity (EC) levels (approximately 3250 µS $cm^{-1}$; Fig. 55), while the barrel leachates started at much lower levels (approximately 650 µS $cm^{-1}$). Between 0 and 10 cm of cumulative leachate, the columns EC fell, while the barrel EC rose until the two became similar. After 10 cm of cumulative leachate, the columns continued to drop, while the barrels peaked at approximately 2700 µS $cm^{-1}$ before dropping in similar fashion. Finally, over the last increments of cumulative leachate, the TNR-1 columns and barrels maintained very similar EC values of around 800 µS $cm^{-1}$. Similar to the pH differences discussed earlier for the spoils, the differences in initial leachate EC are likely due to differences in material preparation and size consist.

The TNR-3 leachate EC followed very different patterns in the columns and barrels. The columns initially peaked at approximately 5400 µS $cm^{-1}$, before quickly falling to 1000 µS $cm^{-1}$ by 10 cm of cumulative leachate, and then slowly dropping to 600 µS $cm^{-1}$. The barrel leachate EC also peaked early at approximately 4750 µS $cm^{-1}$, but unlike the columns, the EC fluctuated greatly for the rest of the experiment and remained at much higher overall levels than the other treatments. After peaking in its early leachates, the EC dropped to approximately 2200 µS $cm^{-1}$ at about 10 cm of cumulative leachate. This was followed by a period of wide variability with a general increase over time and an eventual absolute peak of approximately 9,040 µS $cm^{-1}$ for TNR-3 near the end of the study period. As with differences in pH, the significantly higher EC values in the barrels were obviously driven by pyrite oxidation, which was apparently inhibited in the columns.

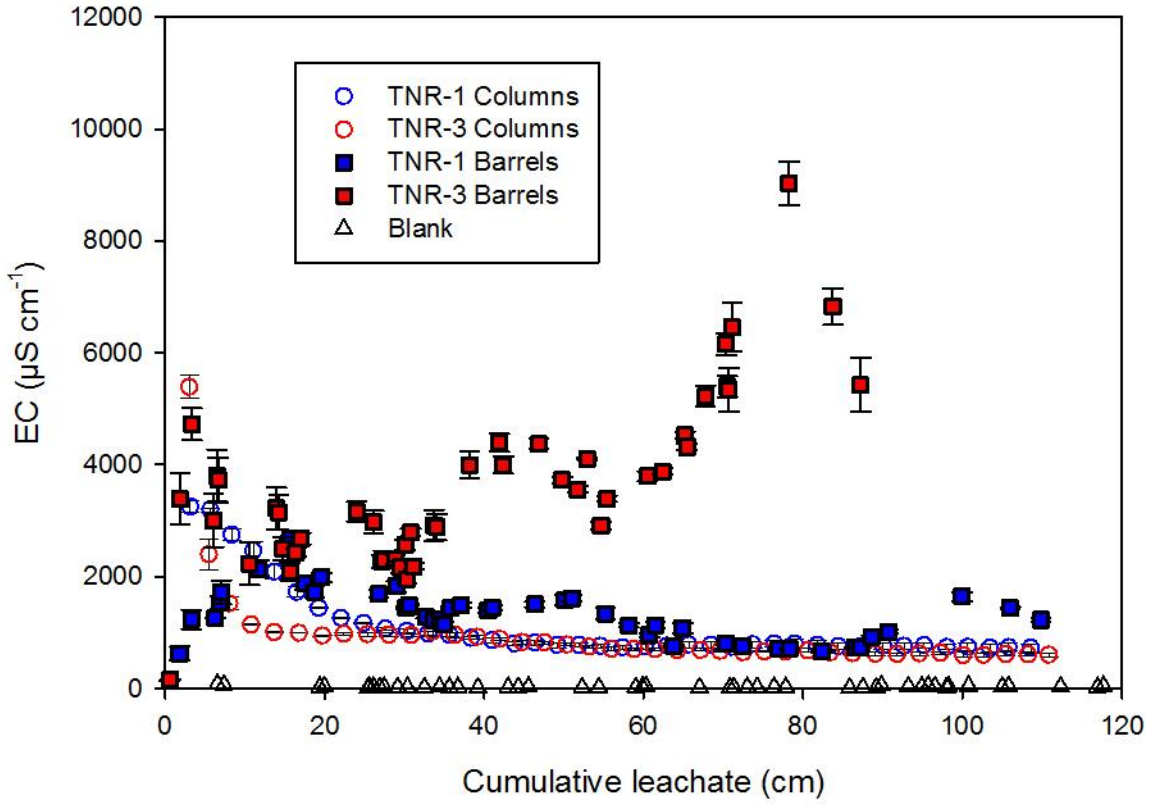


Figure 55. Leachate EC versus cumulative volume eluted for columns and barrels of TNR-1 and TNR-3 refuse material. Values plotted are means (n=3 except for blank n=1) per sample event with one standard error above and below.

*Leachate Bicarbonate*

Bicarbonate levels in the leachates (Fig. 56) varied greatly between the columns and barrels for both materials. First, bicarbonate in the TNR-1 column leachate remained at very low levels (below 5 mg $L^{-1}$) throughout the duration of the study while the barrel leachates fluctuated between 30 mg $L^{-1}$ and 80 mg $L^{-1}$ for the majority of the study. Thus, it appears that the neutralizers present in this material (TNR-1) were much less reactive in the columns and bulk pH remained lower (Fig. 54). For the TNR-3 material, the column leachate produced an early peak

of 275 mg $L^{-1}$ before slowly dropping to 75 mg $L^{-1}$ by the end of the study. The barrels also peaked during the early portion of the study period before dropping, but at significantly lower levels. Between 0 cm and 30 cm of cumulative leachate, bicarbonate fluctuated between 45 mg $L^{-1}$ and 95 mg $L^{-1}$, before dropping to less than 10 mg $L^{-1}$. The drop to very low levels here corresponded with the drop in pH and increase in EC described above; obviously driven by acid-base reactions within the barrels. As discussed above, even though this material appeared to contain a large amount of potential acid neutralizers (CCE = 6.78% or + 68 Mg per 1000 Mg refuse) versus maximum potential acidity (-35 Mg per 1000 material), they were not able to maintain pH control against the rate of S-oxidation at this scale (barrels). However, the neutralizers apparently were able to react more readily at the finer particle size scale and potentially different wetness/humidity conditions in the columns.

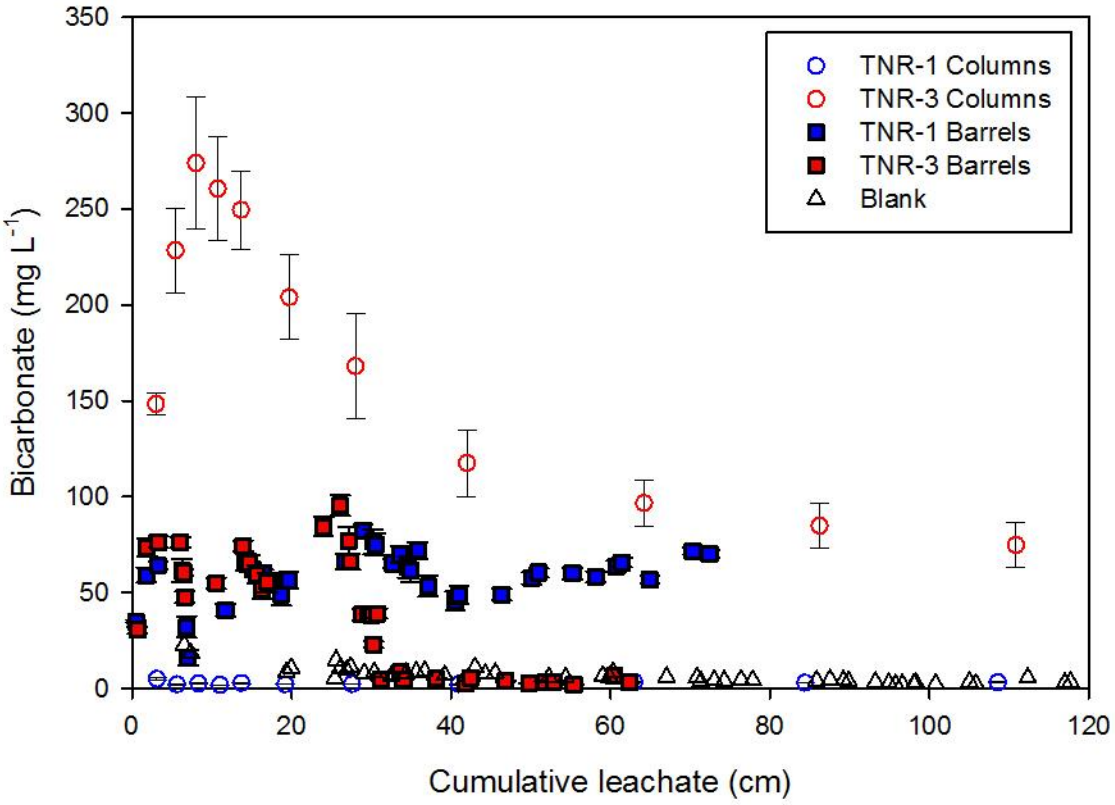


Figure 56. Leachate bicarbonate versus cumulative volume eluted for columns and barrels of TNR-1 and TNR-3 refuse material. Values plotted are means (n=3 except for blank n=1) per sample event with one standard error above and below.

*Leachate Sulfate*

As expected, leachate sulfate patterns (Fig. 57) for both materials closely mirrored EC dynamics over the duration of the study. In the columns, the TNR-1 leachate peaked early at approximately 2200 mg $L^{-1}$, dropped to approximately 600 mg $L^{-1}$ at 30 cm of cumulative leachate, and then declined very slowly for the remainder of the study period. Interestingly, sulfate levels in the barrel leachates were initially very low, and then fluctuated between 250 mg $L^{-1}$ and 950 mg $L^{-1}$ for the duration of the study. Similarly, the TNR-3 column leachates

initially produced a peak sulfate level of approximately 2250 mg $L^{-1}$ before very quickly dropping to 250 mg $L^{-1}$ after 10 cm of cumulative leachate and then leveling off. On the other hand, the TNR-3 barrel leachate fluctuated between 800 mg $L^{-1}$ and 2000 mg $L^{-1}$ from 0 cm to 35 cm of cumulative leachate before reaching its peak sulfate value of approximately 3400 mg $L^{-1}$ at 40 cm of cumulative leachate and remaining above 2500 mg $L^{-1}$ for the remainder of the study. Again, this was likely driven by much more extensive sulfide oxidation in these refuse (TNR-3) barrels in comparison with the other treatments.

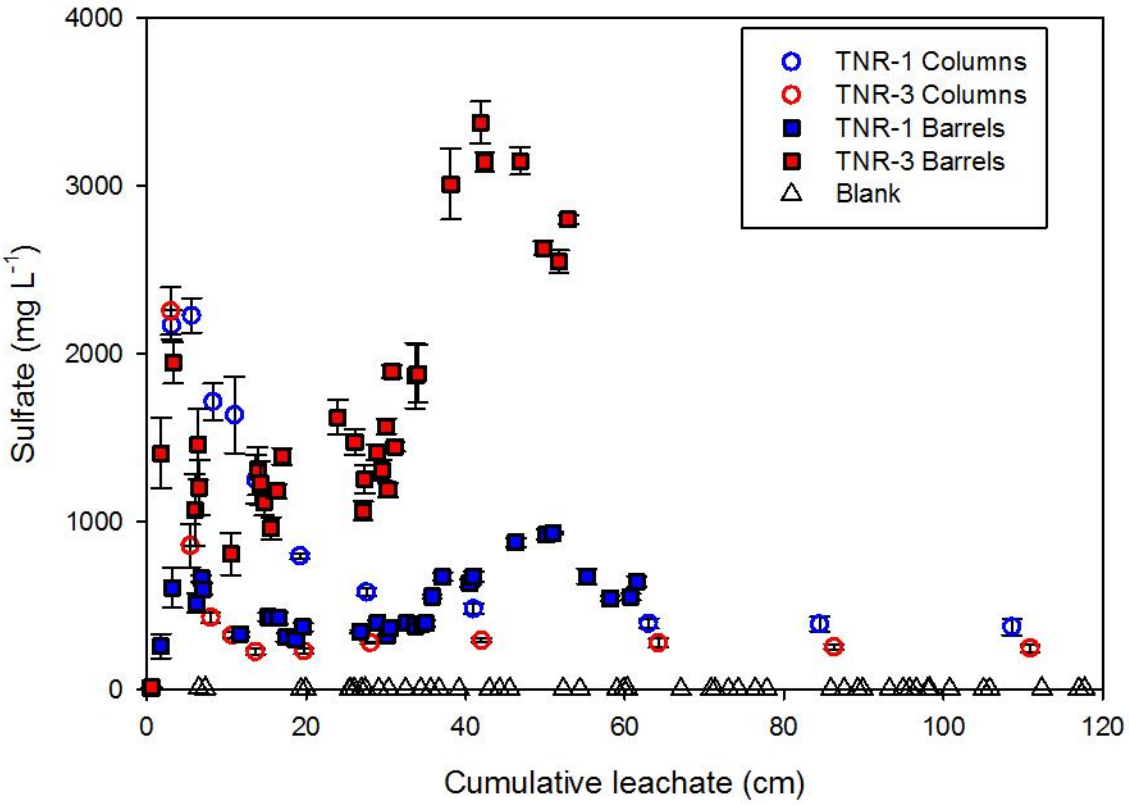


Figure 57. Leachate sulfate versus cumulative volume eluted for columns and barrels of TNR-1 and TNR-3 refuse material. Values plotted are means (n=3 except for blank n=1) per sample event with one standard error above and below.

*Leachate Calcium (Ca)*

There were two major differences in the Ca levels in the TNR-1 leachate from the barrels and columns (Fig. 58). First, the columns peaked with their first leaching event (410 mg $L^{-1}$), while the Ca level was nearly zero for the first leaching event of the barrels. During these initial leaching events and up to 13 cm of cumulative leachate, the column Ca levels dropped while the barrels rose until they were approximately equal at around 260 mg $L^{-1}$. Between 13 cm and 35 cm of cumulative leachate, Ca levels continued to drop in both the columns and barrels at a similar pace. The columns then continued to fall to 60 mg $L^{-1}$ by the end of the study while the barrels exhibited a second peak which reached 245 mg $L^{-1}$.

With the exception of the first few cm of cumulative leachate, the TNR-3 barrel leachates maintained significantly higher Ca levels compared to the TNR-3 column leachates. At approximately 3 cm of cumulative leachate, the columns peaked at 165 mg $L^{-1}$. From there, they fell rapidly to 20 mg $L^{-1}$ by 8 cm of cumulative leachate before slowly rising to approximately 70 mg $L^{-1}$ by the end of the study. Calcium values in the barrel leachates were initially very low, but rose to 330 mg $L^{-1}$ by 3 cm of cumulative leachate. Between 3 cm and 30 cm of cumulative leachate, Ca levels fluctuated between 150 mg $L^{-1}$ and 300 mg $L^{-1}$, before peaking at 425 mg $L^{-1}$ just after 30 cm of cumulative leachate. Towards the end of the study, the barrel leachate contained between 125 mg $L^{-1}$ and 175 mg $L^{-1}$ Ca.

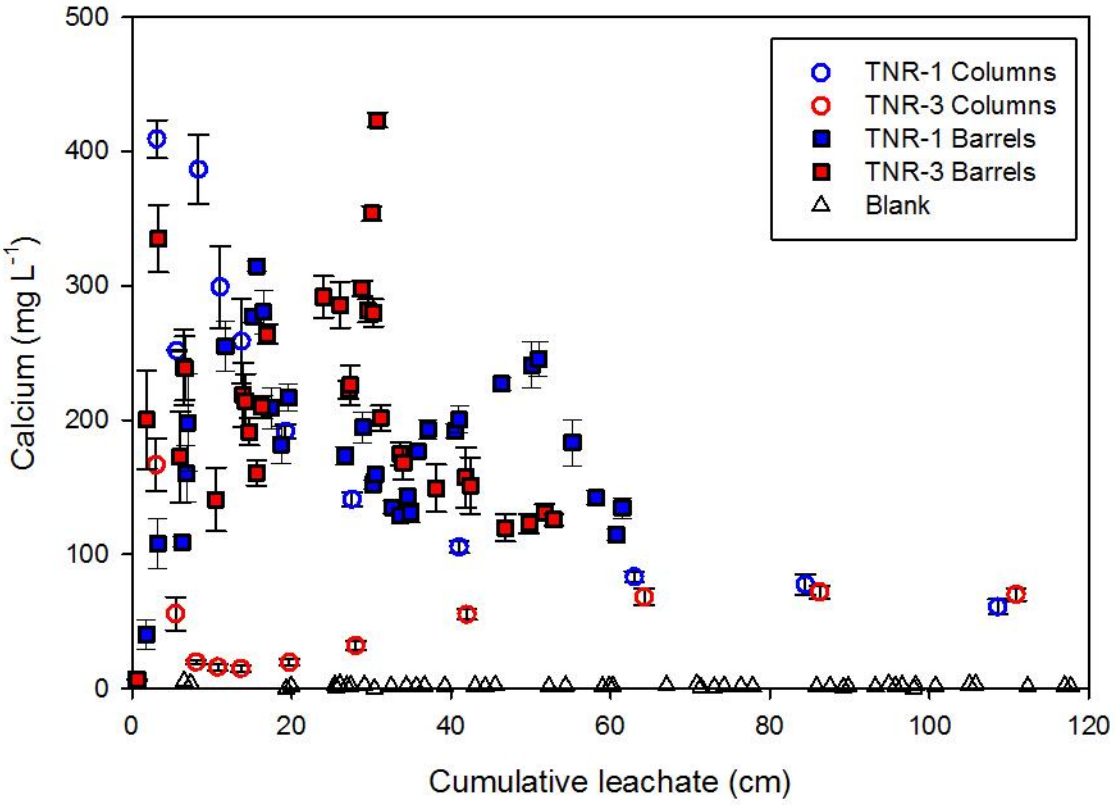


Figure 58. Leachate Ca versus cumulative volume eluted for columns and barrels of TNR-1 and TNR-3 refuse material. Values plotted are means (n=3 except for blank n=1) per sample event with one standard error above and below. Detection limit = 0.01 mg $L^{-1}$.

*Leachate Magnesium (Mg)*

Magnesium levels in the TNR-1 leachate peaked during the initial leaching events (Fig. 59) in the columns (at just above 140 mg $L^{-1}$), but started near detection levels in the barrels. The two scales then converged at approximately 55 mg $L^{-1}$ near 20 cm of cumulative leachate. Between 20 cm and 30 cm of cumulative leachate, Mg levels fell in both scales to approximately 35 mg $L^{-1}$. After this, the columns continued to slowly fall to 18 mg $L^{-1}$ by the end of the study, while the barrels exhibited a peak that reached 58 mg $L^{-1}$ at 50 cm of cumulative leachate.

Towards the end of the study, the barrels appeared to be converging with the columns again between 25 mg $L^{-1}$ and 30 mg $L^{-1}$ at just over 60 cm of cumulative leachate.

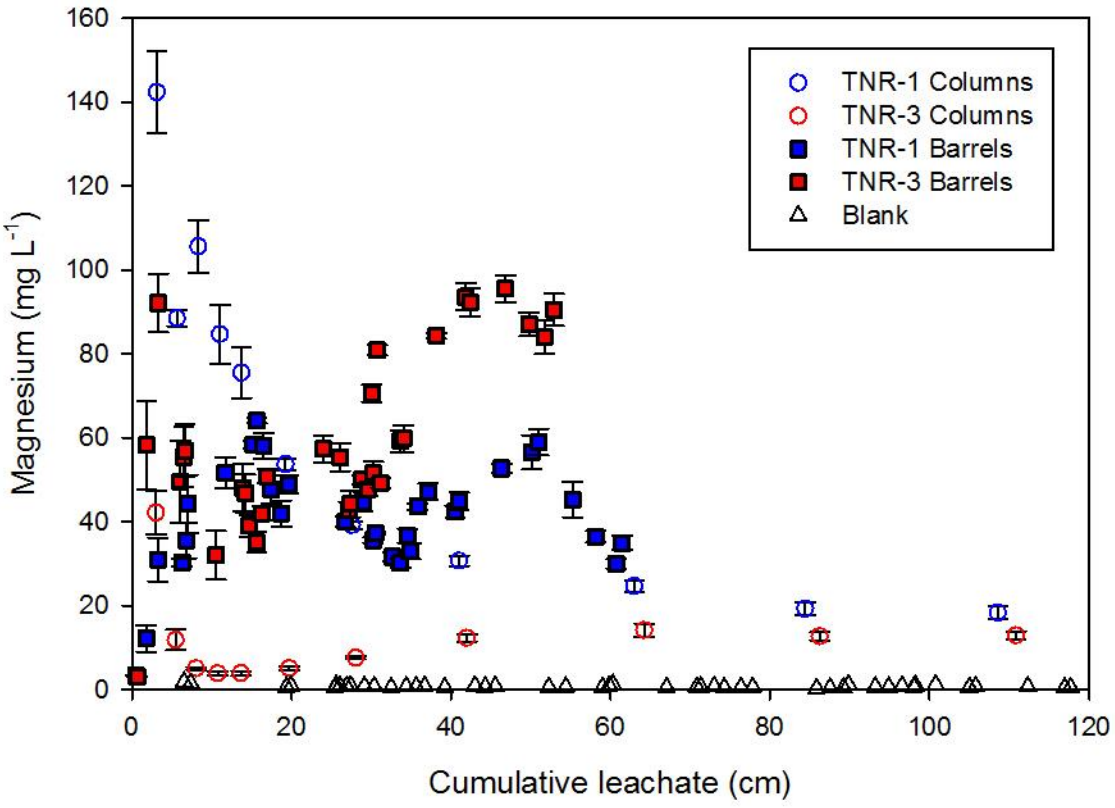


Figure 59. Leachate Mg versus cumulative volume eluted for columns and barrels of TNR-1 and TNR-3 refuse material. Values plotted are means (n=3 except for blank n=1) per sample event with one standard error above and below. Detection limit = 0.005 mg $L^{-1}$.

The leachate from the TNR-3 columns and barrels exhibited peak Mg levels at approximately 3 cm of cumulative leachate. The barrels then peaked again at significantly higher (92 mg $L^{-1}$) levels than the columns (42 mg $L^{-1}$). However, after this point, Mg release patterns differed greatly. The columns quickly dropped to 5 mg $L^{-1}$ before 10 cm of cumulative leachate and fluctuated between this level and 15 mg $L^{-1}$ for the remainder of the study. On the

other hand, the barrels fell to between 35 mg $L^{-1}$ and 55 mg $L^{-1}$ between 3 cm and 30 cm of cumulative leachate before rising quickly to a second peak of 95 mg $L^{-1}$ near the end of the study.

*Leachate Potassium (K)*

Overall, leachate K levels were much higher for both scales for the TNR-1 refuse when compared to TNR-3 (Fig. 60) even though both materials contained similar levels of total K (Table 5) as discussed earlier. With the TNR-1 leachate, K levels rose to a peak during the first few leaching events for both the columns and barrels. The columns peaked at approximately 56 mg $L^{-1}$ at 8 cm of cumulative leachate, while the barrels reached a peak of 45 mg $L^{-1}$ at 15 cm of cumulative leachate. After their peaks, both the columns and the barrels K levels slowly fell, while the barrels maintained about 10 mg $L^{-1}$ higher levels. Once they reached just over 60 cm of cumulative leachate (at the barrels' final measured leaching event), the two scales were approximately equal at 20 mg $L^{-1}$.

The K levels in the TNR-3 leachates followed similar patterns in the columns and barrels, but overall levels were lower than for TNR-1. While the barrels started out at low levels, by 3 cm of cumulative leachate, they were nearly equal at 27 mg $L^{-1}$. After this point, the columns fell to around 10 mg $L^{-1}$ and continued to fluctuate around this level. While the barrels also fell to 10 mg $L^{-1}$, they subsequently rose to approximately 15 mg $L^{-1}$ until just after 30 cm of cumulative leachate, where after they then quickly dropped to approximately 6 mg $L^{-1}$.

The strong overall differences in K elution from these two materials more than likely indicate a major difference in their weatherable mineral content. A higher content of more weatherable K-feldspars or micas (or both) in the TNR-1 refuse is possible, but the total-mass K

content of the two materials (TNR-1 = 11,400 vs. TNR-3 = 10,600 mg $kg^{-1}$; Table 5) was not that different.

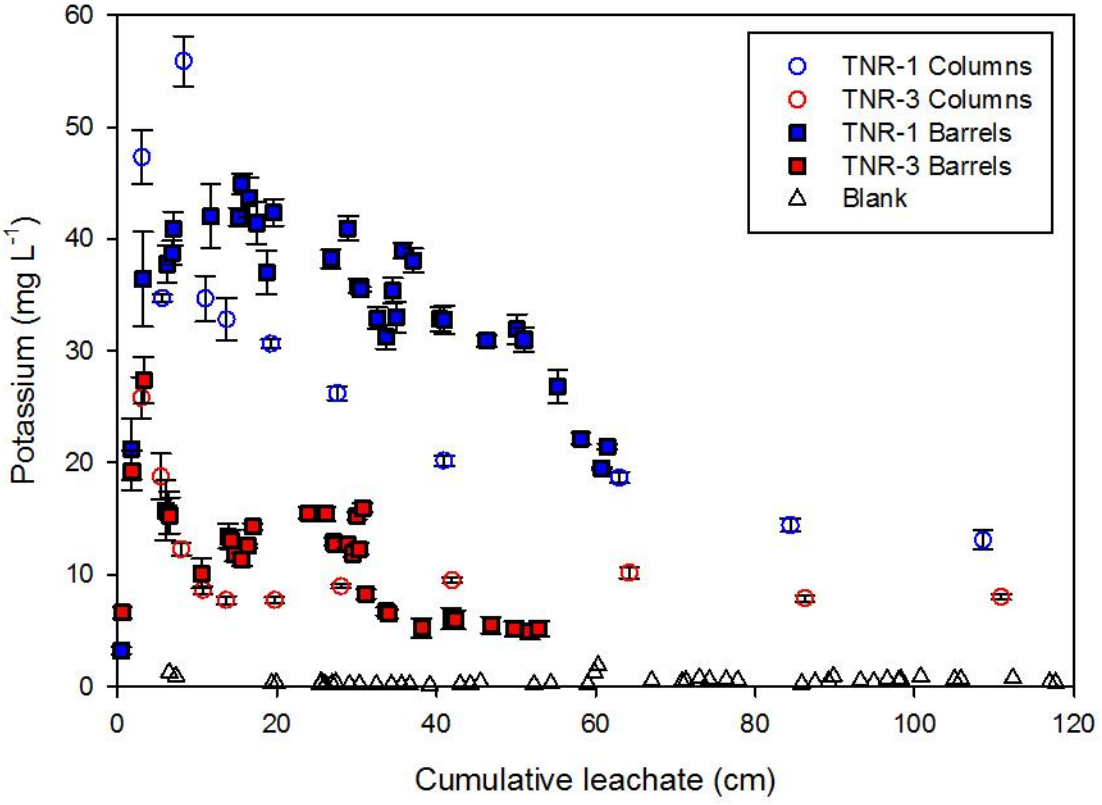


Figure 60. Leachate K versus cumulative volume eluted for columns and barrels of TNR-1 and TNR-3 refuse material. Values plotted are means (n=3 except for blank n=1) per sample event with one standard error above and below. Detection limit = 0.005 mg $L^{-1}$.

*Leachate Sodium (Na)*

In contrast to K, initial mass Na levels in the two refuse materials (TNR-1 = 550 vs. TNR-3 = 945 mg $kg^{-1}$; Table 5) were very different and produced strong differences at both the column and barrel scale. Sodium levels in leachates from the TNR-1 columns (Fig. 61) and barrels were similar and quite low throughout the study. While the barrels started with very low

levels in the first two leaching events, by 3 cm of cumulative leachate, the two scales were nearly equal at approximately 75 mg $L^{-1}$. From this point, leachate Na at both scales slowly decreased for the remainder of the study period to below 50 mg $L^{-1}$. Initial Na levels in the TNR-3 leachates were much higher than TNR-1 and peaked at 3 cm of cumulative leachate for both the columns (at 900 mg $L^{-1}$) and the barrels (at 700 mg $L^{-1}$). From this point, Na levels in both scales decreased through the end of the study. The column release pattern was much more uniform, while the barrels were more variable, but still produced similar values. By 50 cm of cumulative leachate, both the columns and the barrels were similar at approximately 60 mg $L^{-1}$.

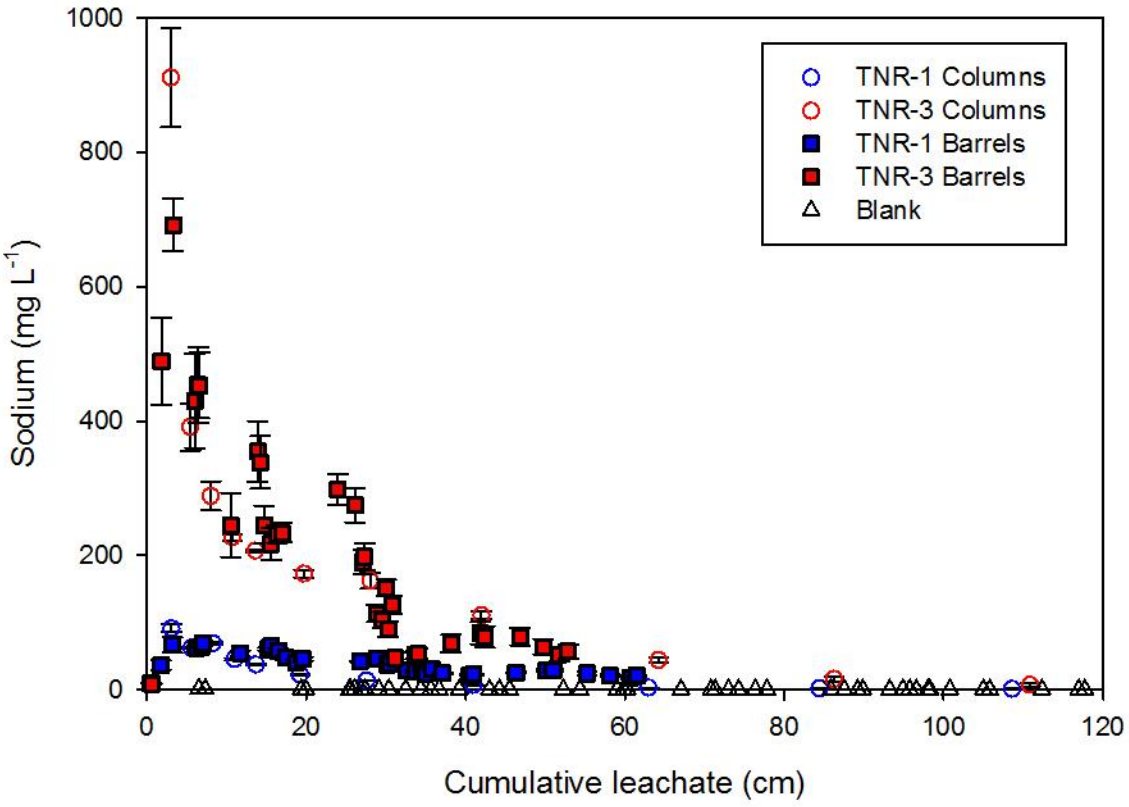


Figure 61. Leachate Na versus cumulative volume eluted for columns and barrels of TNR-1 and TNR-3 refuse material. Values plotted are means (n=3 except for blank n=1) per sample event with one standard error above and below. Detection limit = 0.005 mg $L^{-1}$.

*Leachate Iron (Fe)*

The TNR-1 leachate exhibited low and similar Fe levels in both the columns and barrels (Fig. 62) with the exception of the first leaching event. The columns generated an initially high value at just over 30 mg $L^{-1}$ before immediately dropping below 0.1 mg $L^{-1}$ and remaining below this level for the remainder of the study. For TNR-1, the barrels maintained low Fe levels for the duration of the study. Iron levels in the leachate peaked at around 1.5 mg $L^{-1}$ at just over 10 cm of cumulative leachate. The single initial high value for the column leachates more than likely reflected elution of fine colloidal sized particulate Fe rather than dissolved Fe per se. Parker (2013) reported similar early and often erratic peaks for a number of elements in early leachates for this same mine spoil in a related study. The TNR-3 column leachate maintained very low Fe levels (less than 0.02 mg $L^{-1}$) for the duration of the study. On the other hand, while the barrel leachate remained below 1.5 mg $L^{-1}$ through 35 cm of cumulative leachate, once active sulfide oxidation occurred, Fe levels rapidly increased to just over 12 mg $L^{-1}$ and remained just below this level for the remainder of the study period (> 50 cm cumulative leachate).

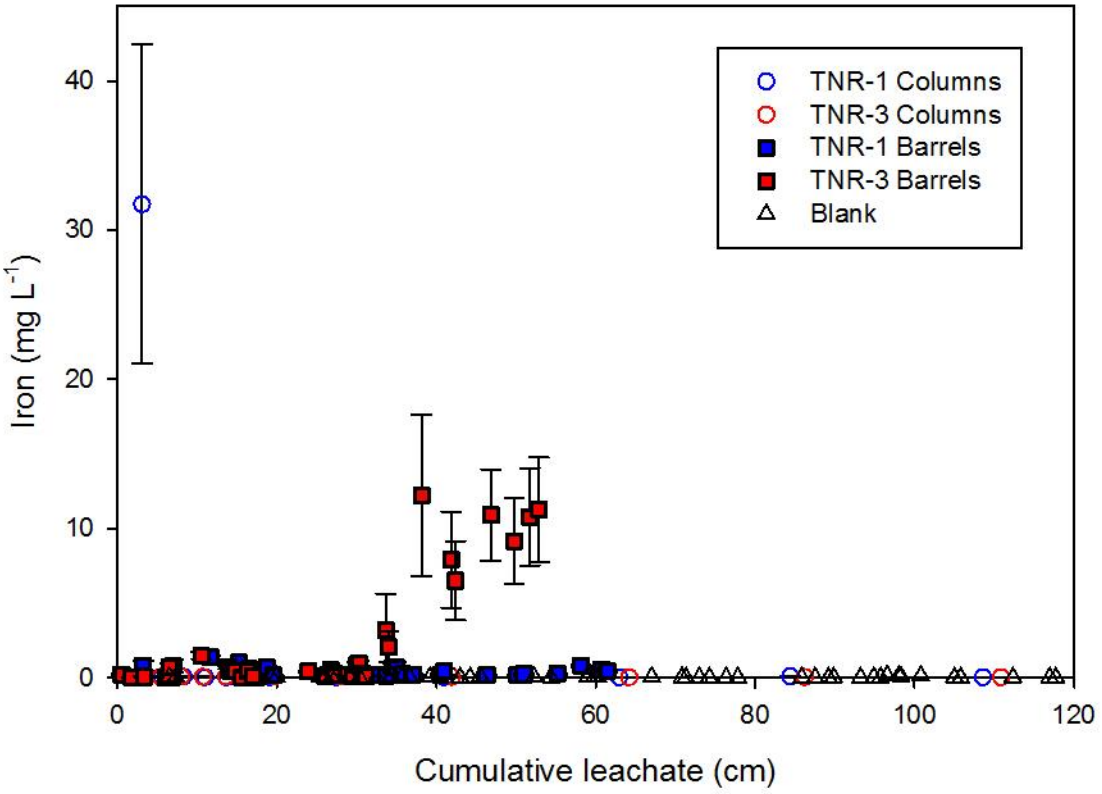


Figure 62. Leachate Fe versus cumulative volume eluted for columns and barrels of TNR-1 and TNR-3 refuse material. Values plotted are means (n=3 except for blank n=1) per sample event with one standard error above and below. Detection limit = 5.0 µg $L^{-1}$.

*Leachate Manganese (Mn)*

Manganese levels in the TNR-1 column leachate (Fig. 63) were significantly higher than the barrels. They peaked during the first leaching event at just above 5 mg $L^{-1}$ and then decreased rapidly to 1.4 mg $L^{-1}$ by 20 cm of cumulative leachate and then to 0.3 by the end of the study (108 cm of cumulative leachate). On the other hand, Mn levels in the barrel leachate started very low, peaked at around 0.3 mg $L^{-1}$ at about 7 cm of cumulative leachate, and then fell to even lower levels through the remainder of the study. While the initial high values for Mn

here were also probably influenced by colloidal particle migration with first leachates, their overall higher levels of elution and prolonger release indicated some other mechanism leading to release of Mn to the solution phase in these columns.

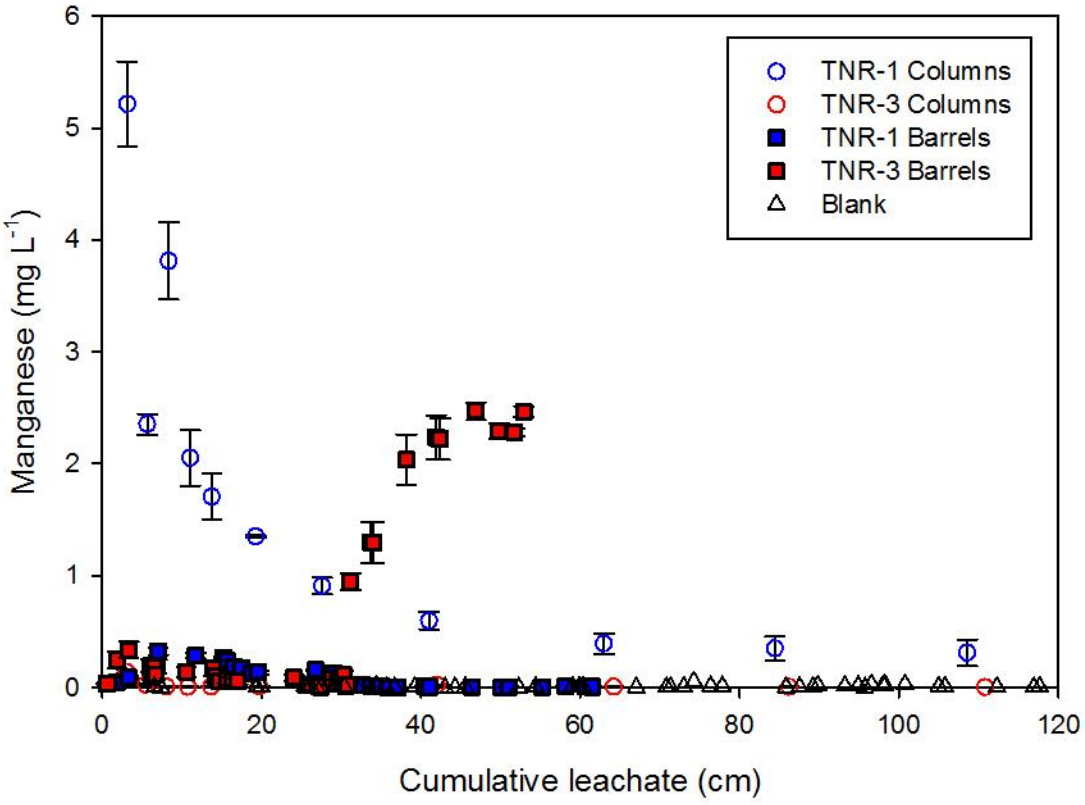


Figure 63. Leachate Mn versus cumulative volume eluted for columns and barrels of TNR-1 and TNR-3 refuse material. Values plotted are means (n=3 except for blank n=1) per sample event with one standard error above and below. Detection limit = 5.0 µg $L^{-1}$.

The Mn levels in the TNR-3 columns peaked during the first leaching event at very low levels of about 0.15 mg $L^{-1}$ and fell throughout the rest of the study. On the other hand, Mn levels in the barrels fluctuated between 0.05 mg $L^{-1}$ and 0.35 mg $L^{-1}$ from 0 cm and 30 cm of cumulative leachate followed by rapid rise to a peak of almost 2.5 mg $L^{-1}$ by the end of the study (just over 50 cm of cumulative leachate) that was associated with sulfide oxidation and pH

reduction induced solubility effects. Evangelou (1995) stated that sulfide oxidation in low oxygen environments can produce large amounts of soluble Mn, as Mn acts as an oxidizing agent. However, the overall Mn levels in these very acidic leachates (<pH 4.0) were relatively low compared to values often seen on actual coal mine discharge sites.

*Leachate Aluminum (Al)*

The TNR-1 leachate from the columns and the barrels displayed similar levels of Al release (Fig. 64) for the majority of the study. The major difference between the two was the initial peak of about 4.5 mg $L^{-1}$ in the columns which was absent in the barrels. As noted above, Parker (2013) also noted early Al release from spoils in a related study which was attributed to an early flush of colloidal materials from the freshly abraded spoil surfaces.

After approximately 10 cm of cumulative leachate, both the columns and the barrels remained below 1.0 mg $L^{-1}$ Al. In contrast, the TNR-3 columns and the barrels produced very different Al release patterns. In the columns, Al levels in the leachate did not rise above 0.1 mg $L^{-1}$, but in the barrels there was a sharp rise beginning at 30 cm of cumulative leachate which peaked near 15.0 mg $L^{-1}$ at the end of the study after just more than 50 cm of cumulative leachate. This obviously coincided with the net acidification of the columns and associated large increases in Al weathering release and solubility.

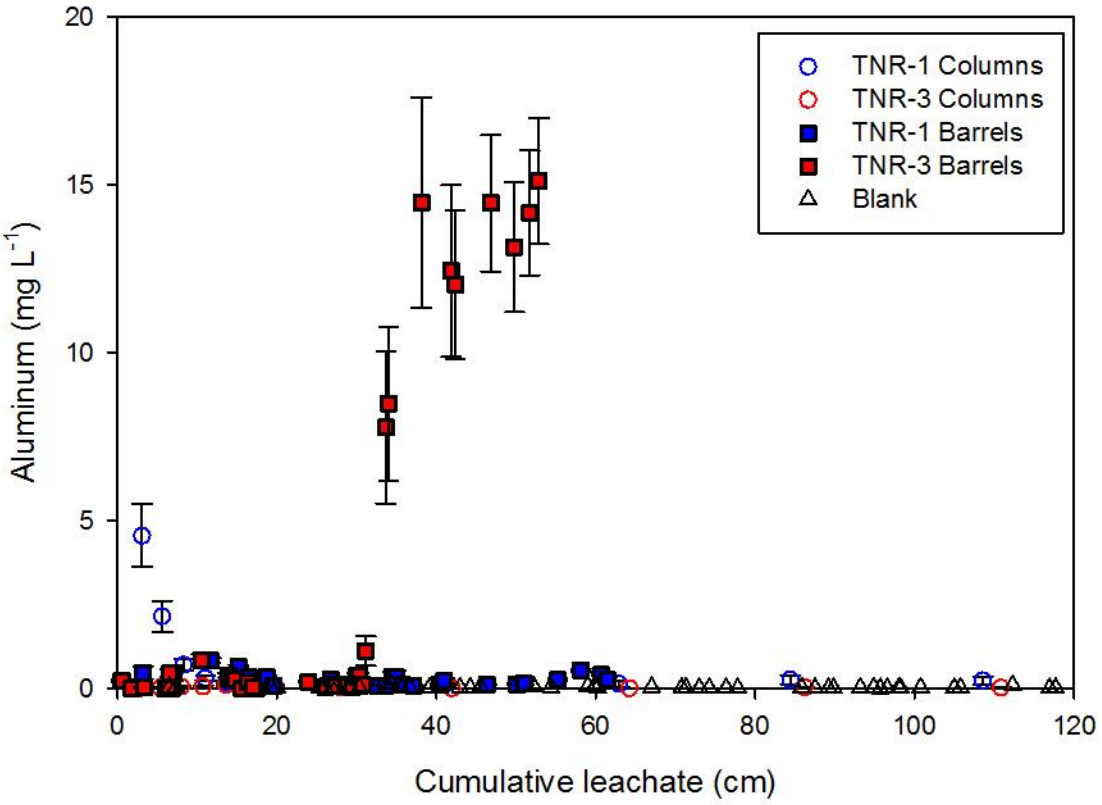


Figure 64. Leachate Al versus cumulative volume eluted for columns and barrels of TNR-1 and TNR-3 refuse material. Values plotted are means (n=3 except for blank n=1) per sample event with one standard error above and below. Detection limit = 1.0 µg $L^{-1}$.

*Leachate Selenium (Se)*

Both refuse materials contained approximately 3.0 mg $kg^{-1}$ total Se (Table 6) but their Se leaching patterns varied strongly. Selenium levels in the TNR-1 barrel leachate (Fig. 65) were significantly higher than Se levels in the TNR-1 columns for the majority of the study. The columns peaked early at 600 µg $L^{-1}$ before dropping to 130 µg $L^{-1}$ at 15 cm of cumulative leachate and then slowing dropping to around 20 µg $L^{-1}$ by the end of the study. Initially, relatively low levels of Se leached from the barrels, but they quickly peaked at 700 µg $L^{-1}$ after

just 5 cm of cumulative leachate. Selenium levels in the barrel leachates then dropped to approximately 250 µg $L^{-1}$ before peaking again at just over 600 µg $L^{-1}$ and then dropping again to approximately 250 µg $L^{-1}$ before the end of the study. Several mechanisms for the higher release of Se from barrels vs. the columns are possible. The leachate pH from the barrels was consistently higher (by 2 to 3 units) than the columns, so simple pH x solubility controls could have at least partially account for the differences. However, the secondary time-lagged peak of Se release from TNR-1 indicates that some sort of longer term weathering event, perhaps refuse fragment slaking or delayed oxidation of more recalcitrant selenides were also involved.

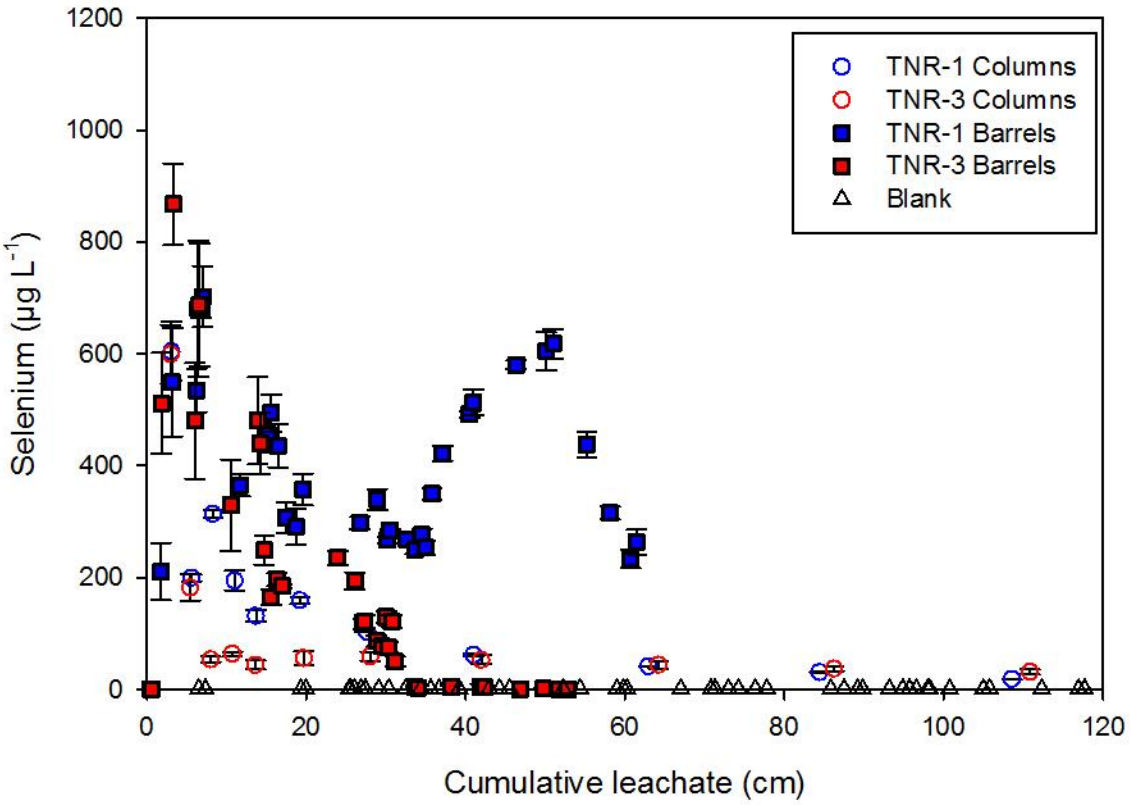


Figure 65. Leachate Se versus cumulative volume eluted for columns and barrels of TNR-1 and TNR-3 refuse material. Values plotted are means (n=3 except for blank n=1) per sample event with one standard error above and below. Detection limit = 0.8 µg $L^{-1}$.

On the other hand, the TNR-3 leachate from the columns and barrels exhibited similar patterns of Se release. However, the columns leachate produced a lower peak and more rapid drop in Se levels. The columns peaked at approximately 600 µg $L^{-1}$, dropped to 50 µg $L^{-1}$ by 8 cm of cumulative leachate, and then stabilized. The barrel leachate produced an early peak of approximately 875 µg $L^{-1}$, followed by a steady drop to below the detection limit of 0.8 µg $L^{-1}$ by 30 cm of cumulative leachate. In strong contrast to TNR-1, this material did not produce the time-lagged secondary peak of Se release, even though it contained essentially the same initial total Se mass (~3 mg $kg^{-1}$). Thus, the form or mineral structure location of the Se probably differed.

Overall, it should be noted that the levels of Se release observed here over the first 40 to 60 cm of leaching were quite high relative to the current surface water standard (5 µg $L^{-1}$). It is also clear that the majority of total Se in these materials appears to be highly reactive, is readily oxidized and mobile, and elutes quite rapidly.

*Leachate Arsenic (As)*

Initial mass As levels in TNR-1 (14 mg $kg^{-1}$; Table 6) were considerably lower than for TNR-3 (34 mg $kg^{-1}$) and this appeared to strongly affect the barrel leachates, but not the columns. The TNR-1 leachates contained As levels below the detection limit of 0.3 µg $L^{-1}$ in both the columns and barrels (Fig. 66) for the majority of the study. One leaching event in the columns (at approximately 11 cm of cumulative leachate) measured approximately 0.6 µg $L^{-1}$. The TNR-1 leachate from the barrels produced measureable levels between approximately 35 cm and 40 cm of cumulative leachate, but never exceeded 0.5 µg $L^{-1}$.

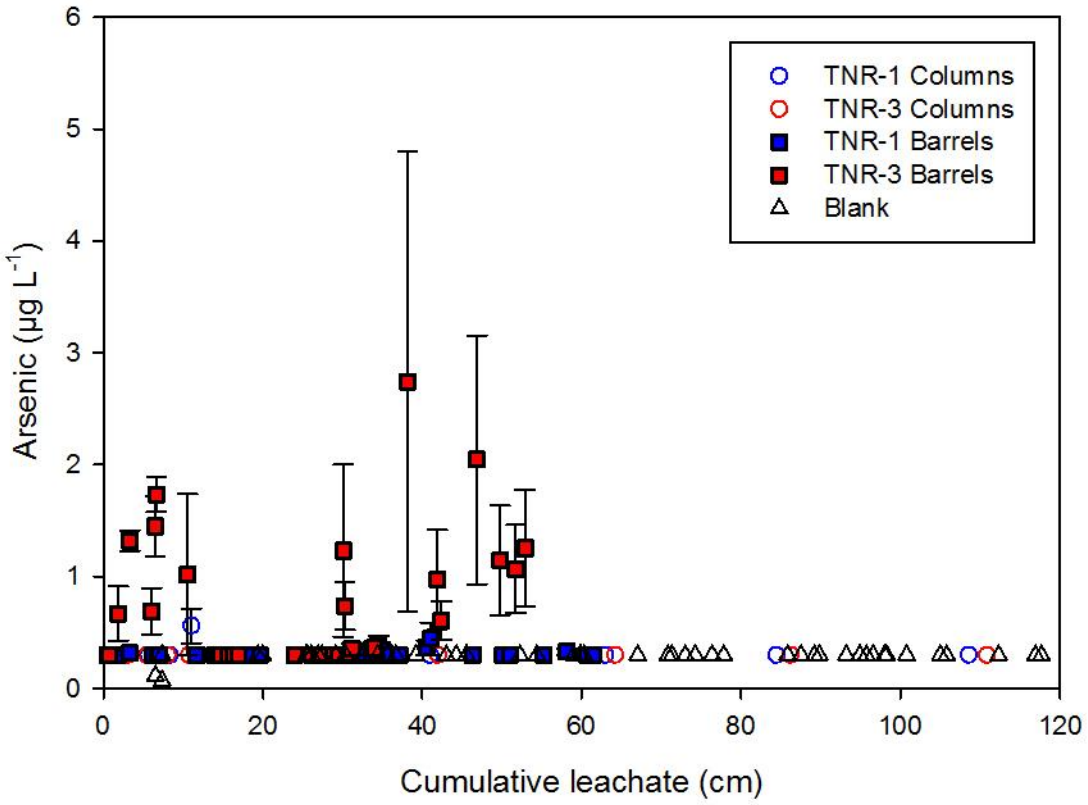


Figure 66. Leachate As versus cumulative volume eluted for columns and barrels of TNR-1 and TNR-3 refuse material. Values plotted are means (n=3 except for blank n=1) per sample event with one standard error above and below. Detection limit = 0.3 µg $L^{-1}$.

However, there were large differences in As levels in the TNR-3 leachate between the columns and barrels. While the columns remained below the detection limit for the duration of the study, the barrels registered quantifiable and much higher levels of As during two extended intervals. Just after 0 cm through 10 cm of cumulative leachate, the barrels produced between 0.7 µg $L^{-1}$ and 1.7 µg $L^{-1}$ of As. Also, between 30 cm and the end of the study, the barrels produced values between 0.6 µg $L^{-1}$ and 2.7 µg $L^{-1}$, with the peak occurring at 38 cm of cumulative leachate. The As values measured from the barrel leachate often fluctuated greatly from measurement to measurement, and varied greatly among replications for a given event. As

with several of the other trace elements, As release from the TNR-3 material was most likely directly driven by sulfide oxidation. This is due to the chalcophilic nature of As (McBride, 1994).

*Leachate Cadmium (Cd)*

Total Cd was very low (<0.3 mg $kg^{-1}$; Table 6) in both refuse materials, but Cd levels in the leachate (Fig. 67) were very different between scales for both refuse materials. The TNR-1 columns exhibited significantly higher Cd levels for the duration of the study. They peaked during the first leaching event at just less than 25 µg $L^{-1}$, before rapidly dropping off to and stabilizing at approximately 3 µg $L^{-1}$. On the other hand, the barrel Cd levels peaked at 1 µg $L^{-1}$ and often hovered just above the detection limit of 0.1 µg $L^{-1}$. Cadmium is very insoluble at high pH (>7.0) in the presence of carbonates and the TNR-1 columns were considerably more acidic than the barrels. The TNR-3 column leachates exhibited Cd levels at or below the detection limit for the duration of the study. The barrel leachate fluctuated at very low values between the detection limit and approximately 0.5 µg $L^{-1}$ Cd between 0 and 35 cm of cumulative leachate. However, just after 30 cm of cumulative leachate, Cd values began to rise and then stabilized at just over 5 µg$L^{-1}$ for the remainder of the study. The higher value at ~30 cm appears to be an outlier, however.

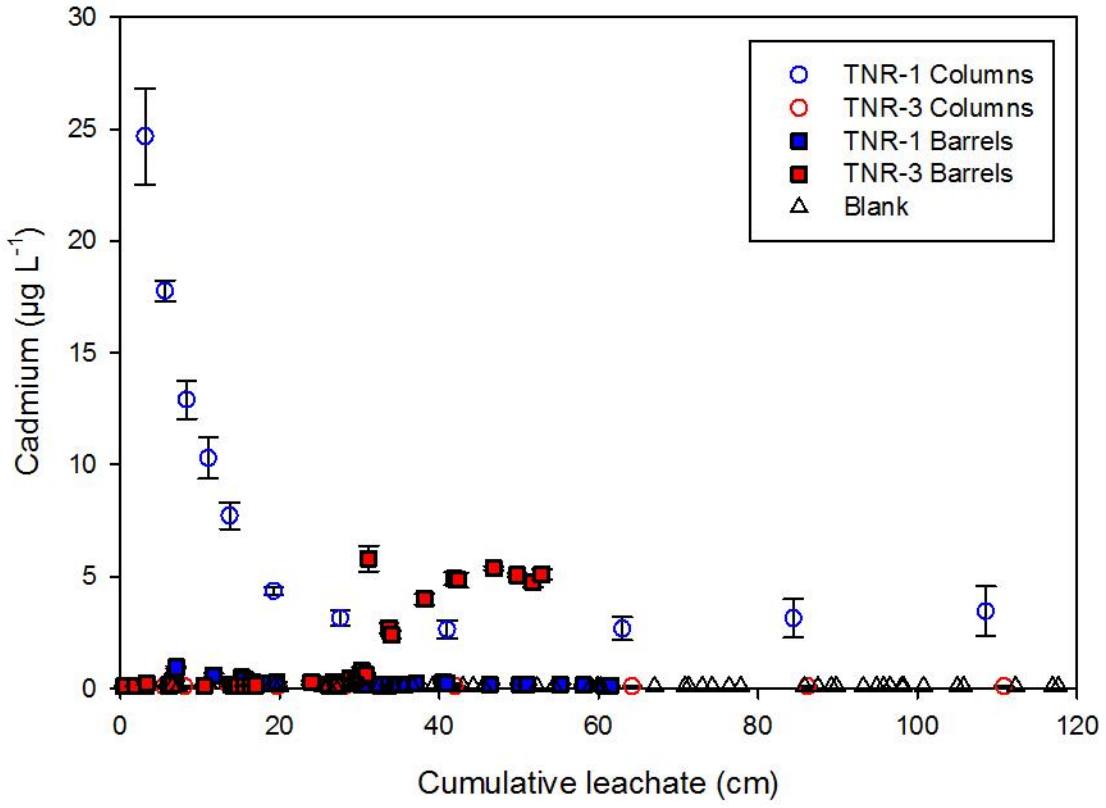


Figure 67. Leachate Cd versus cumulative volume eluted for columns and barrels of TNR-1 and TNR-3 refuse material. Values plotted are means (n=3 except for blank n=1) per sample event with one standard error above and below. Detection limit = 0.1 µg $L^{-1}$.

*Leachate Copper (Cu)*

The TNR-1 columns released significantly more Cu than the barrels (Fig. 68). Copper levels in the column leachate peaked at approximately 265 µg $L^{-1}$ during the first leaching event and quickly dropped to and stabilized at around 10 µg $L^{-1}$ by 15 cm of cumulative leachate. On the other hand the TNR-1 barrel leachate maintained very low Cu levels and fluctuated between the detection limit of 0.6 µg $L^{-1}$ and 4 µg $L^{-1}$. Per earlier comments on Al, Cu levels from the columns may have been due to the initial flush of colloidal materials since pH and sulfide

oxidation interactions were not apparent via sulfate or Fe release. The TNR-3 column leachate Cu peaked at just over 3 µg $L^{-1}$ during the first leaching event and then fluctuated between this value and the detection limit for the remainder of the study. In contrast, the barrels maintained very low values of less than 1 µg $L^{-1}$ through 30 cm of cumulative leachate before beginning to rapidly rise at 35 cm of cumulative leachate and peaking at 235 µg $L^{-1}$ at the end of the study (just over 50 cm cumulative leachate). Again, trace metal release here was likely driven by sulfide oxidation and the dramatic drop in pH.

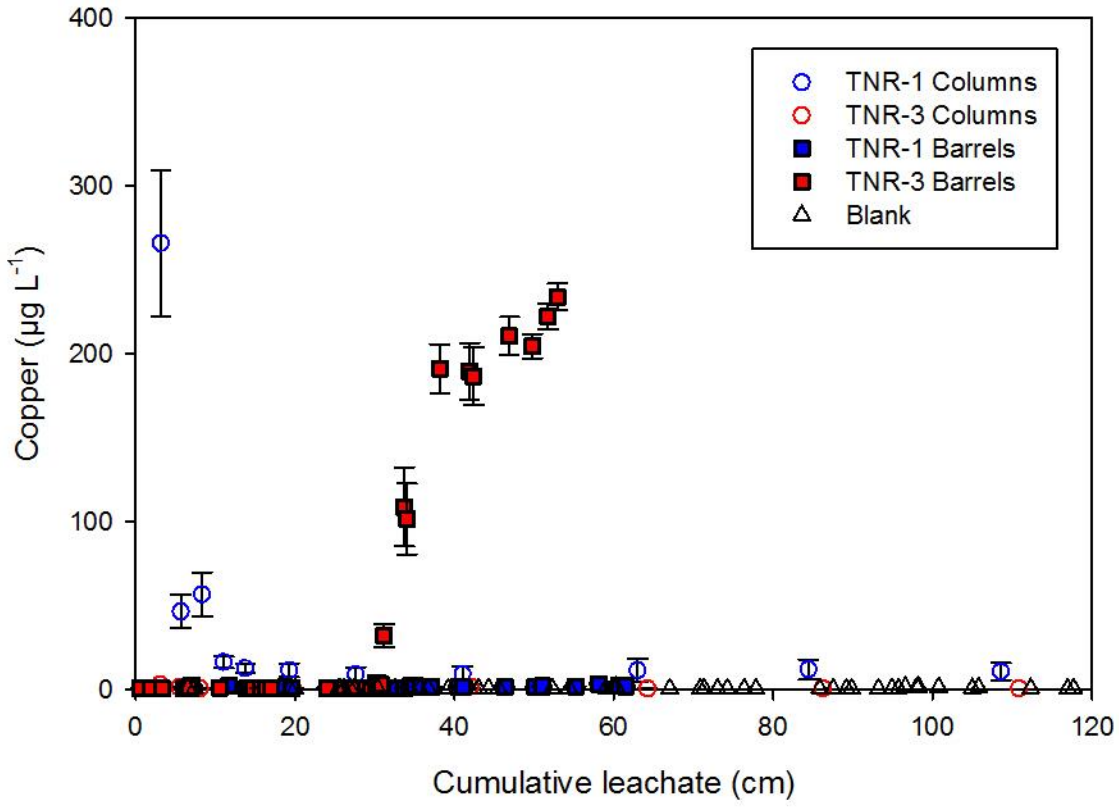


Figure 68. Leachate Cu versus cumulative volume eluted for columns and barrels of TNR-1 and TNR-3 refuse material. Values plotted are means (n=3 except for blank n=1) per sample event with one standard error above and below. Detection limit = 0.6 µg$L^{-1}$.

*Leachate Nickel (Ni)*

Nickel levels in the TNR-1 leachate (Fig. 69) peaked in the columns at almost 1600 µg $L^{-1}$ before falling to below 200 µg $L^{-1}$by 30 cm of cumulative leachate and remaining below this level for the remainder of the study. Nickel levels in the barrels were significantly lower and never reached levels higher than 50 µg $L^{-1}$. The higher and more prolonged release of Ni from the TNR-1 columns was most likely due to the lower pH in that system vs. the barrels.

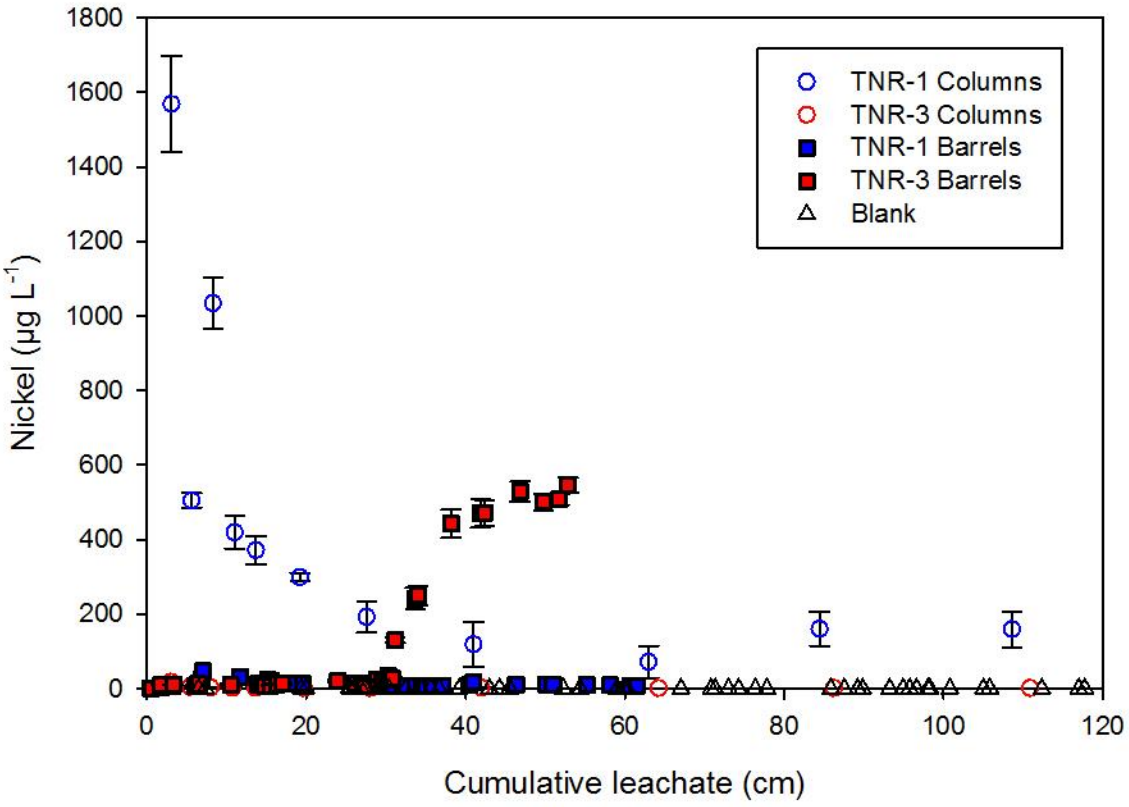


Figure 69. Leachate Ni versus cumulative volume eluted for columns and barrels of TNR-1 and TNR-3 refuse material. Values plotted are means (n=3 except for blank n=1) per sample event with one standard error above and below. Detection limit = 0.3 µg $L^{-1}$.

The Ni levels in the TNR-3 leachates remained at very low levels in the columns and never rose higher than 20 µg $L^{-1}$. Likewise, the barrel Ni levels remained below 20 µg $L^{-1}$

through 30 cm of cumulative leachate, but then rose to between 450 µg $L^{-1}$ and 550 µg $L^{-1}$ through 50 cm of cumulative leachate. Again, the onset of sulfide oxidation and associated pH reduction was accompanied by increased Ni release and solubility for TNR-3.

*Leachate Lead (Pb)*

Similar to Ni, Pb levels in the TNR-1 leachate (Fig. 70) peaked at initially significantly higher values in the columns compared to the barrels. The columns peaked at approximately 18 µg $L^{-1}$, and then quickly fell below 2 µg $L^{-1}$ by 10 cm of cumulative leachate where they remained for the remainder of the study. On the other hand, the barrels did not exhibit a significant initial peak, but rather fluctuated between 0.5 µg $L^{-1}$ and 2.5 µg $L^{-1}$ for the duration of the study. The TNR-3 column leachate Pb levels remained below the detection limit of 0.5 µg $L^{-1}$ for the duration of the study, presumably due to high pH. In contrast, barrel leachate Pb levels fluctuated between the detection limit and 2 µg $L^{-1}$ before rapidly rising at 30 cm of cumulative leachate to a peak of 17 µg $L^{-1}$ at 45 cm of cumulative leachate. The Pb levels then remained above 10 µg $L^{-1}$ in the barrels through the conclusion of the study, but exhibited very high variance between and within sampling events.

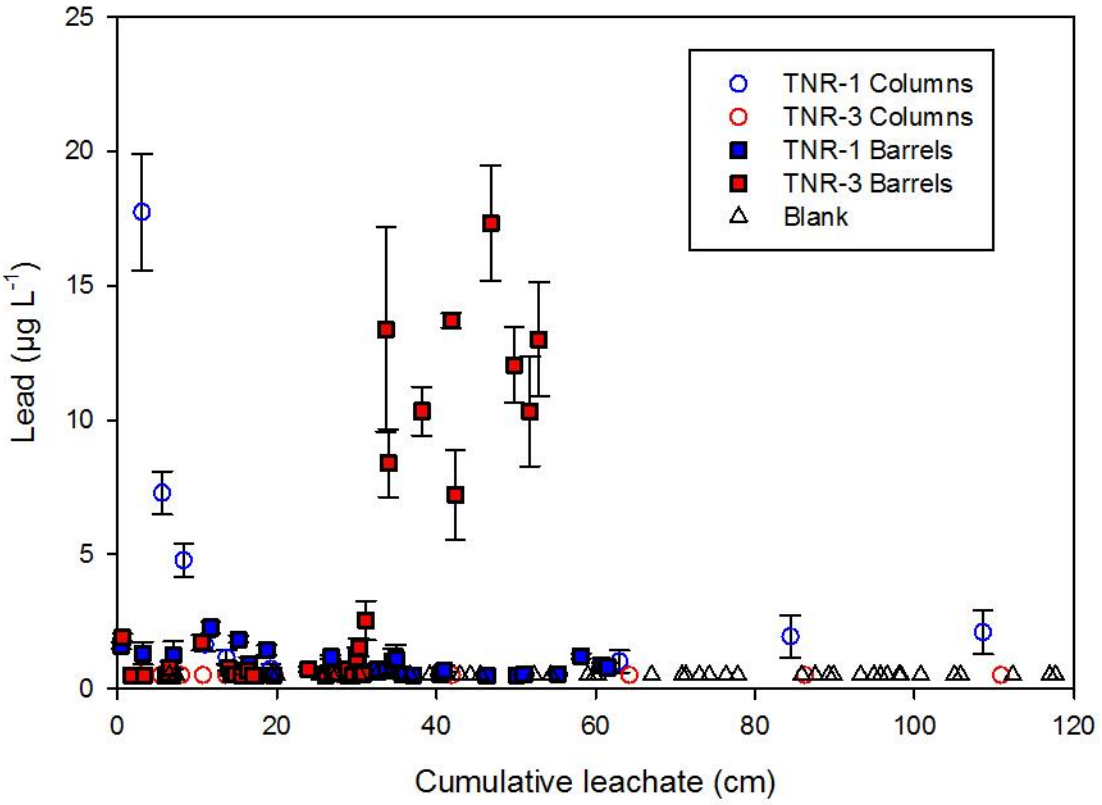


Figure 70. Leachate Pb versus cumulative volume eluted for columns and barrels of TNR-1 and TNR-3 refuse material. Values plotted are means (n=3 except for blank n=1) per sample event with one standard error above and below. Detection limit = 0.5 µg $L^{-1}$.

*Leachate Zinc (Zn)*

Overall treatment effects for Zn were similar to those reported above for Ni and Pb. Zinc levels in the TNR-1 leachate (Fig. 71) were very different between the columns and the barrels, again most likely due to pH solubility effects in the more acidic columns. The column leachate Zn peaked during the first leaching event (just above 4 mg $L^{-1}$) and then dropped quickly before leveling off at approximately 0.4 mg $L^{-1}$ by 20 cm of cumulative leachate.

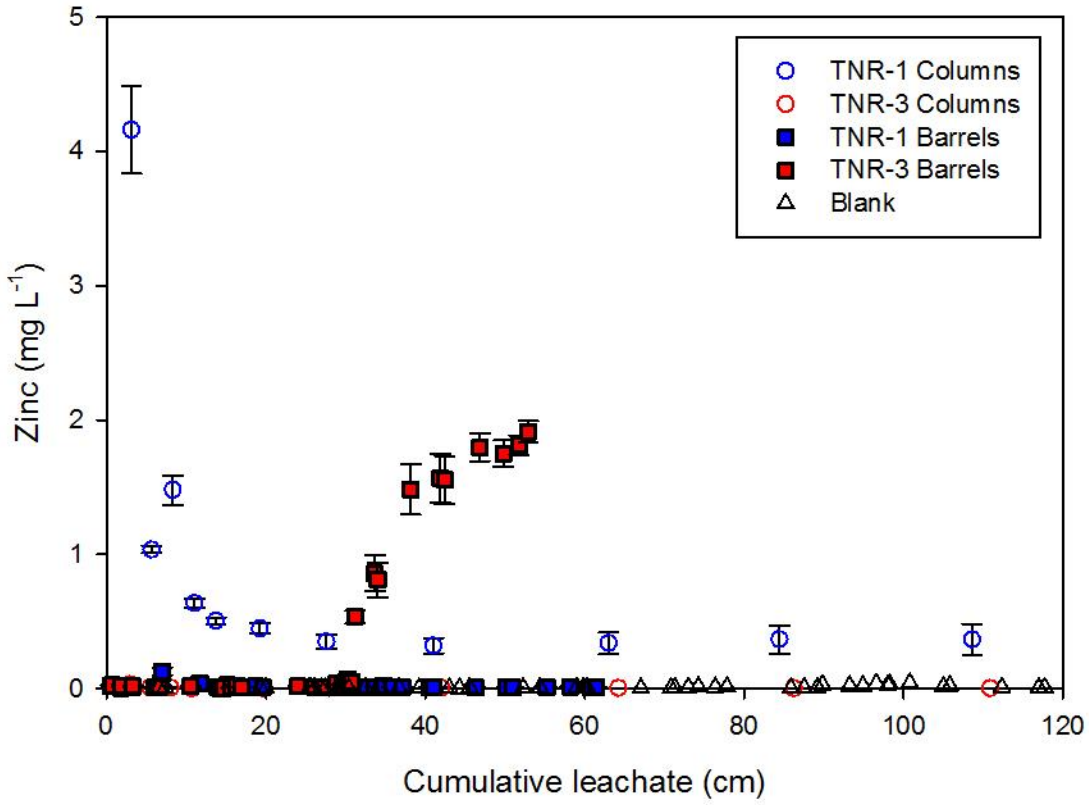


Figure 71. Leachate zinc versus cumulative volume eluted for columns and barrels of TNR-1 and TNR-3 refuse material. Values plotted are means (n=3 except for blank n=1) per sample event with one standard error above and below. Detection limit = 0.008 mg $L^{-1}$.

Zinc levels in the barrel leachates remained significantly lower than in the column leachates for the duration of the study. The barrel leachates peaked at just over 0.1 mg $L^{-1}$ at around 7 cm of cumulative leachate. In contrast, the TNR-3 column leachate peaked at just over 0.03 mg $L^{-1}$ (not visible at scale of Fig. 71) during the first leaching event and then remained at or near detection. On the other hand, the TNR-3 barrel leachates remained below 0.01 mg $L^{-1}$ through 30 cm of cumulative leachate, and then Zn levels began to rise quickly to a peak of about 2 mg $L^{-1}$ by the conclusion of the study (just over 50 cm of cumulative leachate).

*Leachate Chloride (Cl)*

Leachates from the TNR-1 material contained very similar amounts of Cl (Fig. 72) in both the columns and the barrels. The column Cl levels were below the detection limit of 5 mg $L^{-1}$ for the duration of the study. The barrel leachate contained measureable, but very small, amounts of Cl from 0 to 7 cm of cumulative leachate and peaked at approximately 14 mg $L^{-1}$ during the first leaching event. On the other hand, the TNR-3 refuse materials eluted much more Cl, but also exhibited similar Cl release patterns in both the columns and barrels.

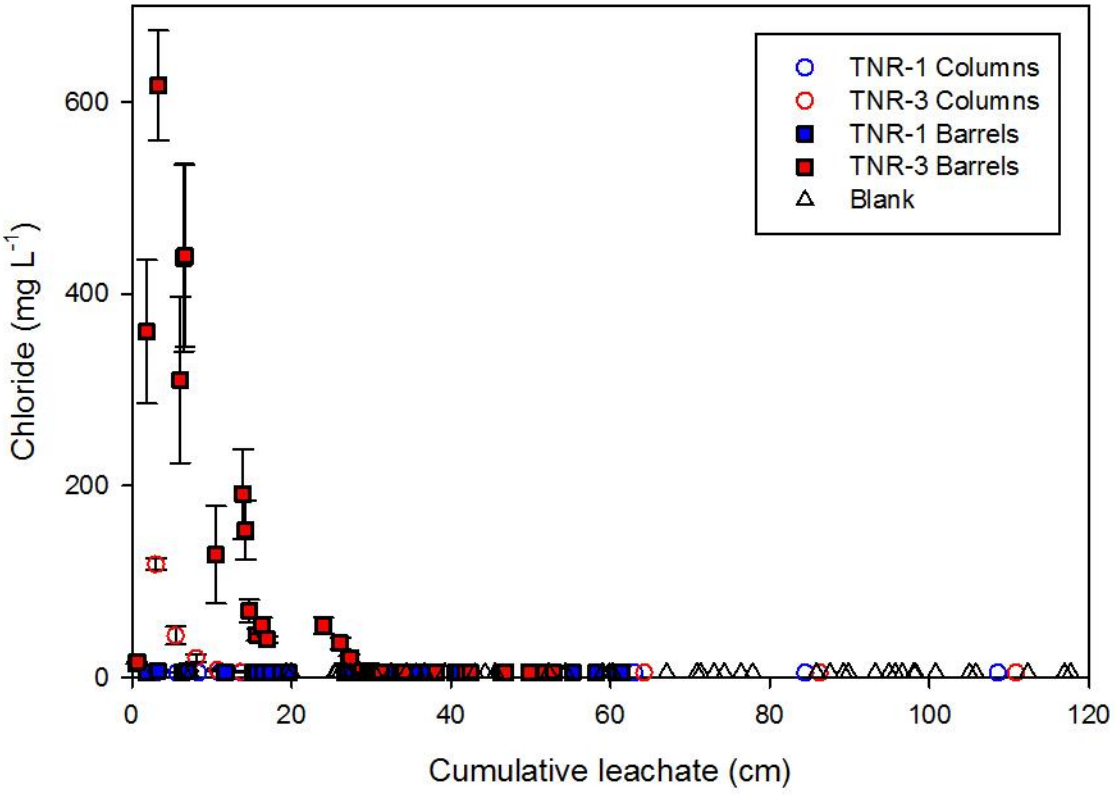


Figure 72. Leachate Cl versus cumulative volume eluted for columns and barrels of TNR-1 and TNR-3 refuse material. Values plotted are means (n=3 except for blank n=1) per sample event with one standard error above and below. Detection limit = 5.0 mg $L^{-1}$.

Both the columns and barrels peaked during the initial leaching event and then rapidly fell to below the detection limit; however the barrels had a significantly higher initial peak. The columns peaked initially at just over 100 mg $L^{-1}$ while the barrels peaked at just over 600 mg $L^{-1}$. Following their peaks, the columns fell to the detection limit (5 mg $L^{-1}$) before 15 cm of cumulative leachate while the barrels eluted ~30 cm of cumulative leachate to reach the same levels. The TNR-3 material also exhibited much higher Na release, so it appears to have retained more traces of NaCl-salinity following deposition and lithification, and these chlorides and Na appeared to be preferentially released via some weathering process, perhaps fragments slaking, in the barrels relative to the columns.

Comparison of Field Leaching Behavior for Barrels by Date

The following section interprets the refuse leaching data as an actual time series rather than by cumulative volume of leachates. Thus, the figures show "date of sampling" on the x-axis and "parameter analyzed" on the y-axis. Leachate data are displayed for the TNR-1 and TNR-3 coarse refuse from the barrels that were placed in the field, and leached under natural environmental conditions. This allows for a better analysis of how leachate characteristics differed over time, between different seasons, and between refuse materials. It is interesting to note that the TNR-3 material produced less leachate compared to the TNR-1 materials. This aligns with the observations discussed earlier and below suggesting more reactive pyrite in the TNR-3 material which presumably would have produced more highly hydrated reaction products and salts. All graphs begin in May of 2013, and extend to January 2014 except for bicarbonate, which extends to March of 2014, and pH and EC which extend through November 2014. Figure 73 displays cumulative rainfall vs. date. This graph displays drier periods in the late summer and early fall of each year, when there was less cumulative rainfall added and visible gaps between

rainfall events. This graph also displays the cumulative leachate that was collected from the barrels and blank.

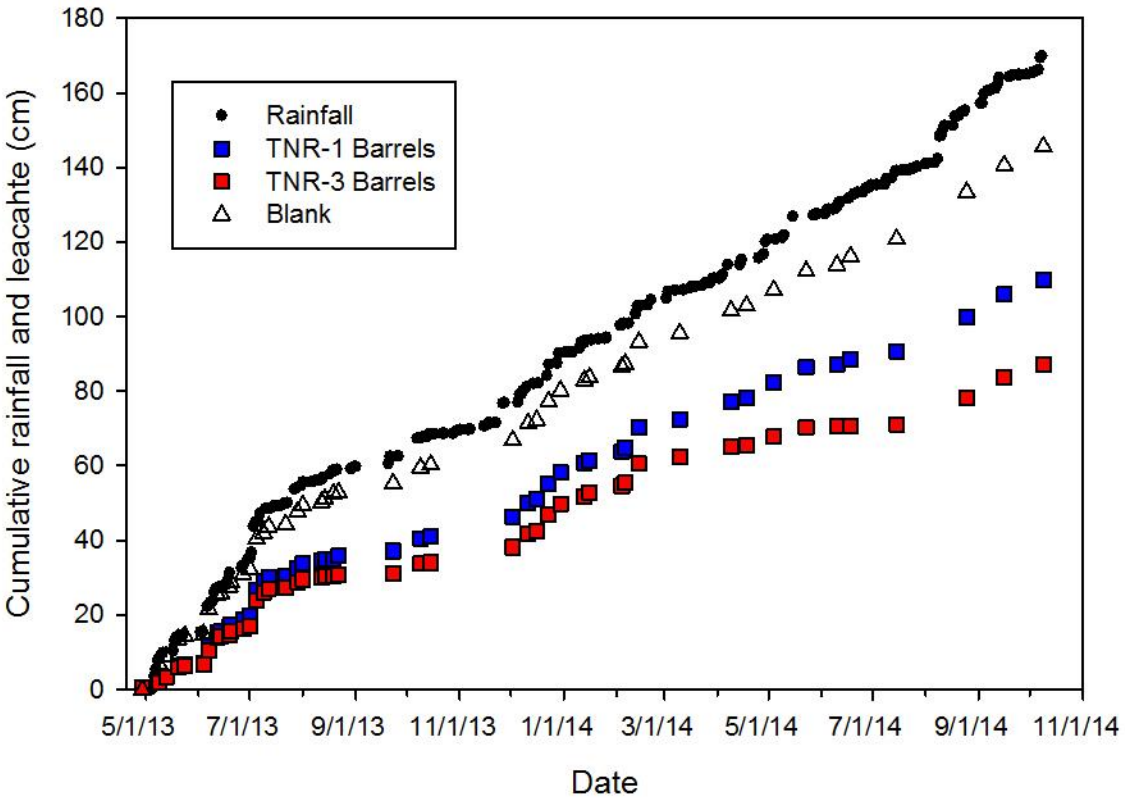


Figure 73. Cumulative rainfall and leachate versus date for the barrels and blank. Values plotted are cumulative rainfall for each measureable rainfall event, or cumulative leachate for each leachate collection date.

*Leachate pH*

There were significant differences in leachate pH over time between the two refuse samples (Fig. 74). The TNR-1 material leachate pH stayed relatively constant, generating between ~7.0 and 7.5 for the entire time period. On the other hand, the TNR-3 leachate pH was ~7.0 to 7.5 through August, but then pH levels dropped significantly. After several dry periods during the late summer and fall of 2013, the pH dropped to 3.5 and continued to drop with a minimum value of 2.4.

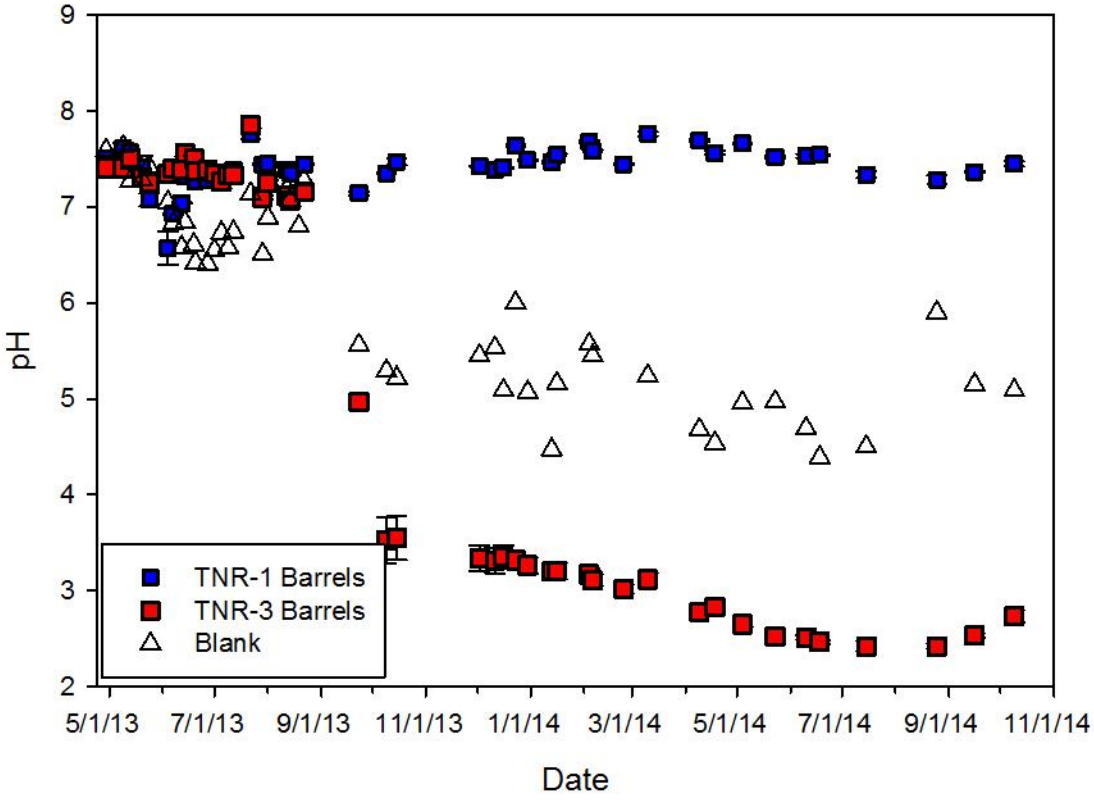


Figure 74. Leachate pH versus date for barrels of TNR-1 and TNR-3 refuse material. Values plotted are means (n=3 except for blank n=1) per sample event with one standard error above and below.

*Leachate EC*

The EC elution patterns were somewhat similar for both refuse materials (Fig. 75), but the TNR-3 leachate maintained significantly higher levels for the majority of the study period. Leachate from both materials showed three EC peaks. First, the initial peaks during the first two months following placement in the spring of 2013 produced an EC of 4750 µS $cm^{-1}$ in the TNR-3 barrels and 2730 µS $cm^{-1}$ in the TNR-1 barrels. Next, a second peak occurred during the winter of 2013/2014 after a dry period during the fall of 2013. This secondary peak was 4400 µS $cm^{-1}$ in the TNR-3 barrels and 1630 µS $cm^{-1}$ in the TNR 1 barrels. Lastly, another peak

occurred after a dry period in the late summer of 2014 which reached 9040 µS $cm^{-1}$ in the TNR-3 barrels and 1660 µS $cm^{-1}$ in the TNR-1 barrels. Overall, the EC peaks were much more pronounced and significant in the TNR-3 barrels compared to the TNR-1 barrels. It is also interesting to note that the TNR-3 barrels produced relatively high EC levels both before and after rapid acidification phase over the summer of 2013 (see Fig. 74). This indicates that sulfides in the refuse were actively oxidizing from the beginning of leaching in these materials, but there were apparently sufficient neutralizers present for the first several months to keep the pH up around 7.0. Over longer periods of time, the EC continued to rise, eventually exceeding 6000 µS $cm^{-1}$ once the pH fell below 4.0. This likely indicated the system had moved into the very rapid phase of pyrite oxidation without inhibition by the neutralizers which had been spent.

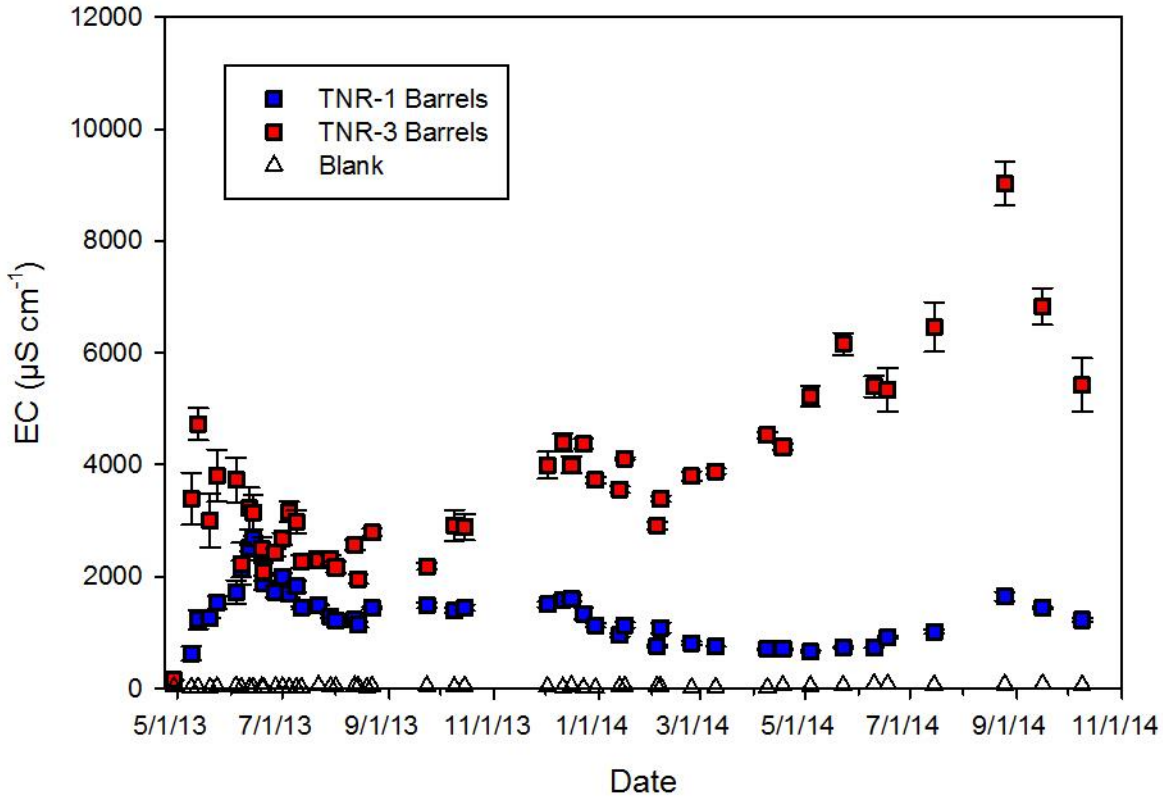


Figure 75. Leachate EC versus date for barrels of TNR-1 and TNR-3 refuse material. Values plotted are means (n=3 except for blank n=1) per sample event with one standard error above and below.

*Leachate Bicarbonate*

Bicarbonate elution (Fig. 76) was similar for the two refuse materials during the first four months of the study, but differed greatly after this time. During the first four months, both materials reached their peak their levels and bicarbonate levels also fluctuated greatly between leachate collections. During this time, leachate bicarbonate generally stayed between 40 mg $L^{-1}$ and 80 mg $L^{-1}$, with the TNR-1 leachate peaking at 83 mg $L^{-1}$ and the TNR-3 leachate peaking at 95 mg $L^{-1}$. After August 2013, the TNR-1 leachate bicarbonate remained between 45 mg $L^{-1}$ and 70 mg $L^{-1}$, while the TNR-3 leachate bicarbonate levels were significantly lower. During this later time period, TNR-3 leachate bicarbonate remained below 10 mg $L^{-1}$.

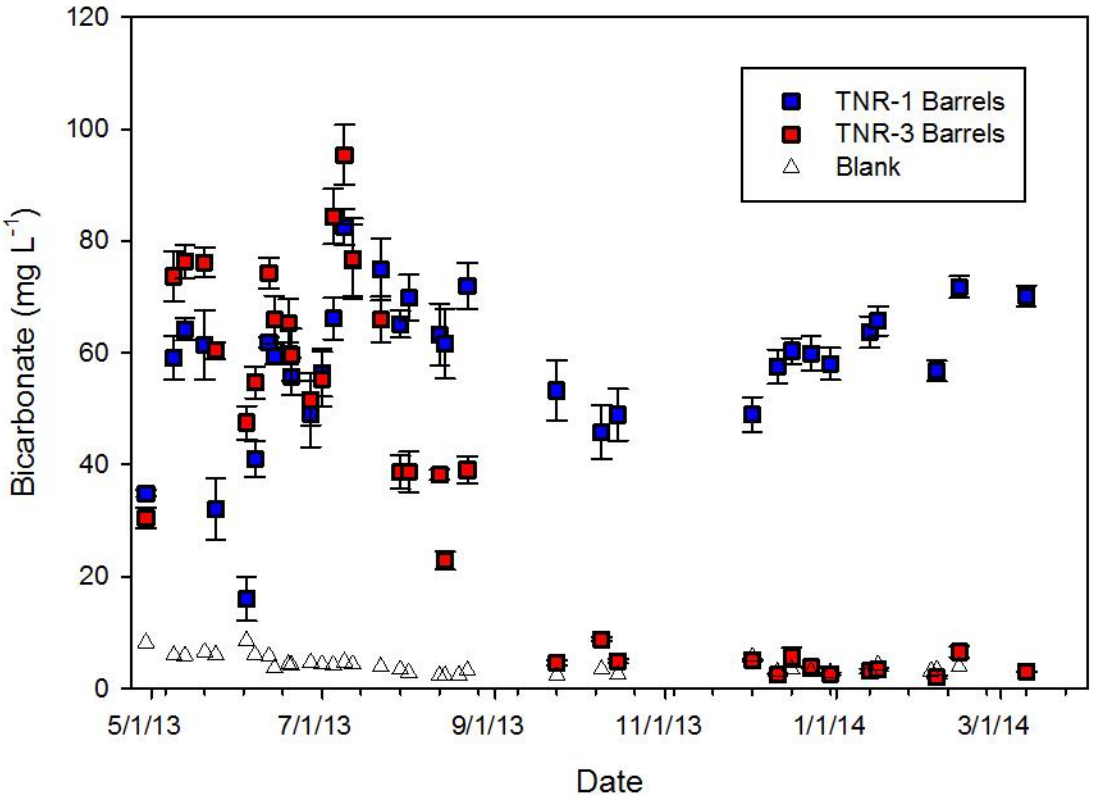


Figure 76. Leachate bicarbonate versus date for barrels of TNR-1 and TNR-3 refuse material. Values plotted are means (n=3 except for blank n=1) per sample event with one standard error above and below.

These data reinforce the assumptions described above for the first several months; specifically that the TNR-3 barrels contained sufficient neutralizers to maintain their alkalinity (as indicated by bicarbonate), but then alkalinity dropped dramatically in the late summer as the neutralizers (presumably complex carbonates and possibly feldspars) were spent. Refuse TNR-1, on the other hand, appeared to contain a large surplus of reactive neutralizers and was able to maintain higher levels of alkalinity and associated leachate pH throughout the study period.

*Leachate Sulfate*

Sulfate levels in the TNR-3 leachate were significantly higher than in the TNR-1 leachate for the duration of the study period (Fig. 77). However, sulfate levels for both refuse samples showed similar elution patterns over time. Sulfate levels started low, peaked during the first month, and then showed a secondary peak later in the study period. The initial peak for the TNR-1 leachate reached 670 mg $L^{-1}$, and 1950 mg $L^{-1}$ in the TNR-3 barrels. This first peak was likely due to an initial flush of accumulated sulfate oxidation and hydration reaction products from the material. The secondary peak in December reached 950 mg $L^{-1}$ in the TNR-1 leachate and 3380 mg $L^{-1}$ in the TNR-3 leachate. This secondary peak followed the dry period in the late fall of 2013. As described earlier, the overall pattern of sulfate elution was controlled by differences in pyrite oxidation over time while the time-lagged peaks reflected the net storage of sulfate reaction products during periods of dry weather and then subsequent release following significant precipitation events.

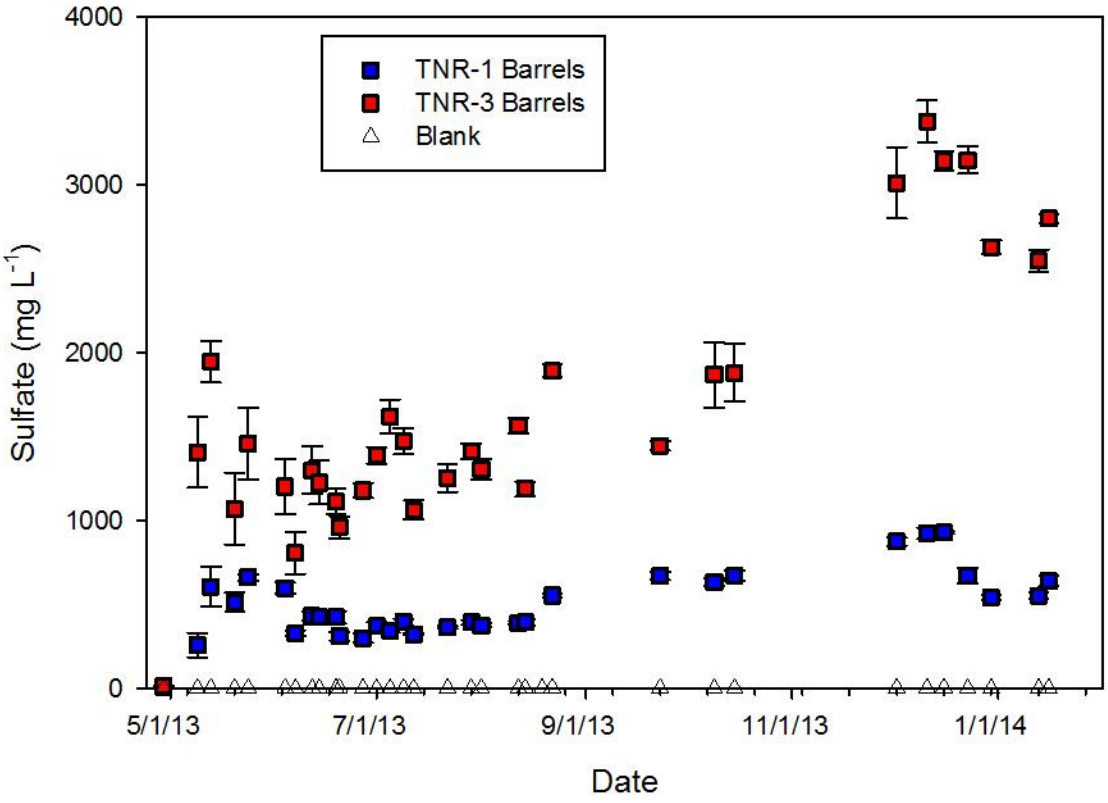


Figure 77. Leachate sulfate versus date for barrels of TNR-1 and TNR-3 refuse material. Values plotted are means (n=3 except for blank n=1) per sample event with one standard error above and below.

*Leachate Calcium (Ca)*

Calcium elution patterns differed significantly between the two refuse materials (Fig. 78). While the TNR-1 leachate Ca levels peaked early and late, the TNR-3 Ca levels peaked early and midway through the study. However, both materials continued to leach significant levels of Ca throughout the study period indicating long term dissolution and reaction of Ca containing mineral phases, most likely carbonates and possibly feldspars. The TNR-1 leachate Ca levels peaked in mid-June at 312 mg $L^{-1}$ and again at 244 mg $L^{-1}$ in mid-December. On the other hand, with the exception of an apparent outlier at the third sampling event, Ca in the TNR-3 leachates

slowly and irregularly increased to a peak of 423 mg $L^{-1}$ in mid-August before tailing off for the rest of the study.

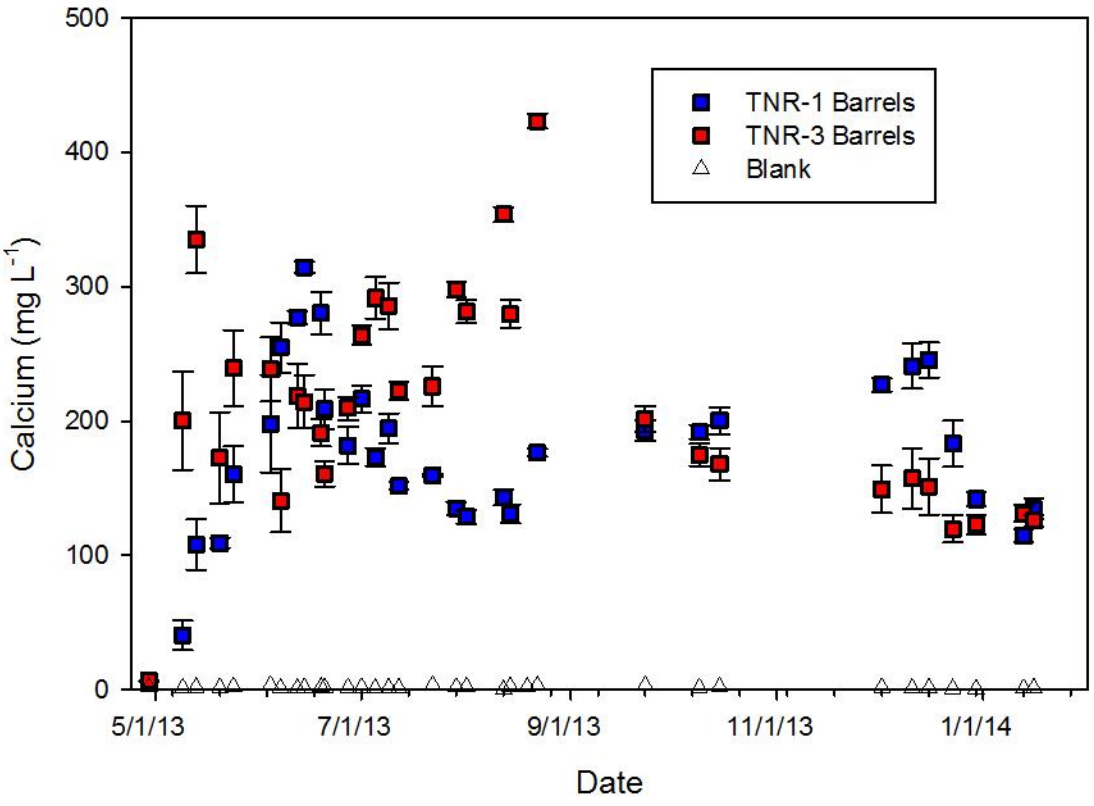


Figure 78. Leachate Ca versus date for barrels of TNR-1 and TNR-3 refuse material. Values plotted are means (n=3 except for blank n=1) per sample event with one standard error above and below. Detection limit = 0.01 mg $L^{-1}$.

*Leachate Magnesium (Mg)*

Overall, the TNR-3 leachate had higher Mg levels compared to the TNR-1 leachate (Fig. 79). Although the patterns over time were similar, the peak Mg levels were significantly higher in the TNR-3 leachate, and after mid-July, Mg levels remained significantly higher in the TNR-3 leachate for the rest of the study period. The initial peak Mg levels for TNR-3 reached 92 mg $L^{-1}$, subsequently declined, and then rebounded to a maximum peak of 95 mg $L^{-1}$ during the

last month of the study. On the other hand, the initial peak Mg level for TNR-1reached 64 mg $L^{-1}$ and the final peak reached 59 mg $L^{-1}$.

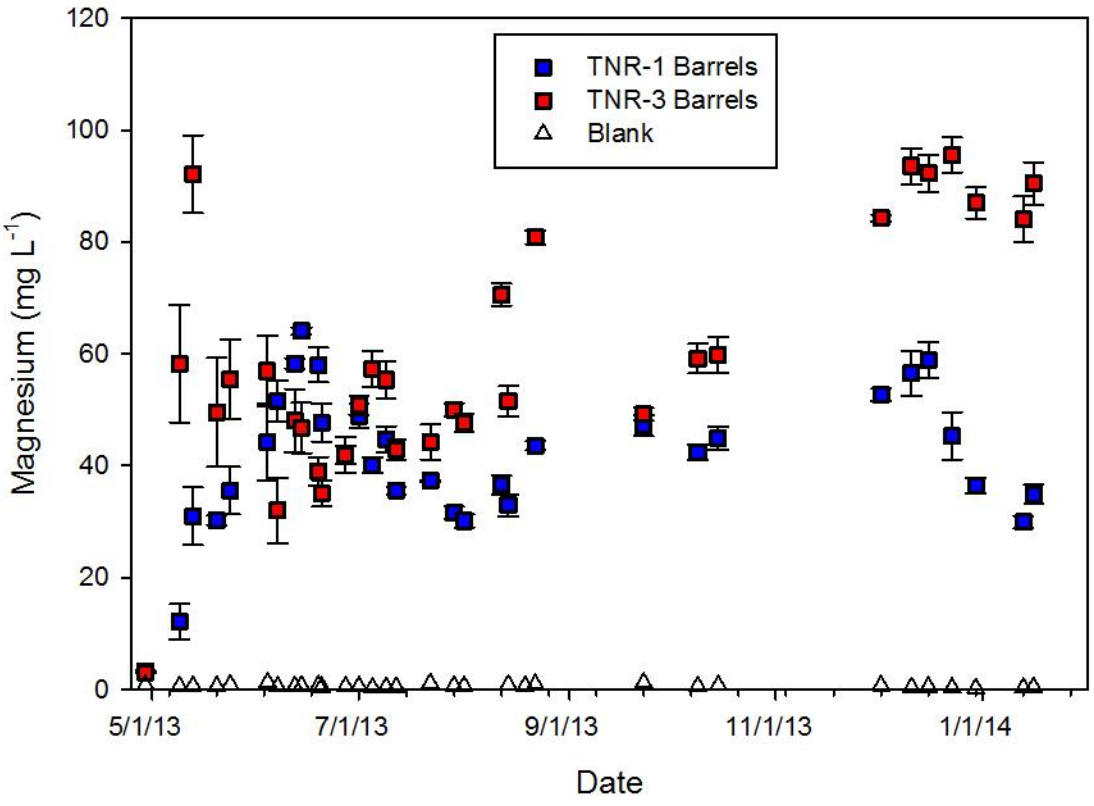


Figure 79. Leachate Mg versus date for barrels of TNR-1 and TNR-3 refuse material. Values plotted are means (n=3 except for blank n=1) per sample event with one standard error above and below. Detection limit = 0.005 mg $L^{-1}$.

*Leachate Potassium (K)*

Potassium elution from the two refuse samples showed very similar patterns over time (Fig. 80) but at different overall levels. Both peaked during the first two months, followed by a slow and gradual decline throughout the rest of the study period. However, K levels in the TNR-1 leachate were significantly higher for the duration of the study compared to the TNR-3 barrels.

The TNR-1 leachate peak K level reached 45 mg $L^{-1}$, while the TNR-3 leachate peaked at 27 mg $L^{-1}$.

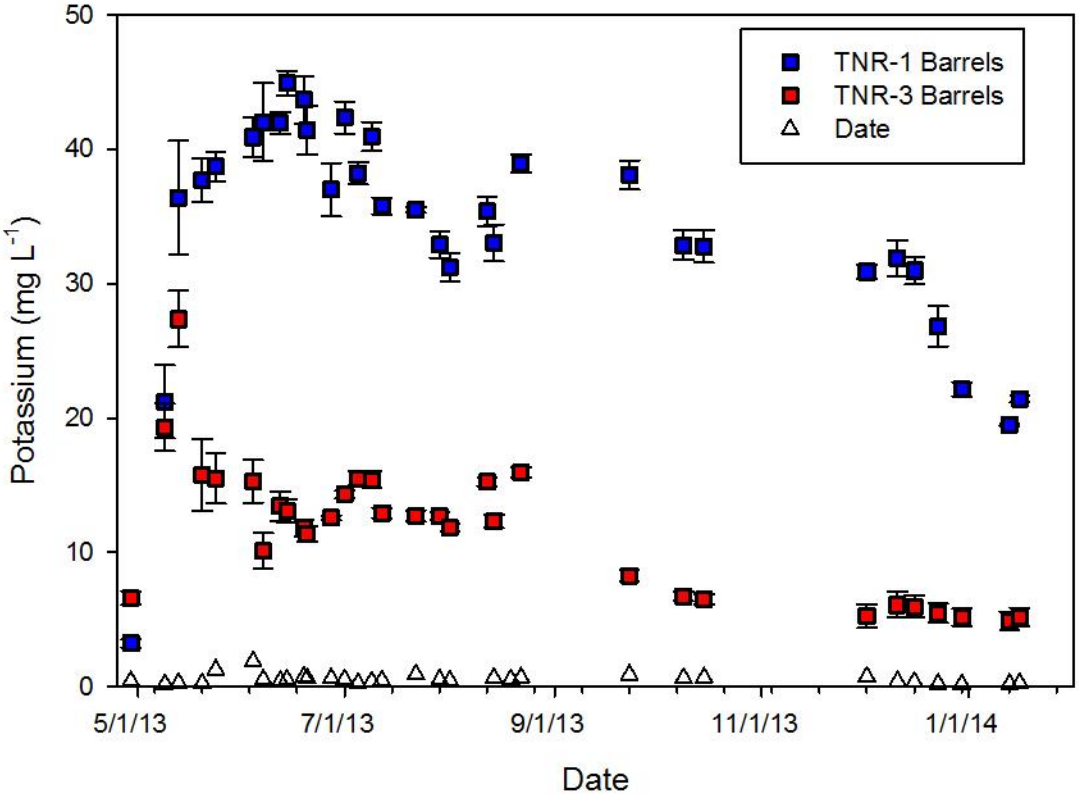


Figure 80. Leachate K versus date for barrels of TNR-1 and TNR-3 refuse material. Values plotted are means (n=3 except for blank n=1) per sample event with one standard error above and below. Detection limit = 0.005 mg $L^{-1}$.

*Leachate Sodium (Na)*

Sodium levels in the TNR-3 leachate remained significantly higher than the TNR-1 barrels for the duration of the study (Fig. 81). Sodium levels in both leachates peaked early, and then declined for the rest of the study period. The TNR-3 barrels peaked at 690 mg $L^{-1}$, while the TNR-1 barrels peaked at 70 mg $L^{-1}$. Also, the decline following this peak was much more

rapid in the TNR-3 barrels. As discussed earlier, the original TNR-3 refuse contained much higher levels of total Na which then rapidly leached out upon exposure and weathering.

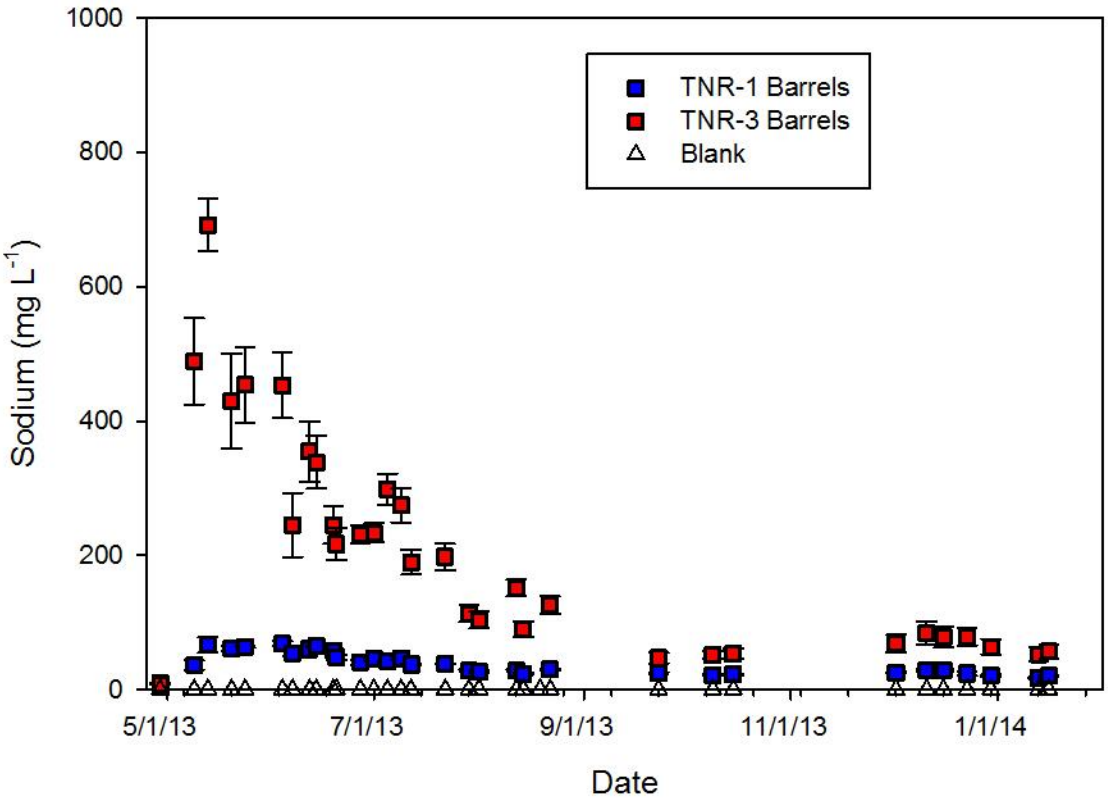


Figure 81. Leachate Na versus date for barrels of TNR-1 and TNR-3 refuse material. Values plotted are means (n=3 except for blank n=1) per sample event with one standard error above and below. Detection limit = 0.005 mg $L^{-1}$.

*Leachate Iron (Fe)*

Overall, Fe levels in the TNR-3 leachate were significantly higher compared to the TNR-1 leachate (Fig. 82). Iron levels in the TNR-1 leachate remained below 1.0 mg $L^{-1}$ for the duration of the study. Iron levels in the TNR-3 leachate remained below 1.5 mg $L^{-1}$ through September 2013, and then began to steadily rise through January with a peak of 12.1 mg $L^{-1}$ during this period. It is interesting to note that significant Fe leaching did not occur in TNR-3

until several months after the system had strongly acidified and the pH dropped to < 4.0. The Fe produced from pyrite oxidation more than likely re-precipitated in the columns in oxy-hydroxide forms, but did eventually remobilize into solution to some extent when the pH dropped even more to < 3.0.

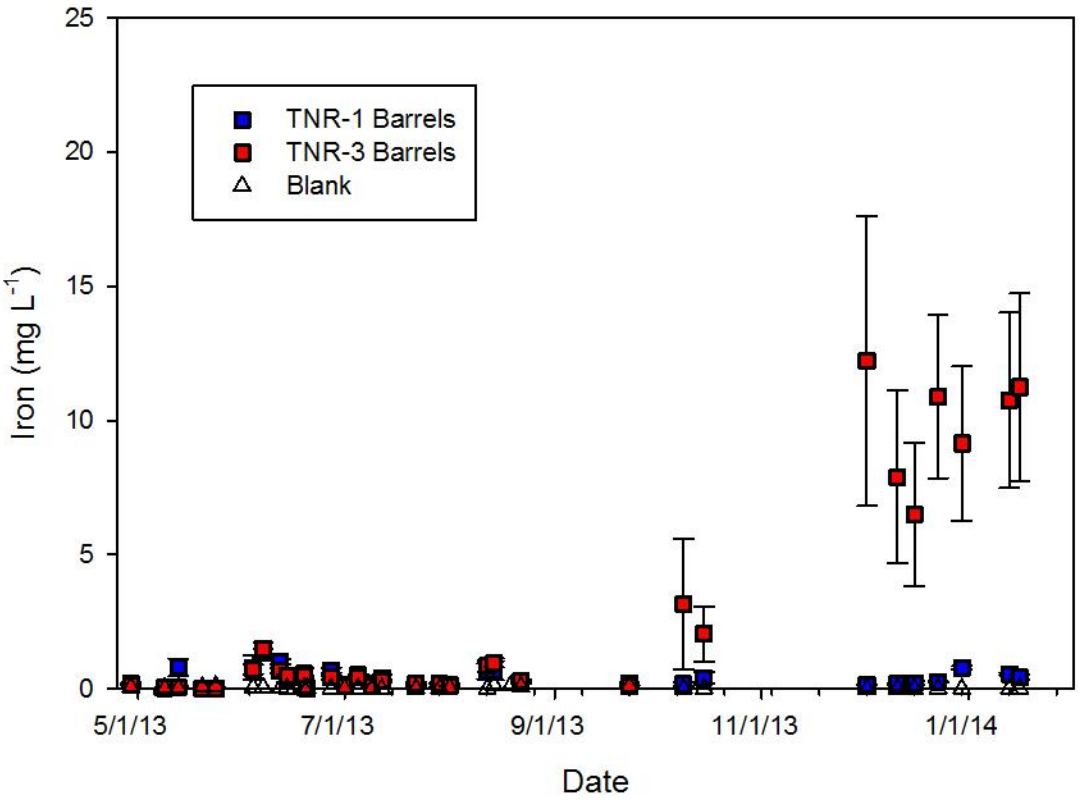


Figure 82. Leachate Fe versus date for barrels of TNR-1 and TNR-3 refuse material. Values plotted are means (n=3 except for blank n=1) per sample event with one standard error above and below. Detection limit = 5.0 µg $L^{-1}$.

*Leachate Manganese (Mn)*

Manganese elution from the two refuse materials (Fig. 83) was very similar during the first half of the study, but changed drastically after September, 2013. There was an initial peak during the first two months for both the TNR-1 and TNR-3 leachates which reached

approximately 330 µg $L^{-1}$. This peak was followed by a steady decline through September for both materials. After September, Mn levels in the TNR-1 leachate remained very low, while steadily increasing in the TNR-3 leachate. The Mn levels in the TNR-3 leachate reached a peak of 2475 µg $L^{-1}$ near the end of the study. Similar to Fe, this later release of large amounts of Mn from TNR-3 was most likely related to the strong acidification of the system to < pH 3.0, while the earlier period of release from both materials was most likely related to the active phase of pyrite oxidation and known Fe-Mn redox interactions discussed earlier.

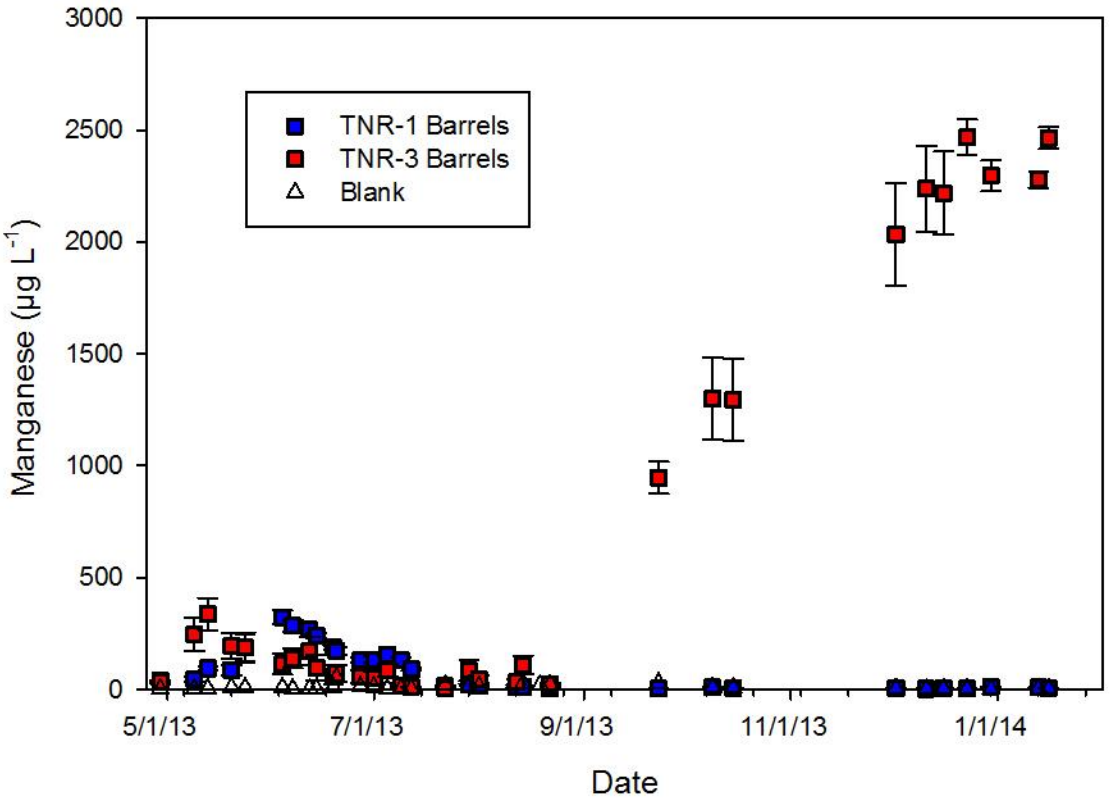


Figure 83. Leachate Mn versus date for barrels of TNR-1 and TNR-3 refuse material. Values plotted are means (n=3 except for blank n=1) per sample event with one standard error above and below. Detection limit = 5.0 µg $L^{-1}$.

*Leachate Aluminum (Al)*

Leachate Al levels were drastically different for the two refuse materials (Fig. 84). Aluminum levels in the TNR-1 leachates never rose above 0.75 mg $L^{-1}$ for the entire study. On the other hand, Al levels in the TNR-3 leachates stayed below 0.75 mg $L^{-1}$ through September 2013, but then suddenly increased to above 7.75 mg $L^{-1}$ for the remainder of the study. During this period the TNR-3 leachate reached a peak of 15.1 mg $L^{-1}$. Again, the later Al release here from the TNR-3 was due to pH solubility control.

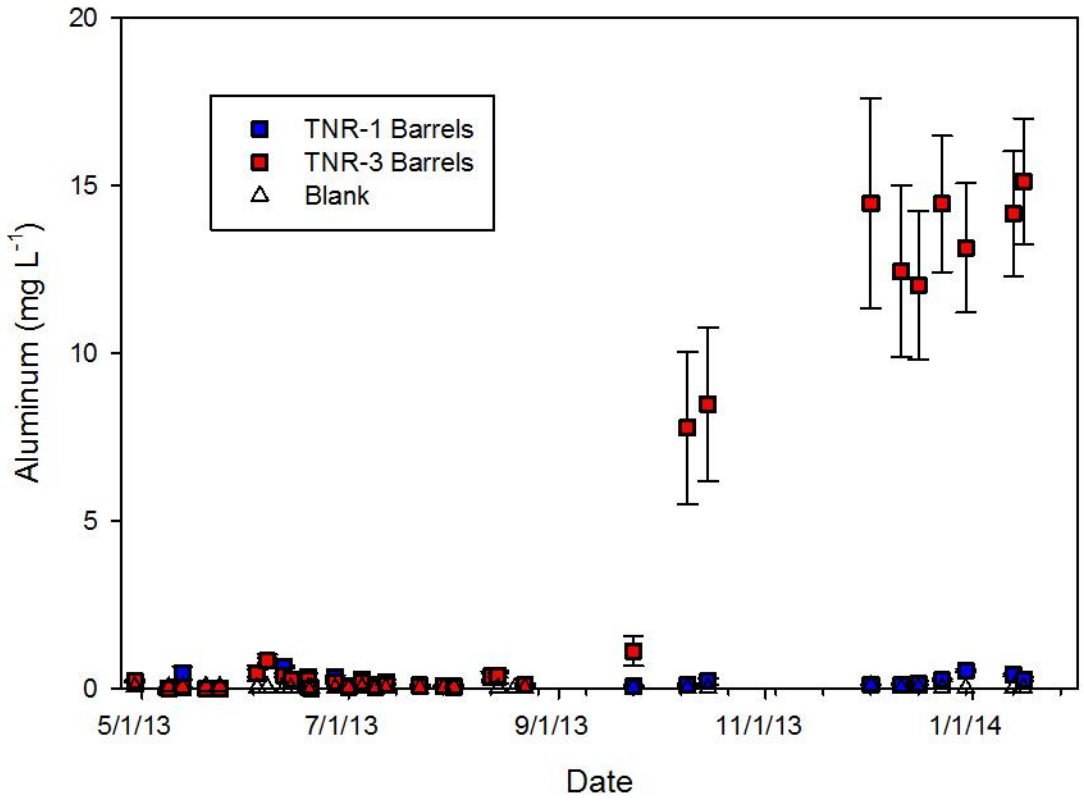


Figure 84. Leachate Al versus date for barrels of TNR-1 and TNR-3 refuse material. Values plotted are means (n=3 except for blank n=1) per sample event with one standard error above and below. Detection limit = 1.0 µg $L^{-1}$.

*Leachate Arsenic (As)*

Arsenic levels in the TNR-1 leachate (Fig. 85) remained at or just above the detection limit of 0.3 µg $L^{-1}$ for the duration of the study. On the other hand, As levels in the TNR-3 leachate were significantly elevated several times throughout the study.

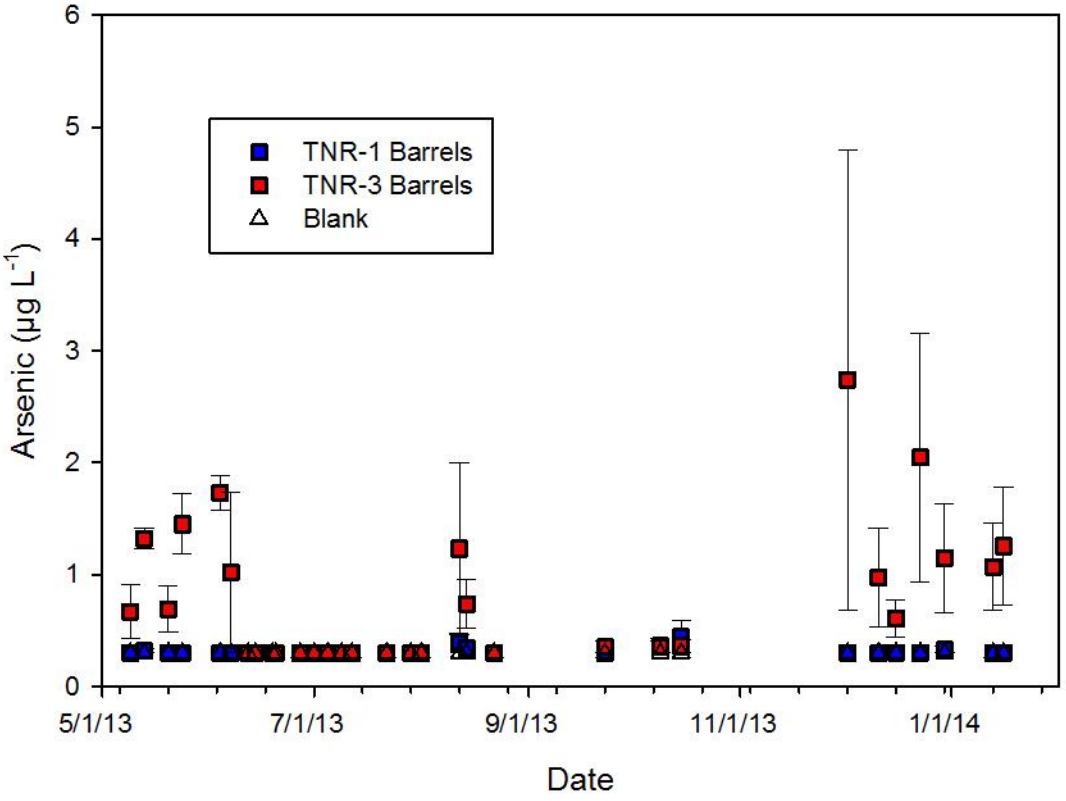


Figure 85. Leachate As versus date for barrels of TNR-1 and TNR-3 refuse material. Values plotted are means (n=3 except for blank n=1) per sample event with one standard error above and below. Detection limit = 0.3 µg $L^{-1}$.

First, there was a period of elevated As levels during the first two months of leachate collection. This was likely associated with the early onset of active pyrite oxidation in the refuse. Later, there was another period of elevated As levels towards the end of the study following a dry period of weather with no rain. This time period included the peak levels of As

for the TNR-3 material at 2.7 µg $L^{-1}$. This most likely reflected As release from the actively weathering pyrites in the refuse, accumulation of arsenate in the accumulated sulfate salt phases of the barrels over the dry summer, and then subsequent flushing following significant precipitation events.

*Leachate Cadmium (Cd)*

Cadmium elution magnitude and patterns differed greatly between the two materials (Fig. 86). First, Cd levels in the TNR-1 leachate remained below 0.25 µg $L^{-1}$ for much of the study, with one noticeable spike after two months that reached almost 1.0 µg $L^{-1}$.

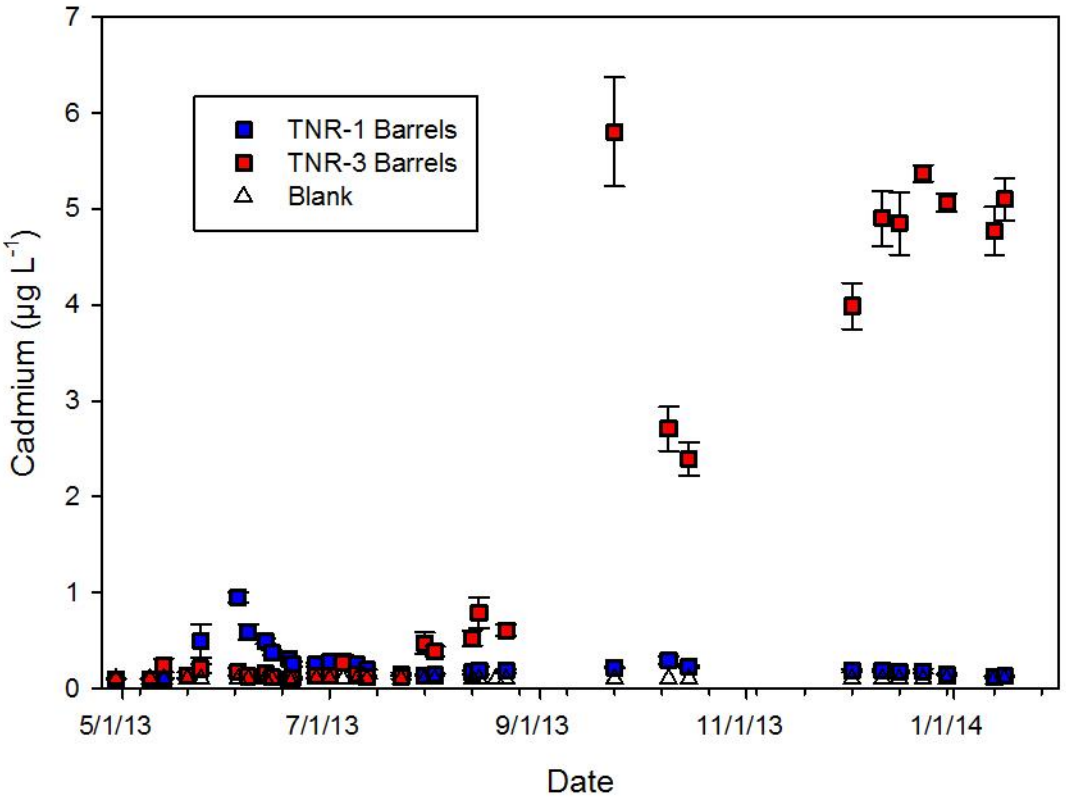


Figure 86. Leachate Cd versus date for barrels of TNR-1 and TNR-3 refuse material. Values plotted are means (n=3 except for blank n=1) per sample event with one standard error above and below. Detection limit = 0.1 µg$L^{-1}$.

Cadmium levels in the TNR-3 leachate remained below 0.25 µg $L^{-1}$ through July, but then steadily increased for the remainder of the study with a peak of 5.8 µg $L^{-1}$. As described for the other acid-soluble metals in this section, the longer term elevated release of Cd for the TNR-3 followed a significant period of intense acid sulfate weathering process with leachate pH < 3.5. Parker (2013) also saw increased leachate Cd related to pyrite oxidation.

*Leachate Copper (Cu)*

Patterns of Cu elution differed greatly between the two refuse samples (Fig. 87). The TNR-1 leachates contained Cu levels at or below the detection limit of 0.6 µg $L^{-1}$ for the majority of the study. On the other hand, Cu levels remained low in the TNR-3 leachate through mid-September, but then began a steady increase to a peak of 235 µg $L^{-1}$ by the end of the study period. This increase occurred following the late summer of 2013 and the associated very low pH conditions. Like the other acid-soluble metals, Cu became soluble in the TNR-3 barrels at these low pH values, so significant amounts were detected in the leachate. No drop in pH occurred in TNR-1 leachate, so Cu did not become soluble during this time.

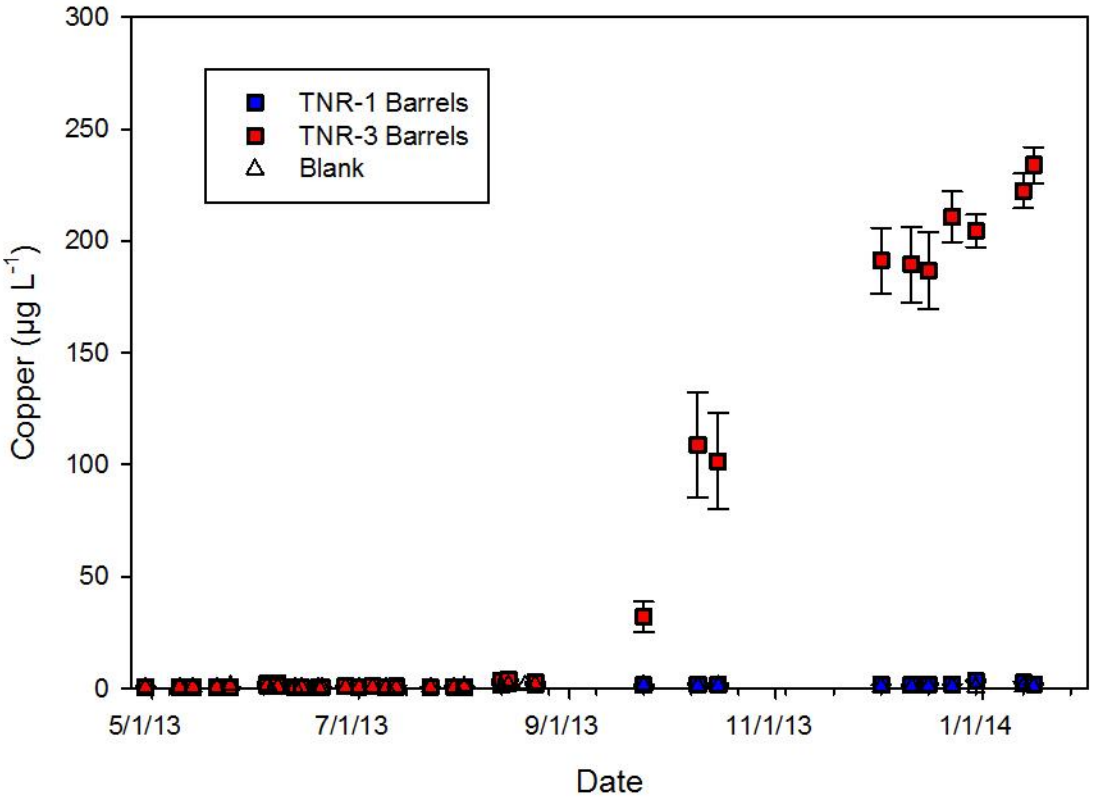


Figure 87. Leachate Cu versus date for barrels of TNR-1 and TNR-3 refuse material. Values plotted are means (n=3 except for blank n=1) per sample event with one standard error above and below. Detection limit = 0.6 µg $L^{-1}$.

*Leachate Nickel (Ni)*

Nickel elution patterns differed greatly between the two refuse samples (Fig. 88). First, Ni levels in the TNR-1 leachate peaked at 48 µg $L^{-1}$ in early June and otherwise remained low for the duration of the study. In contrast, Ni levels in the TNR-3 leachate remained below 40 µg $L^{-1}$ through September, and then peaked at the end of the study period in January at 550 µg $L^{-1}$ following strong leachate acidification.

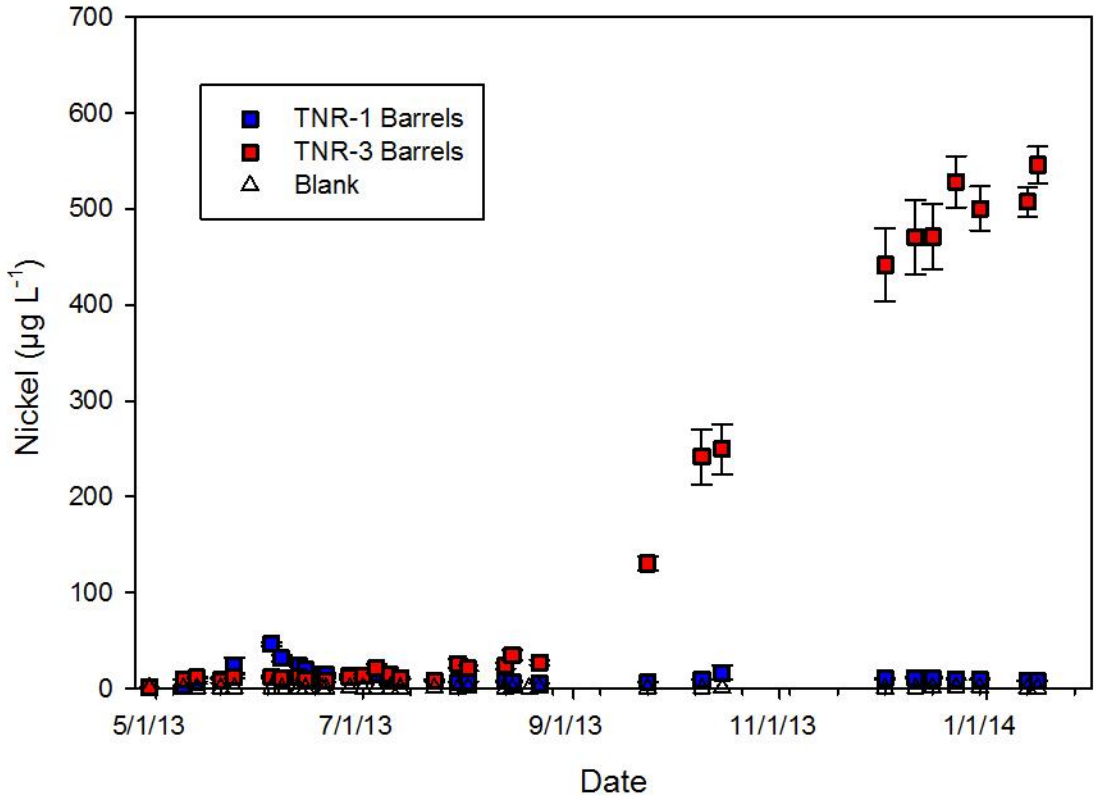


Figure 88. Leachate Ni versus date for barrels of TNR-1 and TNR-3 refuse material. Values plotted are means (n=3 except for blank n=1) per sample event with one standard error above and below. Detection limit = 0.3 µg $L^{-1}$.

*Leachate Lead (Pb)*

Overall, Pb elution in the TNR-3 leachates was significantly higher compared to the TNR-1 leachates (Fig. 89) where they remained below 2.5 µg $L^{-1}$ for the duration of the study. For TNR-3, the leachate Pb levels remained below 2.5 µg $L^{-1}$ through September, after which Pb suddenly increased to above 7.0 µg $L^{-1}$ following leachate acidification and then remained elevated for the remainder of the study with a peak of 17.3 µg $L^{-1}$.

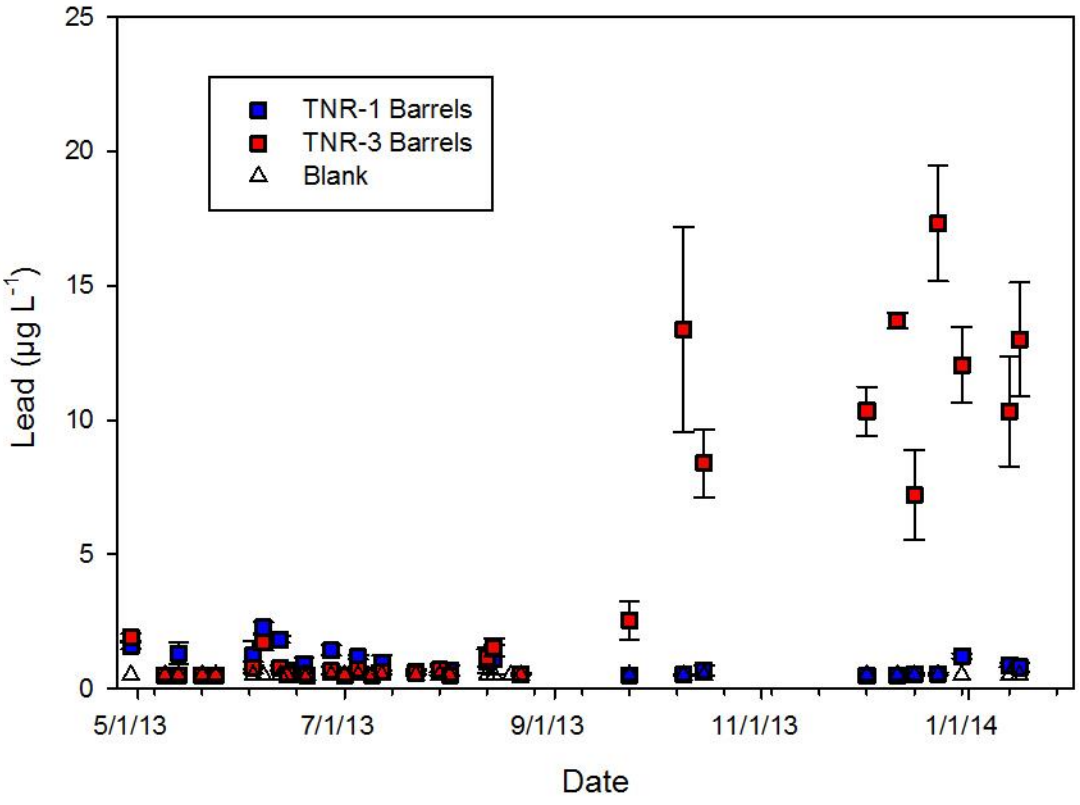


Figure 89. Leachate Pb versus date for barrels of TNR-1 and TNR-3 refuse material. Values plotted are means (n=3 except for blank n=1) per sample event with one standard error above and below. Detection limit = 0.5 µg $L^{-1}$.

*Leachate Selenium (Se)*

Even though total Se levels were relatively low and similar for both materials (~3.0 mg $kg^{-1}$), Se elution patterns differed strongly between the two refuse materials (Fig. 90). The TNR-1 leachate maintained higher Se levels over time, but the TNR-3 leachate reached a higher initial peak value. Overall, the TNR-1 materials Se levels remained above 200 µg $L^{-1}$ for the duration of the study with two noticeable peak elution periods. One peak occurred during the first two months and reached 700 µg $L^{-1}$, and the other occurred following several dry periods in the fall of 2013, reaching a value of 620 µg $L^{-1}$. By comparison, the TNR-3 material Se levels

only produced one initial peak during the first two months followed by a rapid decline to below the detection limit of 0.8 µg $L^{-1}$ after September 2013. The initial peak reached 870 µg $L^{-1}$. Thus, it appears that the Se mineral phase in the TNR-1 material was subject to weathering release over a more extended period of time than the Se in TNR-3. The much higher leachate pH of TNR-1 over the latter half of the study period also would have enhanced Se solubility and transport. As discussed earlier, these observed levels are much higher than the current surface water regulatory standard (5 µg $L^{-1}$).

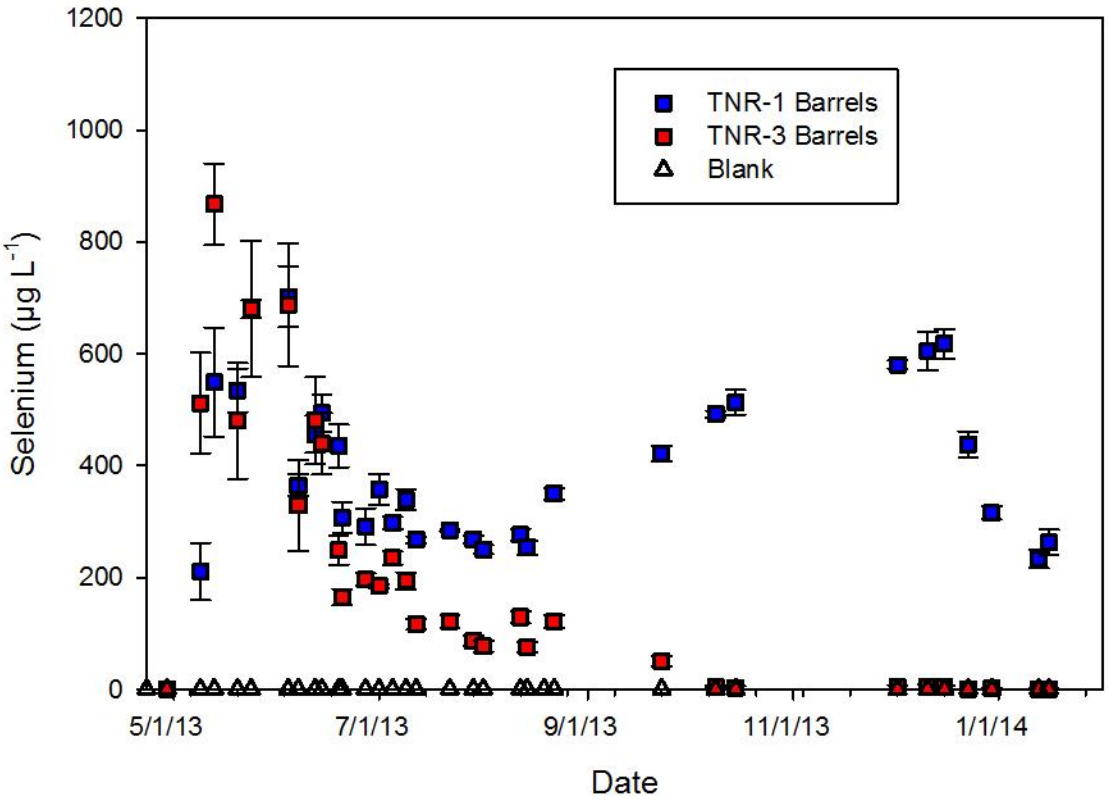


Figure 90. Leachate Se versus date for barrels of TNR-1 and TNR-3 refuse material. Values plotted are means (n=3 except for blank n=1) per sample event with one standard error above and below. Detection limit = 0.8 µg $L^{-1}$.

*Leachate Zinc (Zn)*

Zinc levels in the leachates were significantly different for the two refuse samples (Fig. 91). First, the TNR-1 barrels remained relatively low, but generated a small peak of 130 µg $L^{-1}$ in June 2013. On the other hand, Zn levels in the TNR-3 leachates remained low through late August, where they began a steady increase to 1900 µg $L^{-1}$ by the end of the study period in January. The beginning of this ascent corresponded to the strong drop in leachate pH at the end of the summer. The levels seen here are much greater than those discussed for the Harlan spoil and did not reflect the potential external source(s) observed in the blank as discussed earlier.

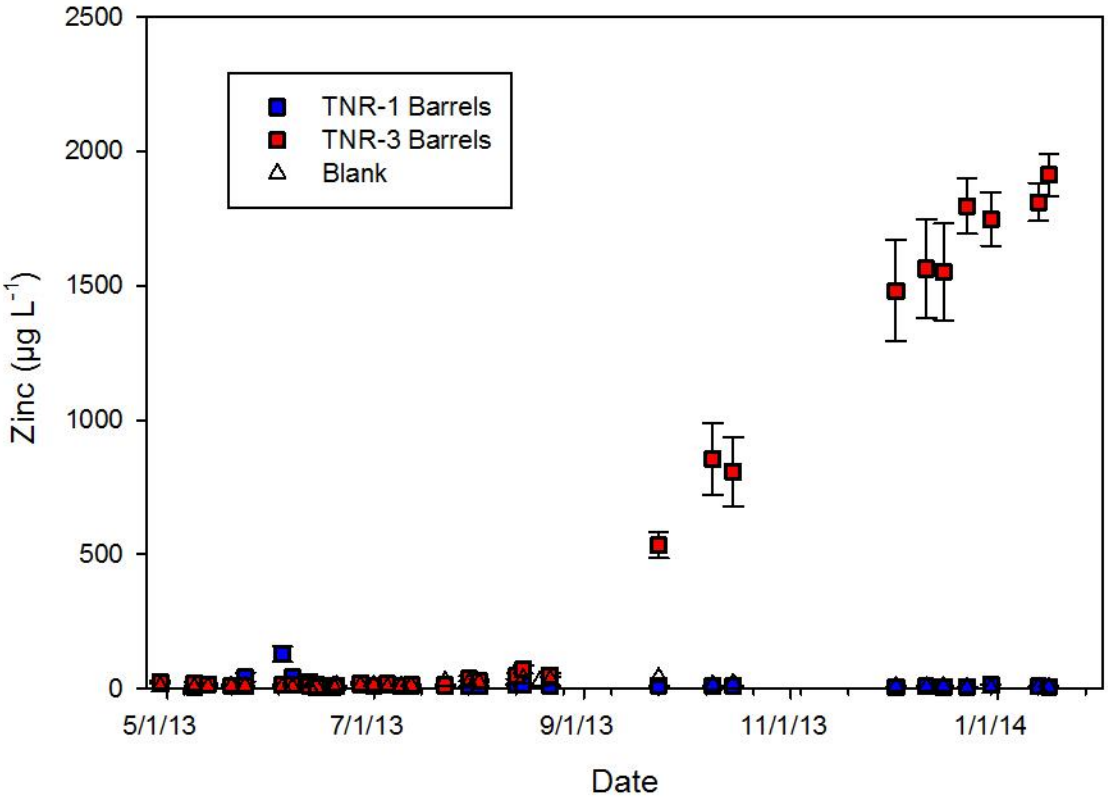


Figure 91. Leachate Zn versus date for barrels of TNR-1 and TNR-3 refuse material. Values plotted are means (n=3 except for blank n=1) per sample event with one standard error above and below. Detection limit = 0.8 µg $L^{-1}$.

*Leachate Chloride (Cl)*

Chloride levels were very different in the leachates of the two refuse materials (Fig. 92). The TNR-1 leachate had very low Cl levels for the duration of the study, and with few exceptions, stayed below the detection limit of 5.0 mg $L^{-1}$. In contrast, TNR-3 had significantly higher Cl levels from the beginning of the study through July 2013. Chloride levels peaked in May at 620 mg $L^{-1}$, and dropped quickly to the detection limit after July. As discussed earlier, the TNR-3 refuse was much higher in Na and Cl than the TNR-1 materials and these components leached rapidly.

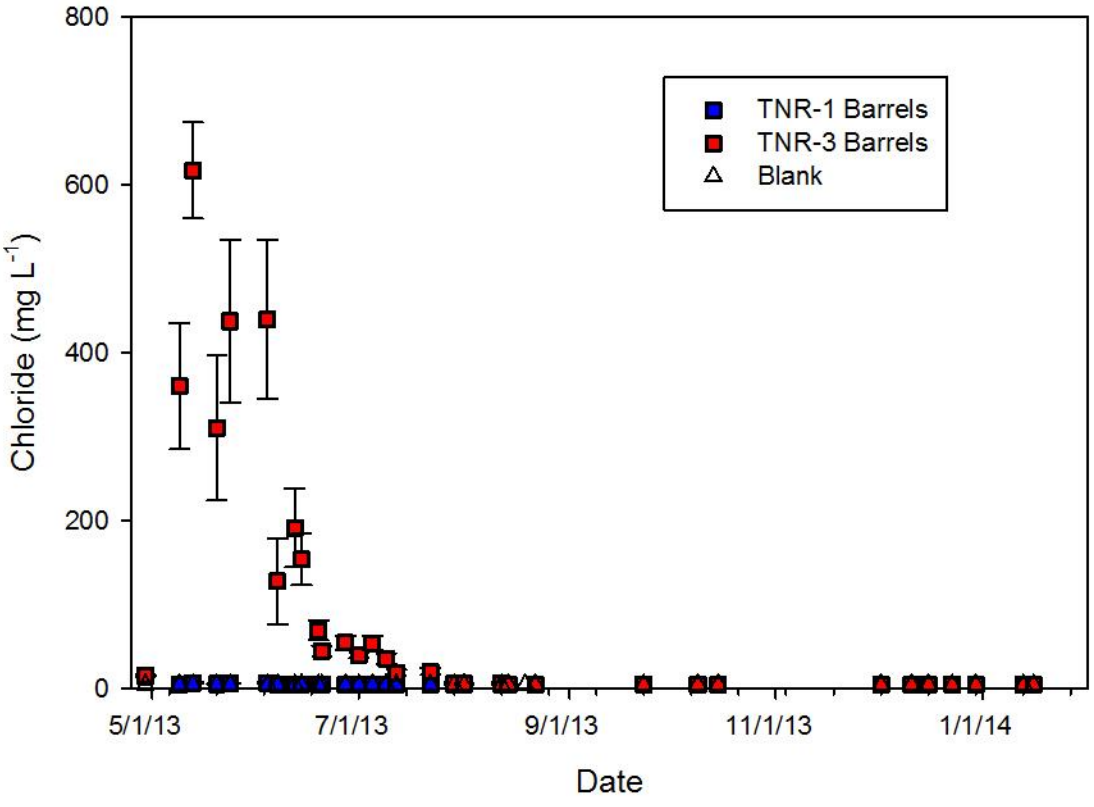


Figure 92. Leachate Cl versus date for barrels of TNR-1 and TNR-3 refuse material. Values plotted are means (n=3 except for blank n=1) per sample event with one standard error above and below. Detection limit = 5.0 mg $L^{-1}$.

## SUMMARY AND CONCLUSIONS

### SUMMARY

#### Effect of Leaching Test Scale on Harlan Spoil Leachate

Leachate EC, sulfate, Se, Ca, Mg, bicarbonate, K, Na, Ni, Fe, Al, Pb, and Cu were all affected by leaching scale. Of these parameters, leachate EC, sulfate, Se, Ca, and Mg responded similarly to changes in scale. In each case, initial peak values were significantly higher in the mesocosms, and in most cases the barrel size was intermediate between the mesocosms and columns. This initial peak was followed by a rapid decline to similar low levels in all three scales. However, the barrels and mesocosms also displayed a secondary peak due to seasonal effects that was not seen in the columns. In each case, the initial peak was likely related to pyrite oxidation and flushing of surface residues and reaction products (Orndorff et al., 2010). The additional peaks later in the study all corresponded to leaching events following the dry period of the year. During this dry period, small rains were able to interact with the spoil and likely produced weathering salts within the spoil, but not collectable leachate. Following a substantial rainfall, these weathering salts were washed through and seen in the leachates. A directly related study by Parker (2013) found that leaching cycle (frequency) had a significant effect on leachate EC. In that study, he determined that columns leached once per week had significantly higher EC levels compared to columns leached daily. Parker's findings align with the results seen in this study, as higher leachate EC levels were seen when times between rainfall events were farther apart. Also, long-term elevated EC levels (> 500 µS $cm^{-1}$) were seen in recent field scale studies by Evans et al. (2014) and Pond et al. (2014) when monitoring valley fills in the field, indicating that the relatively rapid flushing of TDS seen at all three scales of this study probably extends over several decades at full mining field scales.

The overall range of EC produced by the Harlan spoil in this study was very similar to regional reports from field studies (Evans et al., 2014; Pond et al., 2008, 2014; Timpano et al. 2015). Taken together, these combined results indicate that the likelihood of long-term elevated EC levels in the field are likely and are troubling for the health of watersheds affected by mining operations. Many studies have connected diminished stream health to elevated EC levels (Bernhardt et al., 2012; Pond et al., 2008, 2014; Timpano et al., 2015). In this study, the barrels and mesocosms that were located outside under natural conditions produced EC levels greater than 500 µS $cm^{-1}$ several times over the monitoring period and produced initial values > 1500 µS $cm^{-1}$. While the results of my study and others (Daniels et al., 2013; Orndorff et al., 2010) clearly indicate the emission of TDS components from similar non-acidic spoils should be expected to decline significantly over time, recent regional field study results by Evans et al. (2014) and Pond et al. (2014) indicate that most valley fills continue to emit relatively high levels of TDS for decades. The extended TDS release is more than likely the results of many factors including the very large mass of spoil materials in valley fills and the long periods of time and volumes of percolated rainfall required to flush their initially high loads of soluble constituents. Other factors such as the development of preferential flow pathways leading to incomplete leaching of the spoil mass are also possible. However, it is important to point out that Evans et al. (2014) did note that the TDS discharge from many valley fills in SW Virginia did appear to be dropping over extended time periods (15 to 20 y) to levels < 500 µS $cm^{-1}$.

Bicarbonate levels in the columns peaked sooner compared to the barrels and mesocosms, but peak values were not significantly different. This difference could have been due to the crushed spoil, and associate increased surface area, in the columns reacting more readily. Overall, similar patterns were seen when compared to past column leaching studies

including Daniels et al. (2009). Also, the barrels and mesocosms were significantly more variable among replicates later in the study, likely caused by more variation in material packing in the larger vessels affecting aeration, hydration, and gas exchange.

Leachate Cl, K, Na, and Ni showed a different overall treatment effect than the elements discussed above. For these elements, the columns produced a significantly higher initial peak value, but after the first few leaching events they were not significantly different across the different leaching scales studied. The higher initial peak in the columns may have been caused by a significant initial flush caused by material preparation methods which produced finer textured material in the columns, compared to the barrels and mesocosms where the material was not altered.

Aluminum and Pb showed similar treatment effects where leachate levels remained low in the columns, while the barrels and mesocosms exhibited a peak at approximately 40 cm of cumulative leachate. In both cases, the peaks seen in the barrels and mesocosms were presumably caused by washing of colloidal Al in small mineral fragments out of the vessels. Similarly, leachate Fe from the barrels and mesocosms also peaked at approximately 40 cm of cumulative leachate, but the columns produced a distinct initial peak at the beginning of the study. The initial peak in Fe in the column leachate was probably caused by a combination of losses of colloidal mineral fragments and rapid pyrite oxidation, and the later peak in the barrels and mesocosms was most likely caused by time-lagged pyrite weathering. The related study by Parker (2013), which also used the same Harlan sandstone spoil, documented that much of the initial Al and Fe detected in his column leaching experiment was in a colloidal form. In his study, elevated levels of Fe and Al were seen during the first leaching cycles, while in the barrels and mesocosms these two peaks were time-lagged. It is possible that the more irregular and

infrequent leaching events of the barrels and mesocosms caused slower movement of these colloidal fragments. Leachate Cu, Mn, and Zn did not differ significantly based on scale until the middle of the study where the barrels and mesocosms exhibited a significant peak. This peak was caused by an outside factor and not the contents of the spoil, because significant peaks were also seen in the leachate collected from the "blank barrel" at the same time (more significant in Cu and Zn, but also present for Mn). Potential causes of this influx of Cu, Mn, and Zn are deposition of very fine particulates from the upwind Virginia Tech coal fired power plant, or possibly local uses in foliar research applications at the Turfgrass Research Center.

Leachate pH, As, and Cd were not affected by scale.

Effect of Leaching Test Scale on Coarse Coal Refuse Leachate

Every refuse leachate component analyzed (pH, EC, bicarbonate, sulfate, Ca, Mg, K, Fe, Mn, Al, Se, As, Cd, Cl, Cu, Ni, Pb, and Zn) showed a treatment effect (columns vs. barrels). Leachate EC, Ca, Mg, Se, and sulfate displayed similar treatment effects over time. For each of these components, concentrations in column leachates for both TNR-1 and TNR-3 began with an initial peak before rapidly decreasing and stabilizing at a lower level for the remainder of the study. However, elution patterns differed greatly between the columns and barrels for both refuse materials. For both TNR-1 and TNR-3, concentrations began very low before rapidly increasing to an initial peak, followed by a second and higher peak. Leachate concentrations from the barrels ended at relatively high levels, compared to the columns which ended at low concentrations. In the columns, TNR-1 maintained higher concentrations of these components compared to TNR-3, but the opposite was true for the majority of the study in the barrels. Initial differences between the column and barrel leachates could have been due to material preparation

and smaller size consist in the columns. Later differences were likely a result of differential pyrite oxidation driven reactions in the barrels, which were apparently inhibited in the columns. These results are concerning for the health of headwater streams receiving runoff from coal mining operations. As discussed previously, elevated TDS levels impair aquatic life (Bernhardt et al., 2012; Pond et al., 2008; Timpano et al., 2015) and levels seen at both scales for both materials often exceeded the 500 $\mu S\ cm^{-1}$ benchmark considered to be harmful for aquatic life. Furthermore, the TNR-3 barrels leachates were an order of magnitude higher in EC once pyrite oxidation occurred. Also, significant differences between leaching scales in this study indicates that predicting TDS and component ion concentrations is difficult for reactive and sulfide refuse materials.

Leachate pH showed significantly different treatment effects between the two refuse materials. For the TNR-1 material, leachate pH was typically 2.0 to 3.0 units lower in the columns compared to the barrels. Leachate pH for the TNR-3 refuse was similar and stable for both the columns and the barrels (approximately 7.5 to 8.0) for the first 30 cm of cumulative leachate before the pH in the barrel leachates quickly plummeted to 3.5 and continued to slowly drop while the column leachate remained around pH 8.0. Differences in both cases could be due to differences in pyrite form and oxidation/reaction rates among refuse materials (Stewart and Daniels, 1992), or differences in material preparation and size consist between the two scales (columns and barrels) and associated reactive surface area. Regardless, the differences observed in pH and other associated solubility effects between the two leaching scales and refuse materials employed were not expected, and in certain cases were counterintuitive.

Leachate Al, Cd, Cu, Fe, Mn, Ni, Pb, and Zn all displayed the same general treatment effects. For the TNR-1 refuse, concentrations of these components started with an initial peak

followed by a rapid decline before stabilizing at low levels in the columns, while the barrel leachates remained at very low levels throughout the study. On the other hand, for the TNR-3 refuse, these leachate component concentrations remained low in the columns throughout the study, while in the barrels they started off low before rapidly increasing at approximately 30 cm of cumulative leachate. The initial differences between column and barrel leachates for the TNR-1 refuse were likely due to material preparation. The crushed refuse material could have produced an initial flush of colloidal materials. For the TNR-3 material, the differences after 30 cm of cumulative leachate were directly related to the rapid drop in leachate pH that occurred at this time. Sulfide oxidation and the associated drastic pH reduction likely increased metal solubility and release.

Leachate bicarbonate showed treatment effects for both the TNR-1 and TNR-3 refuse materials. For the TNR-1 material, leachate bicarbonate stayed relatively consistent and averaged 50 mg $L^{-1}$, while column leachate bicarbonate remained at or near the detection limit. The neutralizers were likely much less reactive in the columns compared to the barrels. On the other hand, while both column and barrel leachate bicarbonate for the TNR-3 material peak within the first 30 cm of cumulative leachate and then declined to lower levels, the TNR-3 columns maintained at significantly higher concentrations for the duration of the study. In this case, it appears that neutralizers were able to react more readily at the finer particle size of the columns, but could not maintain pH control against the rate of S-oxidation in the barrels.

Leachate As was not affected by leaching scale for the TNR-1 material. Concentrations remained at or near the detection limit throughout the study for both the columns and barrels. In contrast, the TNR-3 material leachate showed strong treatment effects for As. While the column leachate As remained at or near the detection limit, leachate As from the barrels showed two

significant peaks. These peaks were likely driven by sulfide oxidation in the barrels, which was inhibited in the columns.

Similarly, leachate Cl from the TNR-1 refuse showed no treatment effect, while leachate Cl from the TNR-3 refuse showed a strong treatment effect. For the TNR-1 refuse, leachate Cl concentrations remained at or below the detection limit. Leachate Cl from the TNR-3 barrels was significantly higher than in the column leachate for the first 25 cm of cumulative leachate. This was likely due to a weathering process, such as slaking, that occurred in the barrels but not the columns. Regardless, overall Cl levels were low, so this difference may not be of environmental importance.

Leachate K showed similar treatment effects for both refuse materials. In each case, leachate K concentrations began low in the barrels, but high in the columns. However, both leaching scales peaked for K within the first 20 cm of cumulative leachate. The TNR-1 refuse leachate contained significantly higher leachate concentrations compared to the TNR-3 material. These differences were likely due to differences in weatherable minerals, because total mass K content were similar. Leaching test scale showed no effect on leachate Na. However, the TNR-3 material consistently produced higher concentrations compared to the TNR-1 material. These differences were due to sizeable differences in initial mass Na levels.

## CONCLUSIONS

The TDS elution patterns from the Harlan spoil produced by the columns, barrels, and mesocosms (estimated by EC) were similar, but there were some key differences. First, initial peak leachate EC values in the mesocosm leachates were significantly higher than the barrels and columns. Also, the initial peak leachate EC values from the barrels were intermediate between the columns and mesocosms, further supporting a scaling effect. These findings suggest larger scales of spoil material (e.g. actual field mining site fills) could produce higher initial peak EC values. These results also suggest that the scale of leaching has a more important influence on TDS production than particle size/surface area per se since the coarsest materials (e.g. in the mesocosms) produced higher EC values. Secondly, the barrel and mesocosm leachates exhibited a second and third peak during the late summer and early fall of 2013 and 2014, respectively. These peaks were not seen in the column leachate EC values and suggest that leaching environment and simple variations in field rainfall patterns are an important factor in TDS elution from coal mine spoils. It appears that when the spoils were subjected to dry periods of weather, weathering salts accumulated and then flushed through once a significant rainfall occurred. Other leachate components analyzed also differed, likely due to differences in size consist at the three scales due to material preparation, as well as time-lagged pyrite weathering in coal refuse that obvious at the larger scale (barrels), but not in the columns.

Overall, comparing the column method results to the larger scale experiments confirmed that the column method is likely a reasonable predictor of overall TDS release from coal mine spoil, but probably under-predicts peak levels relative to full field conditions. However, as noted earlier, the observed range of EC from all three scales was quite similar to that reported by numerous regional field studies and thus supports the use of the column technique for general

TDS prediction for non acidic spoils. That being said, it is important to note that the column technique more than likely somewhat underpredicts peak initial TDS elution from a given mass of spoil and does not adequately reproduce field secondary peaks results from expected seasonal water budget variations.

Leachates from the two coarse coal refuse materials, TNR-1 and TNR-3, were very different at both scales of study (columns vs. barrels) throughout the study. While, this was expected based on the different preliminary characterizations data, the completely different relative response between the columns and the barrel was unanticipated. To a large extent, the two materials behaved differently relative to one another in the barrels vs. the columns. Results suggest significant scaling effects between the columns and barrels for the majority of the leachate components analyzed, often due to differences in leaching environment, which likely caused pyrite oxidation driven weathering processes to differ greatly between the two scales. Due to the significant differences seen between the results from the columns and barrels, leaching vessel size appeared to have a more significant effect on TDS prediction with refuse materials compared to spoil materials. Therefore, results from the column leaching technique for refuse materials may not be directly applicable to field scale situations, and more research is needed to determine the best leaching method for TDS prediction with refuse.

**REFERENCES**


Agouridis, C., P. Angel, T. Taylor, C. Barton, R. Warner, X. Yu, and C. Wood. 2012. Water quality characteristics of discharge from reforested loose-dumped mine spoil in eastern Kentucky. J. Environ. Qual. 41:454-468.

AOAC International. 2002. Official Methods of Analysis of AOAC, International 17th Ed. AOAC International, Gaithersburg, MD, USA, Official Method 955.01.

Berner, R.A, and J.W. Morse. 1974. Dissolution kinetics of calcium carbonate in seawater; IV, Theory of calcite dissolution. Amer. J. of Science 274(2): 108-134.

Bernhardt, E.S., B.D. Lutz, R.S. King, J.P. Fay, C.E. Carter, A.M. Helton, D. Campagna, and J. Amos. 2012. How many mountains can we mine? Assessing the regional degradation of central Appalachian rivers by surface coal mining. Environ. Sci. and Tech. 46(15): 8112-8115.

Burger J.A., D. Graves, P. Angel, V. Davis and C.E. Zipper. 2005. The Forestry Reclamation Approach. ARRI Forest Reclamation Advisory No.2. US Office of Surface Mining, 4p. http://arri.osmre.gov/FRA/Advisories/FRA_No.2.7-18-07.Revised.pdf

Buttermore, W.H., E.J. Simcoe, and M.A. Malloy. 1978. Characterization of Coal Refuse. Coal Res. Bureau, Tech. Rep. 159. West Virginia University, Morgantown WV.

Caruccio F., W. Bradham, and G. Geidel. 1993. Overburden analyses; some important factors. West Virginia Surface Mine Drainage Task Force Symposium, April 1993, Morgantown, WV. p 27-28 In; J. Skousen et al. (eds), 14th Ann. Symp. West Virginia Surf. Mine Drain. Task Force, Morgantown, WV.

Chapman, P.M., H.B. Bailey, and E. Canaria. 2000. Toxicity of total dissolved solids associated with two mine effluents to chironomid larvae and early life stages of rainbow trout. Environ. Toxic. and Chem. 19(1): 210-214.

Cormier, S.M., G.W. Suter, and L. Zheng. 2013. Derivation of a benchmark for freshwater ionic strength. Environ. Toxic. and Chem. 32:263 - 271.

Daniels, W. L., M. Beck, M. J. Eick and Z. W. Orndorff. 2009. Predicting Contaminant Leaching Potentials for Central Appalachian Overburden and Coal Refuse Materials. Final Report to OSM Applied Science Research Program, December 2009. http://www.osmre.gov/programs/TDT/appliedScience/2007VTLeachingPotentialNPointonFR.pdf

Daniels, W.L., Z.W. Orndorff, M.J. Eick, and C.E. Zipper. 2013. Predicting TDS release from Appalachian mine spoils. p. 275-285. *In*: J.R. Craynon (ed.), Environmental Considerations in

Energy Production, April 14-18, 2013, Charleston, WV. Soc. For Mining Metal. & Explor., Englewood, CO. www.smenet.org.

Daniels, W.L., C.E. Zipper, and Z.W. Orndorff. 2014a. Predicting release and aquatic effects of total dissolved solids from Appalachian USA coal mines. Int. J. of Coal Science & Tech. 1(2): 152-162.

Daniels W.L., Z.W. Orndorff, L.C. Ross, S. Koropchak, C. Zipper, D. Evans, and M. Eick. 2014b. Correlation of TDS Release Potentials with Field Leaching Behaviors for Appalachian Coal Mine Spoils and Coarse Refuse. Final Report to OSM Applied Science Research Program, July, 2014. http://www.osmre.gov/programs/TDT/appliedScience/2011VT-WDanielsCorrelationTDSReleasePotentialsFR.pdf

Evangelou, V. P. 1995. Pyrite Oxidation and its Control. CRC Press, Inc., New York.

Evans, D.M., C.E. Zipper, P.F. Donovan and W.L. Daniels. 2014. Long-term trends of specific conductance in waters discharged by coal-mine valley fills in Central Appalachia, USA. J. Amer. Water Res. Assoc. 50(6): 1449-1460. DOI: 10.1111/jawr.12198

Green, J., M. Passmore, and H. Childers. 2000. A Survey of the Condition of Streams in the Primary Region of Mountaintop Mining/Valley Fill Programmatic Environmental Impact Statement. U.S. Environmental Protection Agency, Region III, Wheeling, WV. http://www.cet.edu/pdf/mtmvfbenthics.pdf (accessed 19 January 2015)

Halverson, H.G., and C.E. Gentry. 1990. Long-term leaching of mine spoil with simulated precipitation. p 27-32 In Skousen et al., (eds). Proc., 1990 Mining and Reclamation Conference and Exhibition, Charleston, WV. 23-26 Apr. 1990. Amer. Soc. Mining and Rec., 1305 Weathervane, Champaign, IL 61821. http://www.asmr.us/Publications/Conference%20Proceedings/1990%20Meetings%20Vol%201/Halverson%2027-32.pdf

Hartman, K.J., M.D. Kaller, J.W. Howell, and J.A. Sweka, 2005. How much do valley fills influence headwater streams? Hydrobiologia 532:91-102.

Hood, W.C., and A.O. Oertel. 1984. A leaching column method for predicting effluent quality from surface mines. P. 271-277. In D. Graves (ed.). Proc., 1984 National Symp. on Surface Mining, Hydrology, Sed., and Rec., Lexington Ky., 2-7 Dec. 1984. Univ. of Kentucky College of Eng., Lexington, KY.

Lindberg, T.T., E.S. Bernhardt, R. Bier, A.M. Helton, R.B. Merola, A. Vengosh, and R.T. Di Giulio, 2011. Cumulative impacts of mountaintop mining on an Appalachian watershed. Proc. Nat. Acad. of Sci. 108:20929-20934.

McBride, M. B. (1994). Environmental Chemistry of Soils. USA. Oxford University Press.

Móricz, F., F. Mádai, and I.F. Walder. 2012. Pyrite oxidation under circumneutral pH conditions. Geosci. Eng. 1(2):111-116.

Orndorff, Z.W., W. L. Daniels, M. Beck, and M. J. Eick. 2010. Leaching potentials of coal spoil and refuse: acid-base interactions and electrical conductivity. p. 736-766 In: R.I. Barnhisel (ed.), Proc., 2010 National Meeting of the Amer. Soc. Mining and Rec., Pittsburgh, PA, June 5 - 11, 2010. Published by ASMR, 1305 Weathervane, Champaign, IL 61821. http://www.asmr.us.

Palmer, M.A., E.S. Bernhardt, W.H. Schlesinger, K.N. Eshleman, E. Foufoula-Georgiou, M.S. Hendryx, A.D. Lemly, G.E. Likens, O.L. Loucks, M.E. Power, P.S. White, and P.R. Wilcock. 2010. Mountaintop mining consequences. Science 327: 148-149.

Parker, J.M. 2013. The Effect of Various Saturation Levels, Leaching Solution pH, and Leaching Cycle on Electrical Conductivity from Coal Mine Spoil Leachate. M.S. Thesis, Virginia Tech, Blacksburg. http://vtechworks.lib.vt.edu/handle/10919/51807.

Pond, G. J., M.E. Passmore, F.A. Borsuk, L. Reynolds, and C.J. Rose. 2008. Downstream effects of mountaintop coal mining: comparing biological conditions using family- and genus-level macroinvertebrate bioassessment tools. Jour. North Amer. Benth. Soc. 27(3):717-737.

Pond, G.J. 2010. Patterns of Ephemeroptera taxa loss in Appalachian headwater streams (Kentucky, USA). Hydrobiologia, 641:185–201. DOI 10.1007/s10750-009-0081-6.

Pond, G.J., M.E. Passmore, N.D. Pointon, J.K. Felbinger, C.A. Walker, K.J. Krock, J.B. Fulton, and W.L. Nash. 2014. Long-term impacts on macroinvertebrates downstream of reclaimed mountaintop mining valley fills in central Appalachia. J. Environ. Manag. 54(4):919-33. doi: 10.1007/s00267-014-0319-6.

Rhoades, J.D. 1996. Salinity: Electrical conductivity and total dissolved solids. p. 417-435. In: D.L. Sparks (ed.), Methods of Soil Analysis. Part 3. Chemical Methods. Soil Sci. Soc. Amer. Book Series 5. SSSA and ASA, Madison, WI.

Roberts, J.A., W.L. Daniels, J.C. Bell, and J.A. Burger. 1988. Early stages of mine soil genesis in a Southwest Virginia spoil lithosequence. Soil Sci. Soc. Am. J. 52:716-723.

Sena, K. C. Barton, P. Angel, C. Agouridis, and R. Warner. 2014. Influence of spoil type on chemistry and hydrology of interflow on a surface coal mine in a eastern US coalfield. Water, Air, & Soil Poll. October 2014, 225:217.

Schatzel, S.J., and B.W. Stewart. 2012. A provenance study of mineral matter in coal from Appalachian Basin coal mining regions and implications regarding the respirable health of underground coal workers: a geochemical and Nd isotope investigation. Int. J. Coal Geol. 94:123-136.

Skousen J, J. Simmons J, and P. Ziemkiewicz (2002) Acid-base accounting to predict post-mining drainage quality on surface mines. J. Environ. Qual. 31(6):2034–204.

Stewart, B.R., and W.L. Daniels. 1992. Physical and chemical properties of coal refuse from southwest Virginia. J. Environ. Qual. 21: 635–642.

Stewart, B.R., W.L. Daniels and M.L. Jackson. 1997. Evaluation of leachate quality from the codisposal of coal fly ash and coal refuse. J. Environ. Qual. 26: 1417-1424.

Stewart, B.R., W.L. Daniel, L.W. Zelazny and M.L. Jackson. 2001. Evaluation of leachates from coal refuse blended with fly ash at different rates. J. Environ. Qual.. 30:1382-1391.

Timpano, A., S. Schoenholtz, C. Zipper, and D. Soucek. 2010. Isolating effects of total dissolved solids on aquatic life in central Appalachian coalfield streams. p. 1284 – 1302 in R.I. Barnhisel (Ed.), Proc., 2010 National Meeting of the Amer. Soc. of Mining and Rec., Pittsburgh, PA, June 5 - 11, 2010. Amer. Soc. Mining & Rec., 1305 Weathervane, Champaign, IL 61821 http://www.asmr.us.

Timpano, A.J., Schoenholtz, S.H., Soucek, D.J. and Zipper, C.E. 2015. Salinity as a limiting factor for biological condition in mining influenced central Appalachian headwater streams. Amer. Water Res. Assoc. 51:1 240-250. DOI: 10.1111/jawr.12247.

U.S. EPA. 2001. Inductively Coupled Plasma Mass Spectrometry, Method 6010B, Rev.2. *In* SW-846: Test Methods for Evaluating Solid Waste, Physical/Chemical Methods. USEPA, Office of Solid Waste, Washington, DC.

U.S. EPA. 2007a. Microwave Assisted Acid Digestion of Sediments, Sludges, Soils and Oils, Method 3051A, Rev.1. In SW-846: Test Methods for Evaluating Solid Waste, Physical/Chemical Methods. USEPA, Office of Solid Waste, Washington, DC.

U.S. EPA. 2007b. Inductively Coupled Plasma Mass Spectrometry, Method 6020A, Rev.1. *In* SW-846: Test Methods for Evaluating Solid Waste, Physical/Chemical Methods. USEPA, Office of Solid Waste, Washington, DC.

U.S. Geological Survey (USGS), 2014. Harlan Sandstone. Mineral Resources On-line Spatial Data. http://mrdata.usgs.gov/geology/state/sgmc-unit.php?unit=VAPAh%3B0 (accessed 7 July 2014)

Walton, R. B. (2012). Final decision, National Mining Association vs. USEPA and Sierra Club, Case 1:10-cv-01220-RBW Document 167 Filed 07/31/12, United States District Court, Washington, DC.